Title
Self-similar intermediate structures in turbulent boundary layers at large Reynolds numbers

Journal
Journal of Fluid Mechanics, 410

Author
Barenblatt, G.I.

Publication Date
1999-05-01

LBNL-43194
Preprint

ERNEST ORLANDO LAWRENCE
BERKELEY NATIONAL LABORATORY

Self-similar Intermediate Structures in Turbulent Boundary Layers at Large Reynolds Numbers

G.I. Barenblatt, A.J. Chorin, and V.M. Prostokishin

Computing Sciences Directorate
Mathematics Department

May 1999

To be submitted
for publication

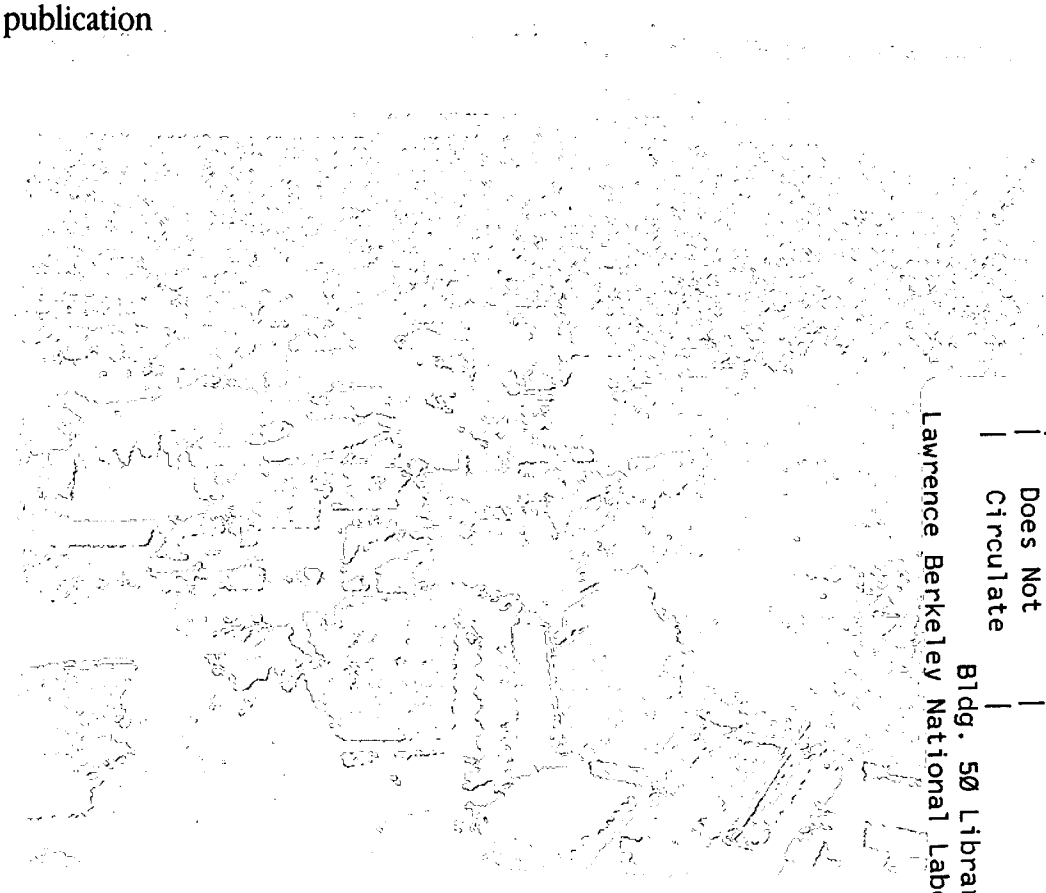

DISCLAIMER

LBNL-43194

SELF-SIMILAR INTERMEDIATE STRUCTURES IN TURBULENT BOUNDARY LAYERS AT LARGE REYNOLDS NUMBERS*

G.I. Barenblatt and A.J. Chorin
Mathematics Department
Computing Sciences Directorate
Lawrence Berkeley National Laboratory
and
Department of Mathematics
University of California
Berkeley, CA 94720, USA

and
V.M. Prostokishin
P.P. Shirshov Institute of Oceanology
Russian Academy of Sciences
36 Nakhimov Prospect
Moscow 117218, Russia

May 1999

*This work was supported in part by the Office of Science, Office of Computational and Technology Research, Mathematical, Information, and Computational Sciences Division, Applied Mathematical Sciences Subprogram, of the U.S. Department of Energy, under Contract No. DE-AC03-76SF00098, and by the National Science Foundation under Grants DMS94-14631 and DMS97-32710.

Self-similar Intermediate Structures in Turbulent Boundary Layers at Large Reynolds Numbers

G. I. Barenblatt, A. J. Chorin

Department of Mathematics
and Lawrence Berkeley National Laboratory
University of California
Berkeley, California 94720, USA

and

V. M. Prostokishin

P. P. Shirshov Institute of Oceanology
Russian Academy of Sciences
36 Nakhimov Prospect
Moscow 117218, Russia

Abstract. Processing the data from a large variety of zero-pressure-gradient boundary layer flows shows that the Reynolds-number-dependent scaling law, which the present authors obtained earlier for pipes, gives an accurate description of the velocity distribution in a self-similar intermediate region of distances from the wall adjacent to the viscous sublayer. The appropriate length scale that enters the definition of the boundary layer Reynolds number is found for all the flows under investigation.

Another intermediate self-similar region between the free stream and the first intermediate region is found under conditions of weak free stream turbulence. The effects of turbulence in the free stream and of wall roughness are assessed, and conclusions are drawn.

1 Introduction

Asymptotic laws for wall-bounded turbulent shear flows at large Reynolds numbers are considered. Classical examples of such flows are the flows in pipes, channels, and boundary layers. This class of flows is of major fundamental and practical importance. All these flows share as dimensional governing parameters the shear stress at the wall τ and the fluid's properties, its density ρ and dynamic viscosity μ. From these parameters two important quantities can be formed: the *dynamic* or *friction* velocity $u_* = (\tau/\rho)^{\frac{1}{2}}$ and the length scale $\delta = \nu/u_*$, where $\nu = \mu/\rho$ is the fluid's kinematic viscosity. The length scale δ is tiny at large Reynolds numbers, and in the layer where the dimensionless distance of the wall y/δ is less than, say, 70 (viscous sublayer) the viscous stress is comparable with the Reynolds stress created by vortices. Outside this viscous sublayer, at $y/\delta > 70$, the contribution of the viscous stress is small. We emphasize that 'small' is not always synonymous with 'negligible', and indeed we will see that here is a case where it is not.

In 1930, the great mechanician Th. von Kármán proposed in explicit form the hypothesis that outside the viscous sublayer the contribution of viscosity can be neglected. On the basis of this assumption he derived the *universal* (i.e. Reynolds number independent) *logarithmic law* for the distribution of the mean velocity u over the cross-section:

$$\phi = \frac{u}{u_*} = \frac{1}{\kappa} \ln \eta + C \,, \qquad \eta = \frac{u_* y}{\nu} \tag{1}$$

where y is the distance from the wall; the constants κ (the von Kármán constant) and C should be identical for all turbulent wall-bounded shear flows at high Reynolds numbers, and the law (1) should be valid in intermediate regions between, on one hand, the viscous sublayer and, on the other, the external parts of the flows, e.g. vicinity of the axis in pipe flow, or vicinity of the external flow in the boundary layer. In 1932, L. Prandtl, the greatest mechanician of this century, came to the law (1) using a different approach, but effectively with the same basic assumption. The law (1) is known as the von Kármán-Prandtl universal logarithmic law. More recent derivations which, however, follow the same ideas and the same basic assumption, often in an implicit form, can be found in monographs by Landau and Lifshits (1987), Monin and Yaglom (1971), Schlichting (1968) and in a recent textbook by Spurk (1997).

According to the von Kármán-Prandtl law (1), all experimental points corresponding to the intermediate region should collapse on a single universal straight line in the traditional coordinates $\ln \eta, \phi$.

Subsequent investigations showed, however, that this is not what happens. First, the experiments showed systematic deviations from the universal logarithmic law (1) even if one is willing to tolerate a variation in the constants κ and C (from less than 0.4 to 0.45 for κ, and from less than 5.0 to 6.3 for C). Furthermore, using analytic and experimental arguments, the present authors showed [Barenblatt (1991, 1993); Barenblatt and Prostokishin (1993); Barenblatt, Chorin and Prostokishin (1997b); Chorin (1998)] that the fundamental von Kármán hypothesis on which the derivation of the universal law (1) was based, i.e. the assumption that the influence of viscosity disappears totally outside the viscous sublayer, is inadequate. In fact, this hypothesis should be replaced by the more complicated one of incomplete similarity, so that the influence of viscosity in the intermediate region remains, but the viscosity enters only in power combination with other factors. This means that the influence of the Reynolds number, i.e. both of the viscosity and the external length scale, e.g. the pipe diameter, remains and should be taken into account in the intermediate region.

For the readers' convenience we present here briefly the concept of incomplete similarity; a more detailed exposition can be found in Barenblatt, (1996). The mean velocity gradient $\partial_y u$ in turbulent shear flows can be represented in the general form suggested by dimensional analysis

$$\partial_y u = \frac{u_*}{y}\Phi(\eta, \mathrm{Re}) \ .$$

In the intermediate region, $\eta = u_* y/\nu$ is large, and we consider the case of large Reynolds number. The basic von Kármán hypothesis corresponds to the assumption that the dimensionless function $\Phi(\eta, \mathrm{Re})$ at large η and Re can be replaced by a constant $1/\kappa$, its limit as $\eta \to \infty$, $\mathrm{Re} \to \infty$. This corresponds to *complete similarity* both in η and Re. The assumption of *incomplete similarity* in η means that at large η a finite limit of the function Φ does not exist, but that this function can be represented as

$$\Phi = C(\mathrm{Re})\eta^{\alpha(\mathrm{Re})}$$

i.e., the velocity gradient has a *scaling* intermediate asymptotics. Here the functions $C(\mathrm{Re})$ and $\alpha(\mathrm{Re})$ should be specified.

Using some additional analytic and experimental arguments the present authors came to the Reynolds-number-dependent *scaling* law of the form

$$\phi = \frac{u}{u_*} = (C_0 \ln \mathrm{Re} + C_1)\eta^{c/\ln \mathrm{Re}} \ . \tag{2}$$

where the constants C_0, C_1 and α must be universal. The scaling law (2) was compared with what seemed (and seems to us up to now) to be the best available data for turbulent

pipe flows, obtained by Nikuradze (1932), under the guidance of Prandtl at his Institute in Göttingen. The comparison has yielded the following values for the coefficients

$$c = \tfrac{3}{2}\,, \qquad C_0 = \frac{1}{\sqrt{3}}\,, \qquad C_1 = \tfrac{5}{2} \tag{3}$$

when the Reynolds number Re was taken in the form

$$\mathrm{Re} = \frac{\bar{u}d}{\nu}\,. \tag{4}$$

Here $\bar{u}$ is the average velocity (the total flux divided by the pipe cross-section area) and d is the pipe diameter. The final result has the form

$$\phi = (\frac{1}{\sqrt{3}}\ \ln\ \mathrm{Re} + \tfrac{5}{2})\eta^{3/2\ \ln\ \mathrm{Re}} \tag{5}$$

or, equivalently

$$\phi = \left(\frac{\sqrt{3}+5\alpha}{2\alpha}\right)\eta^{\alpha}\,, \qquad \alpha = \frac{3}{2\ln\ \mathrm{Re}}\,. \tag{6}$$

The scaling law (5) produces separate curves $\phi(\ln\ \eta$,Re) in the traditional $(\ln\ \eta, \phi)$ plane, one for each value of the Reynolds number. This is the principal difference between the law (5) and the universal logarithmic law (1). We showed that the family (5) of curves having Re as parameter has an envelope, and that in the $\ln\eta, \phi$ plane this envelope is close to a straight line, analogous to (1) with the values $\kappa = 0.4$ and $C = 5.1$. Therefore, if the experimental points are close to the envelope they can lead to the illusion that they confirm the universal logarithmic law (1).

The Reynolds-number-dependent scaling law can be reduced to a self-similar universal form

$$\psi = \frac{1}{\alpha}\ln\ \left(\frac{2\alpha\phi}{\sqrt{3}+5\alpha}\right) = \ln\ \eta\,, \qquad \alpha = \frac{3}{2\ln\ \mathrm{Re}}, \tag{7}$$

so that contrary to what happens in the $(\ln\ \eta, \phi)$ plane, in the $(\ln\ \eta, \psi)$ plane the experimental points should collapse onto a single straight line—the bisectrix of the first quadrant. This statement received a ringing confirmation from the processing of Nikuradze's 1932 data (Barenblatt and Prostokishin (1993); Barenblatt, Chorin and Prostokishin (1997b)).

An important remark should be made here. Izakson, Millikan and von Mises (IMM, see, e.g. Monin and Yaglom (1971)) gave an elegant derivation of the universal logarithmic law based on what is now known as matched asymptotic expansions. This derivation, which seemed to be unbreakable, persuaded fluid dynamicists that this law was a truth which will enter future turbulence theory essentially unchanged. In the papers of the present

authors (Barenblatt, Chorin (1996, 1997)), it was demonstrated that the scaling law (2) is compatible with the properly modified IMM procedure. The method of vanishing viscosity (Chorin, (1988, 1994)) was used in this modification.

Let us turn now to shear flows other than flows in pipes. By the same logic, the scaling law (5) should be also valid for an intermediate region adjacent to the viscous sublayer for all good quality experiments performed in turbulent shear flows at large Re.

The first question is, what is the appropriate definition of the Reynolds number for these flows which will make the formula (5) applicable? This is a very important point—if the universal Reynolds-number-independent logarithmic law were valid, the definition of the Reynolds number would be irrelevant provided it were sufficiently large. For the scaling law (5) this is not the case. Indeed, if the scaling law (5) has general applicability it should be possible to find, for every turbulent shear flow at large Reynolds number, an appropriate definition of the Reynolds number which will make the scaling law (5) valid.

There exists nowadays a large amount of data for an important class of wall-bounded turbulent shear flows: turbulent zero-pressure-gradient boundary layers. These data were obtained over the last 25 years by various authors using various set-ups. For boundary layers the traditional definition of the Reynolds number is

$$\mathrm{Re}_\theta = \frac{U\theta}{\nu} \tag{8}$$

where U is the free stream velocity, and θ is a characteristic length scale—the momentum displacement thickness. The question which we asked ourselves was, is it possible to find for each of these flows a particular length scale Λ, so that the scaling law (5) will be valid for all of them with the same values of the constants. Of course, in each case the length-scale Λ could be influenced by the contingencies of the particular experiment, but the question of decisive importance is whether such a length scale exists. The answer within the accuracy of the experiments is affirmative.

We present here the results of the processing all the experimental data available to us, in particular, all the data collected in a very instructive review by Fernholz and Finley (1996). We show that for all of these flows, without any exception, the scaling law (5) is observed with an instructive accuracy over the whole intermediate region, if the Reynolds number is defined properly, i.e., if the characteristic length Λ entering the Reynolds number

$$\mathrm{Re} = \frac{U\Lambda}{\nu} \tag{9}$$

is properly determined. Moreover, we show that for all the flows where the turbulence in the external flow is small, there exists a sharply distinguishable second intermediate region

between the first one where the scaling law (5) is valid and the external homogeneous flow. The average velocity distribution in this second intermediate region is also self-similar of scaling type:

$$\phi = B\eta^{\beta} \tag{10}$$

where B and β are constants.

However, a Reynolds number dependence of the power β was not observed. Within the accuracy of the experimental data β is close to $1/5$. When the turbulence in the external homogeneous flow becomes significant, the second self-similar region deteriorates and the power β decreases with growing external turbulence until the second intermediate region disappears completely.

2 The first group of zero-pressure-gradient boundary layer experiments

We will explain later why we divided the experimental data into three groups. Here it is sufficient to note that all available sets of experimental data were eventually taken into account.

The original data were always presented by their authors in the form of graphs in the traditional ($\ln \eta, \phi$) plane, suggested by the universal logarithmic law (1). The shape of original graphs was always similar to the one presented qualitatively in Figure 1a. Therefore, the first rather trivial step was to replot the data in the doubly logarithmic coordinates ($\lg \eta, \phi$) appropriate for revealing the scaling laws. The result was instructive: for all experiments of the first group (in chronological order), specifically: Collins, Coles, Hike,[1] (1978); Erm and Joubert (1991); Smith[2] (1994); Naguib[3] (1992), and Nagib and Hites[4] (1995); Krogstad and Antonia (1998), the data outside the viscous sublayer ($\lg \eta > 1.5$) have the characteristic shape of a broken line, shown qualitatively in Figure 1b and quantitatively in Figures 2–6.

Thus, the two straight lines forming the broken line that were revealed in the $\lg \eta, \lg \phi$ plane have as equations

$$\text{(I)} \quad \phi = A\eta^{\alpha} \; ; \qquad \text{(II)} \quad \phi = B\eta^{\beta} \; . \tag{11}$$

The coefficients A, α, B, β were obtained by us through statistical processing.

[1]The data were obtained by scanning the graphs in the review by Fernholz and Finley (1996).
[2]The data were obtained by scanning the graphs in the review by Fernholz and Finley (1996).
[3]The data in digital form were provided to us by Dr. M. Hites.
[4]The data in digital form were provided to us by Dr. M. Hites.

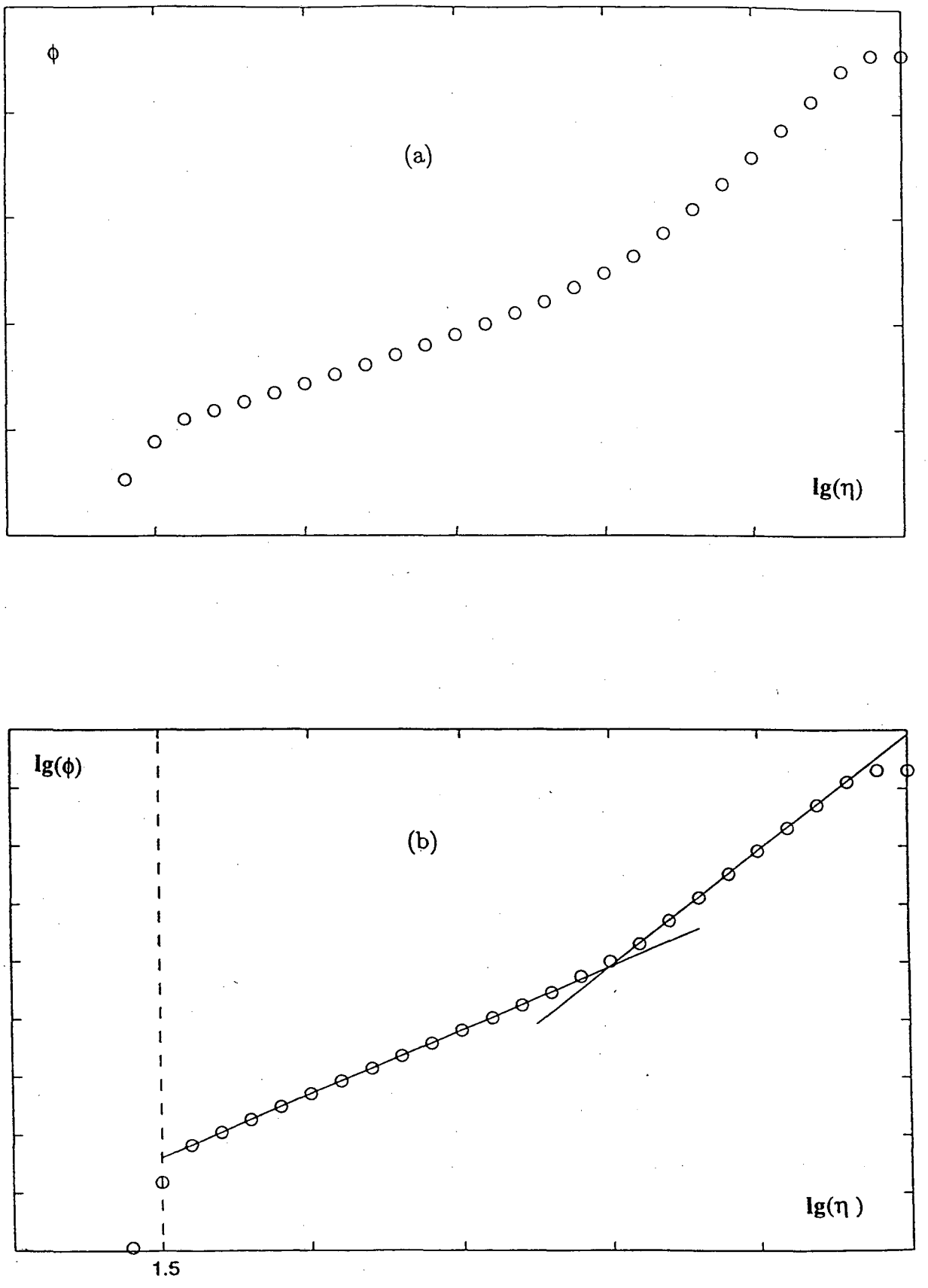

Figure 1. (a) Schematic representation of the experimental data in traditional coordinates $\ln \eta, \phi$. (b) Schematic representation of the experimental data in $(\ln \eta, \ln \phi)$ coordinates for experiments of the first group.

We assume as before that the effective Reynolds number Re has the form (9): $\mathrm{Re} = U\Lambda/\nu$, where U is the free stream velocity and Λ is a length scale. The basic question is, whether one can find in each case a length scale Λ which plays the same role for the intermediate region (I) of the boundary layer as the diameter does for pipe flow? In other words, whether it is possible to find a length scale Λ, perhaps influenced by individual features of the flow, so that the scaling law (5) is valid for the first intermediate region (I)? To answer this question we have taken the values A and α, obtained by statistical processing of the experimental data in the first intermediate scaling region, and then calculated two values $\ln \mathrm{Re}_1$, $\ln \mathrm{Re}_2$, by solving the equations suggested by the scaling law (5):

$$\frac{1}{\sqrt{3}}\ln \mathrm{Re}_1 + \tfrac{5}{2} = A \ , \qquad \frac{3}{2\ln \mathrm{Re}_2} = \alpha \ . \tag{12}$$

If these values $\ln \mathrm{Re}_1$, $\ln \mathrm{Re}_2$ obtained by solving the two different equations (12) are indeed close, i.e., if they coincide within experimental accuracy, then the unique length scale Λ can be determined and the experimental scaling law in the region (I) coincides with the basic scaling law (5).

Table 1 shows that these values are close, the difference slightly exceeds 3% in only two cases; in all other cases it is less. Thus, we can introduce for all these flows the mean Reynolds number

$$\mathrm{Re} = \sqrt{\mathrm{Re}_1 \mathrm{Re}_2} \ , \qquad \ln \mathrm{Re} = \tfrac{1}{2}(\ln \mathrm{Re}_1 + \ln \mathrm{Re}_2) \tag{13}$$

and consider Re as an estimate of the effective Reynolds number of the boundary layer flow. Naturally, the ratio $\mathrm{Re}_\theta/\mathrm{Re} = \theta/\Lambda$ is different for different flows.

Table 1

Figure	Re_θ	α	A	$\ln Re_1$	$\ln Re_2$	$\ln Re$	Re_θ/Re	β
	Collins D.J., Coles D.E., and Hiks J.W. (1978)							
Fig.2 (a)	5,938	0.129	9.10	11.43	11.63	11.53	0.06	0.203
Fig.2 (b)	6,800	0.125	9.23	11.66	12.00	11.83	0.05	0.195
Fig.2 (c)	7,880	0.123	9.41	11.97	12.21	12.09	0.04	0.202
	Erm L.P. and Joubert P.N. (1991)							
Fig.3 (a)	697	0.163	7.83	9.23	9.20	9.22	0.07	0.202
Fig.3 (b)	1,003	0.159	7.96	9.46	9.43	9.45	0.08	0.192
Fig.3 (c)	1,568	0.156	7.99	9.51	9.62	9.56	0.11	0.202
Fig.3 (d)	2,226	0.148	8.28	10.01	10.14	10.07	0.09	0.214
Fig.3 (e)	2,788	0.140	8.66	10.67	10.71	10.69	0.06	0.206
	Naguib A.M. (1992) and Hites M. and Nagib H. (1995)							
Fig.4 (a)	4,550	0.154	7.95	9.44	9.74	9.59	0.31	0.22
Fig.4 (b)	6,240	0.152	8.08	9.66	9.87	9.77	0.36	0.20
Fig.4 (c)	9,590	0.143	8.37	10.17	10.49	10.33	0.31	0.206
Fig.4 (d	13,800	0.131	8.94	11.15	11.45	11.30	0.17	0.193
Fig.4 (e)	21,300	0.138	8.61	10.58	10.87	10.73	0.47	0.22
Fig.4 (f)	29,900	0.130	8.99	11.24	11.54	11.39	0.34	0.204
Fig.4 (g)	41,800	0.124	9.30	11.78	12.10	11.94	0.27	0.201
Fig.4 (h)	48,900	0.122	9.39	11.93	12.30	12.11	0.27	0.192
	Smith R.W. (1994)							
Fig.5 (a)	4,996	0.146	8.36	10.15	10.27	10.21	0.18	0.20
Fig.5 (b)	12,990	0.130	9.08	11.40	11.54	11.47	0.14	0.167
	Krogstad P.-A. and Antonia R.A. (1998)							
Fig.6	12,570	0.146	8.38	10.18	10.27	10.23	0.45	0.201

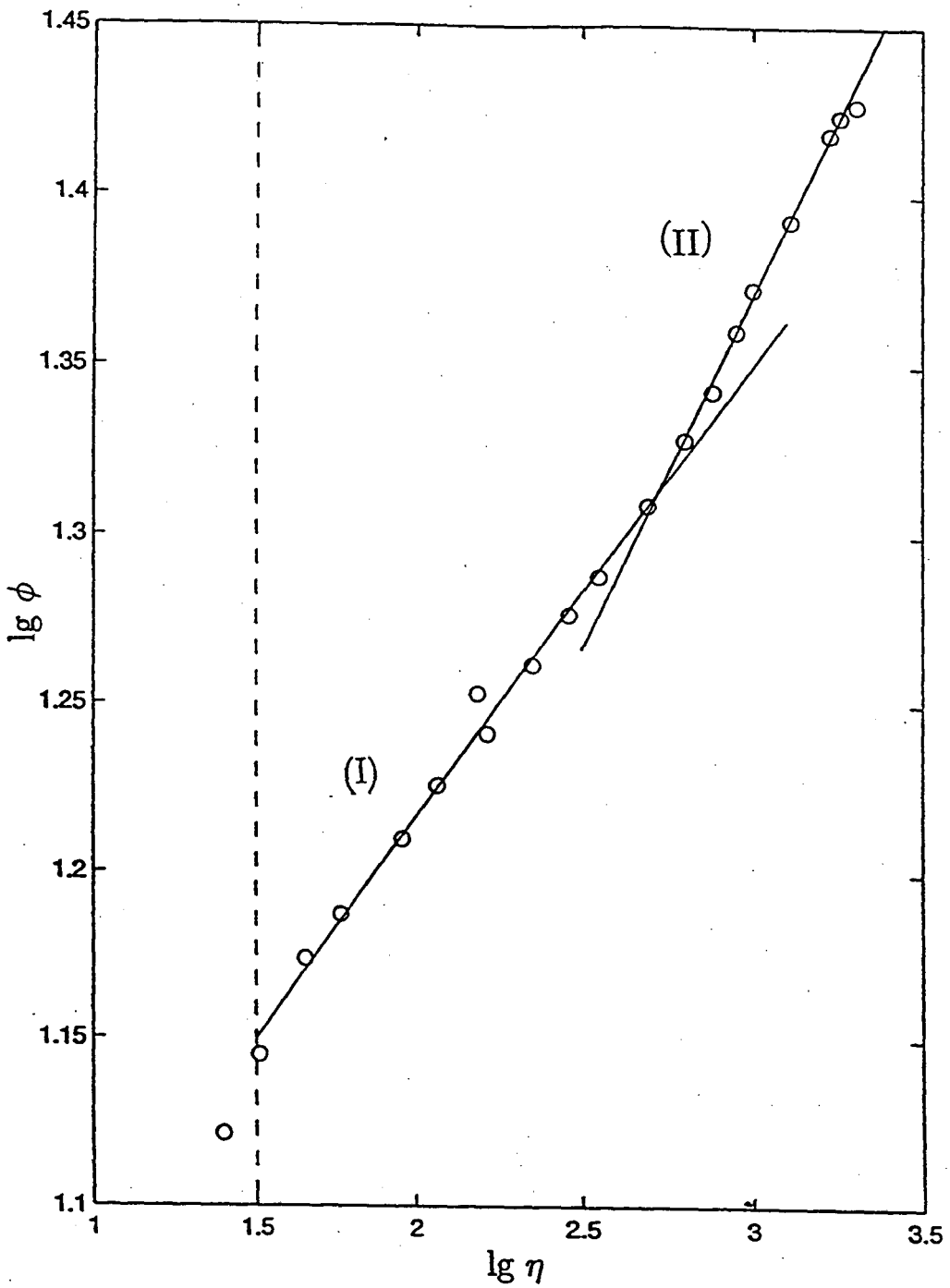

Figure 2. (a) The experiments by Collins, Coles, Hike, (1978) $\mathrm{Re}_\theta = 5,938$. Both self-similar intermediate regions (I) and (II) are clearly seen.

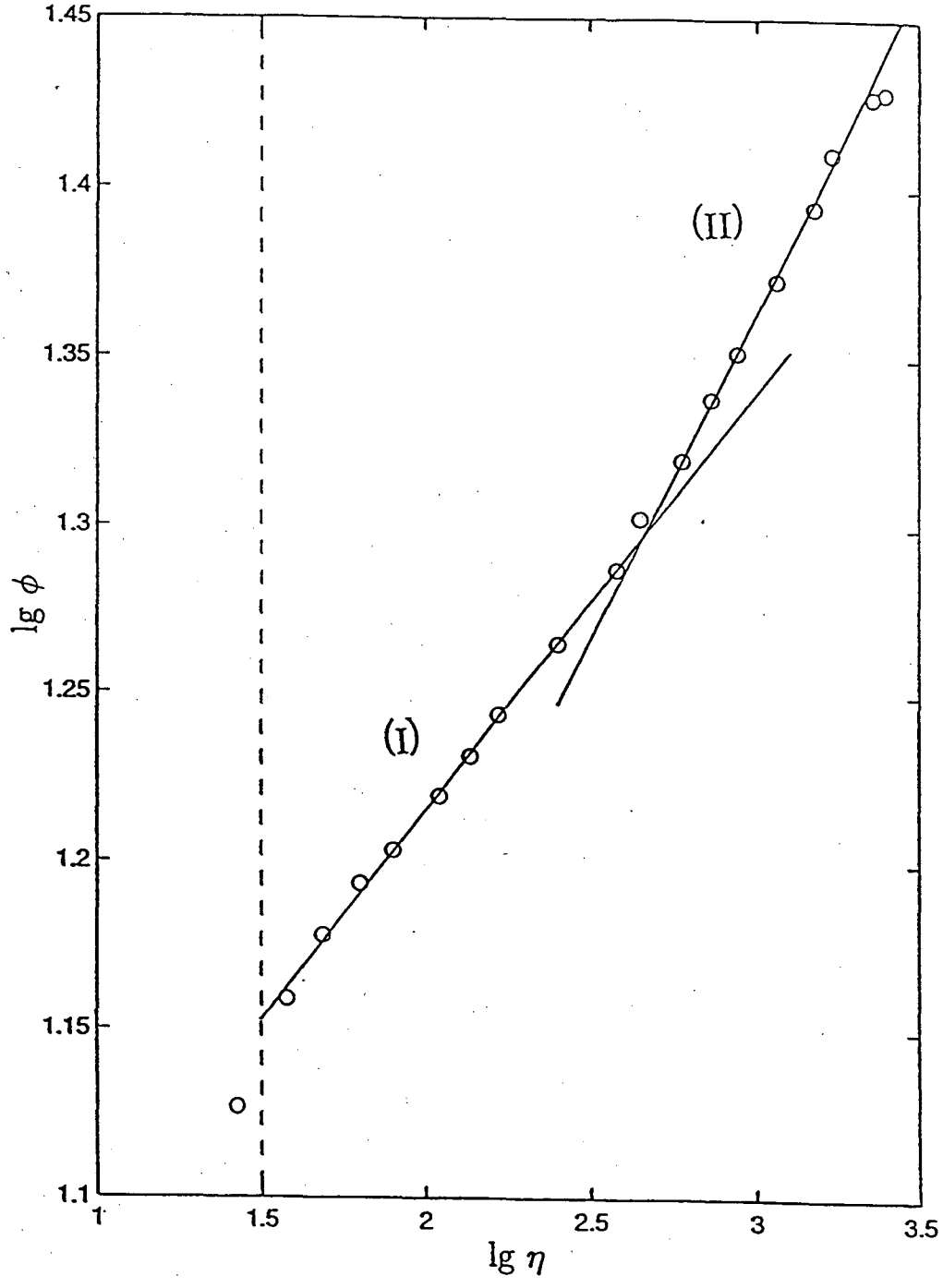

Figure 2. (b) The experiments by Collins, Coles, Hike,(1978) $\mathrm{Re}_\theta = 6,800$. Both self-similar intermediate regions (I) and (II) are clearly seen.

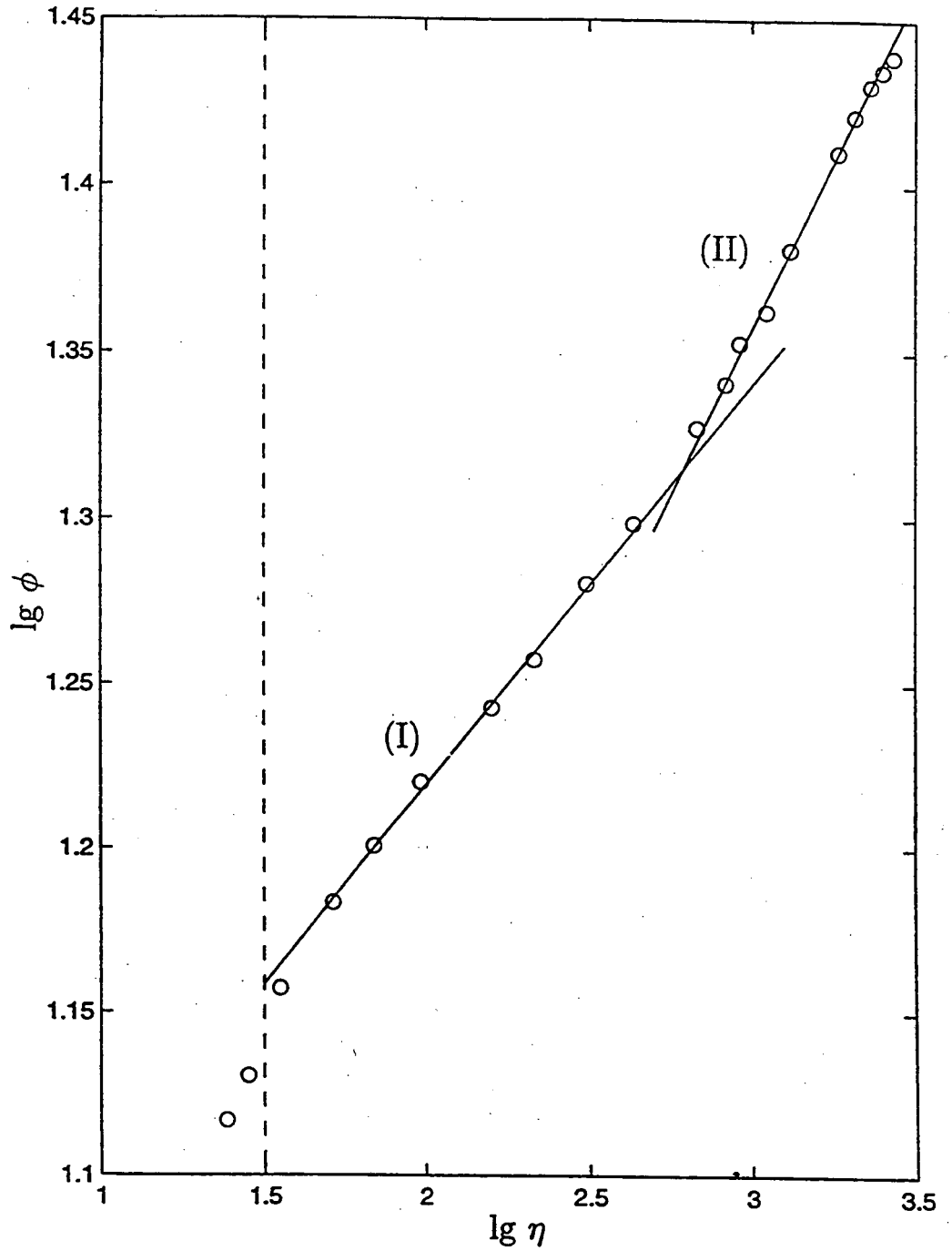

Figure 2. (c) The experiments by Collins, Coles, Hike, (1978). $\mathrm{Re}_\theta = 7,880$. Both self-similar intermediate regions (I) and (II) are clearly seen.

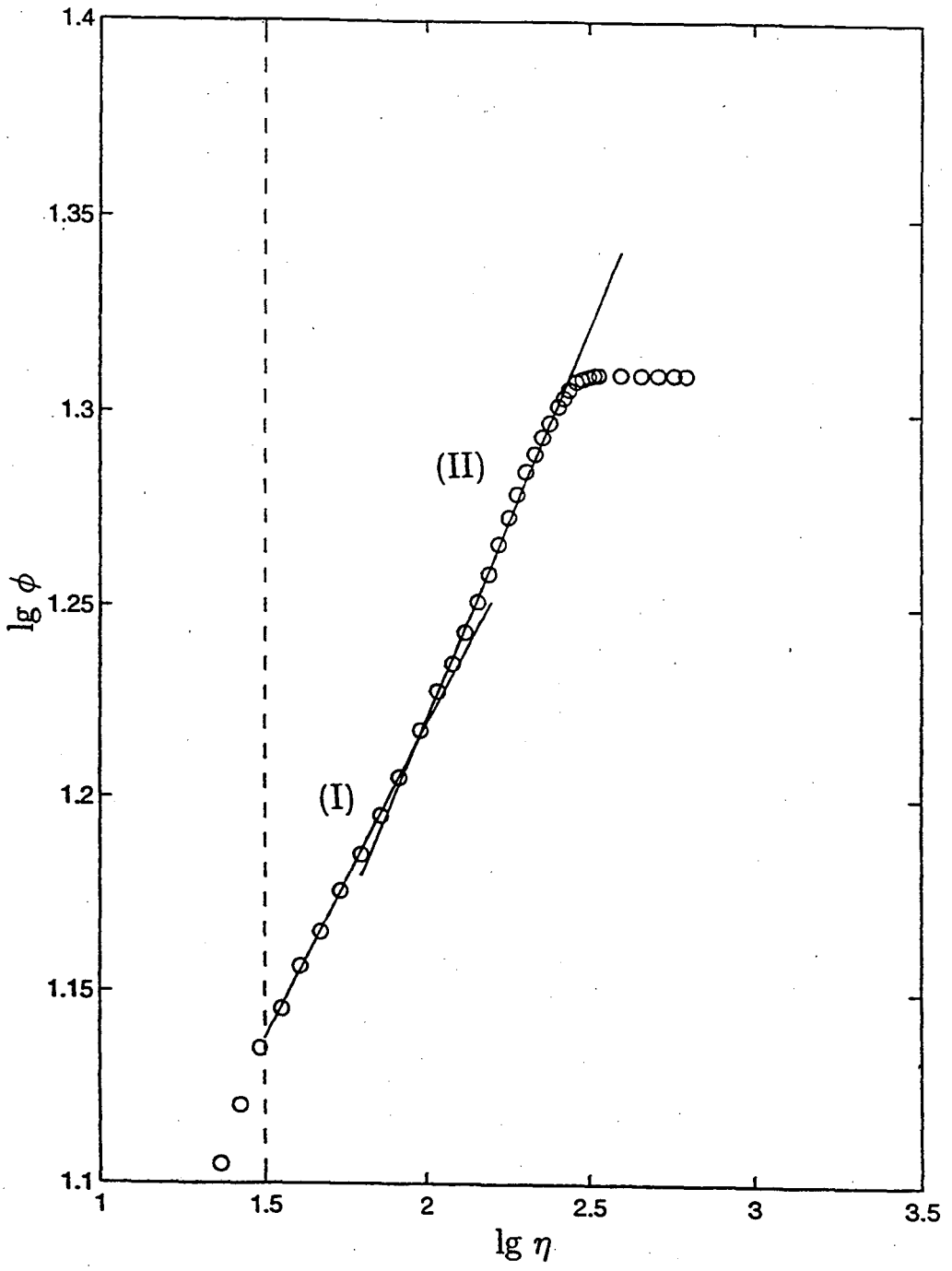

Figure 3. (a) The experiments by Erm and Joubert, (1991). $Re_\theta = 697$. Both self-similar intermediate regions (I) and (II) are clearly seen.

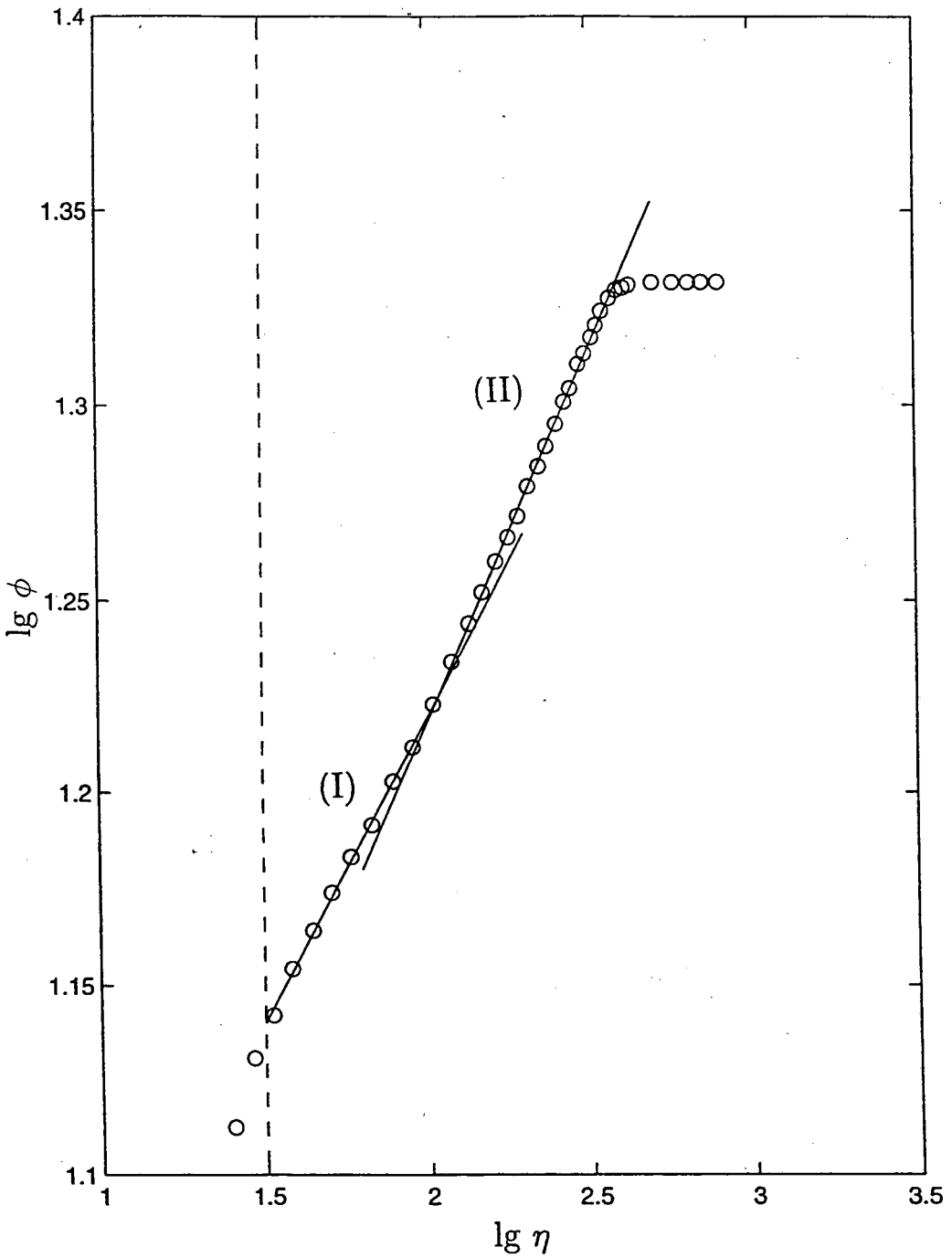

Figure 3. (b) The experiments by Erm and Joubert, (1991). $Re_\theta = 1,003$. Both self-similar intermediate regions (I) and (II) are clearly seen.

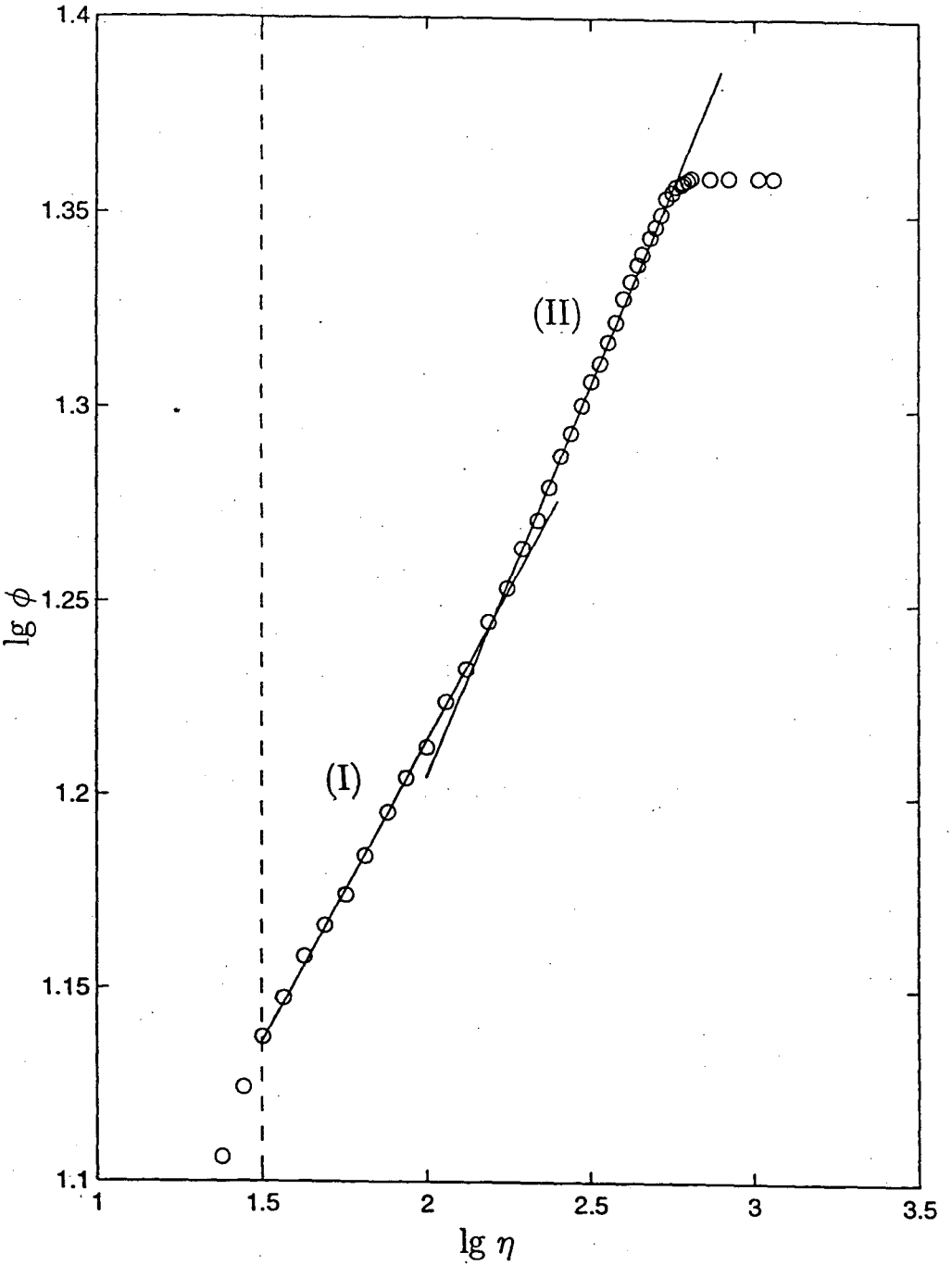

Figure 3. (c) The experiments by Erm and Joubert, (1991). $Re_\theta = 1,568$. Both self-similar intermediate regions (I) and (II) are clearly seen.

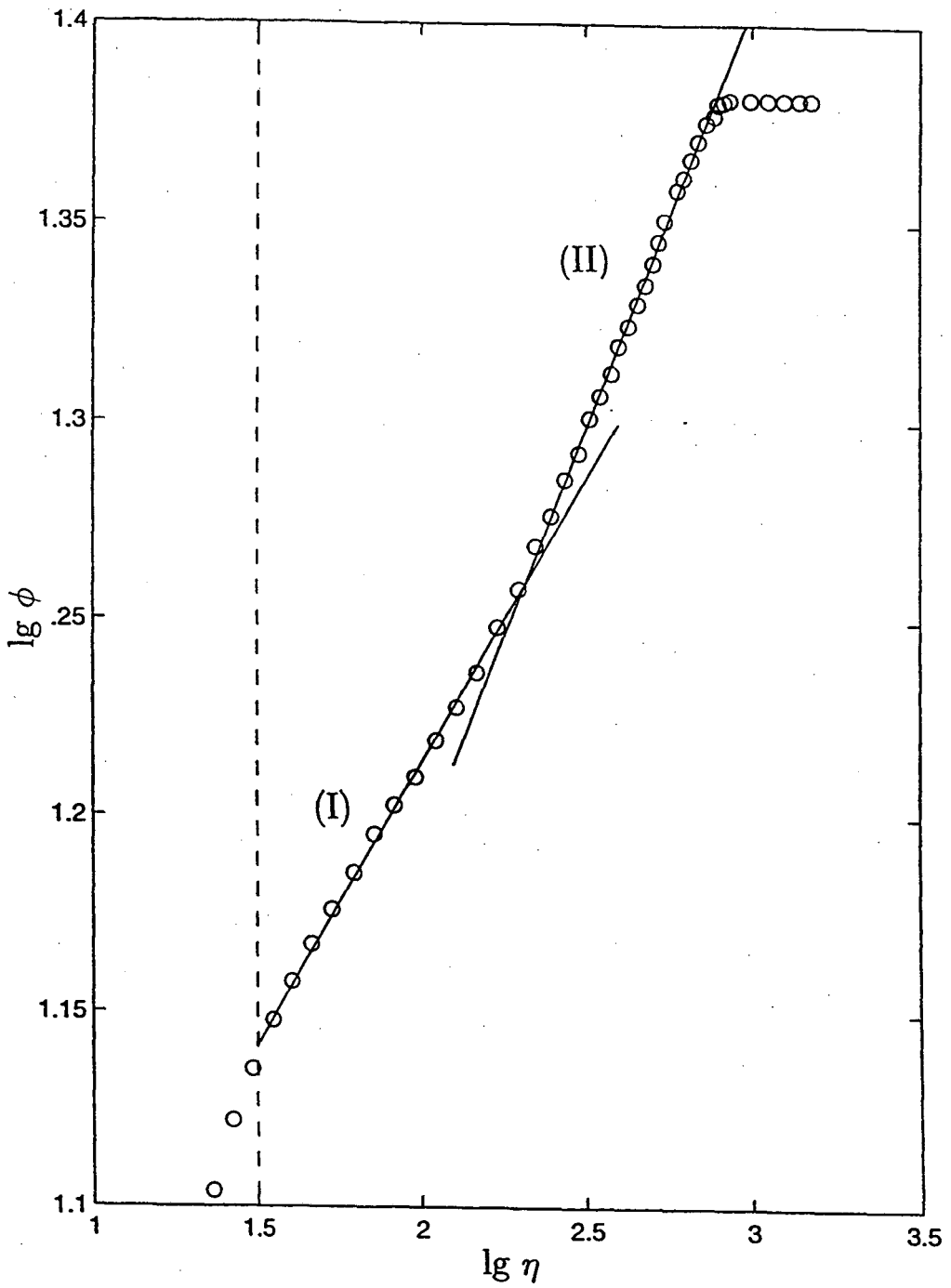

Figure 3. (d) The experiments by Erm and Joubert, (1991). $Re_\theta = 2,226$. Both self-similar intermediate regions (I) and (II) are clearly seen.

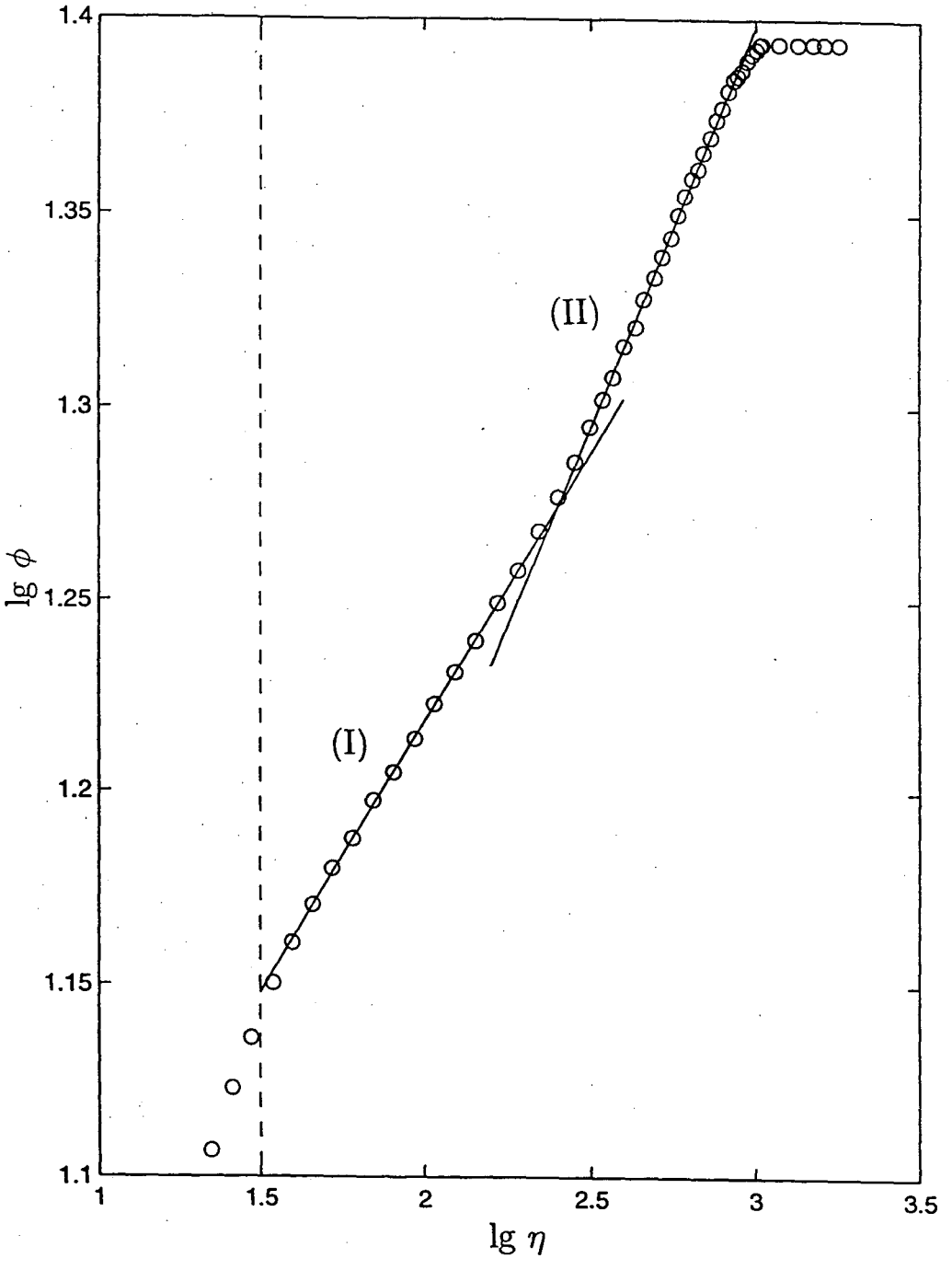

Figure 3. (e) The experiments by Erm and Joubert, (1991). $\mathrm{Re}_\theta = 2,788$. Both self-similar intermediate regions (I) and (II) are clearly seen.

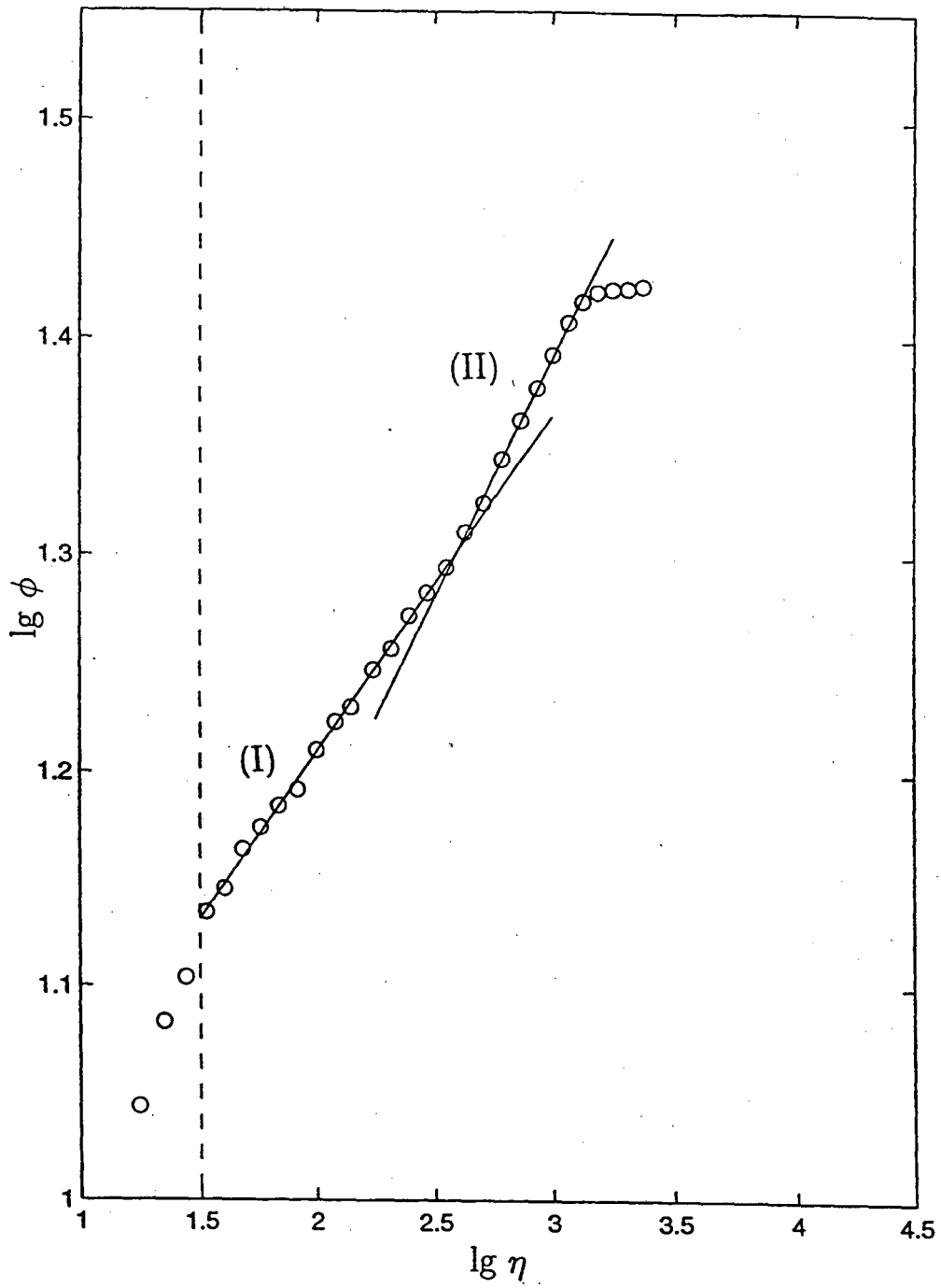

Figure 4. (a) The experiments by Naguib, (1992). $\mathrm{Re}_\theta = 4,550$. Both self-similar intermediate regions (I) and (II) are clearly seen.

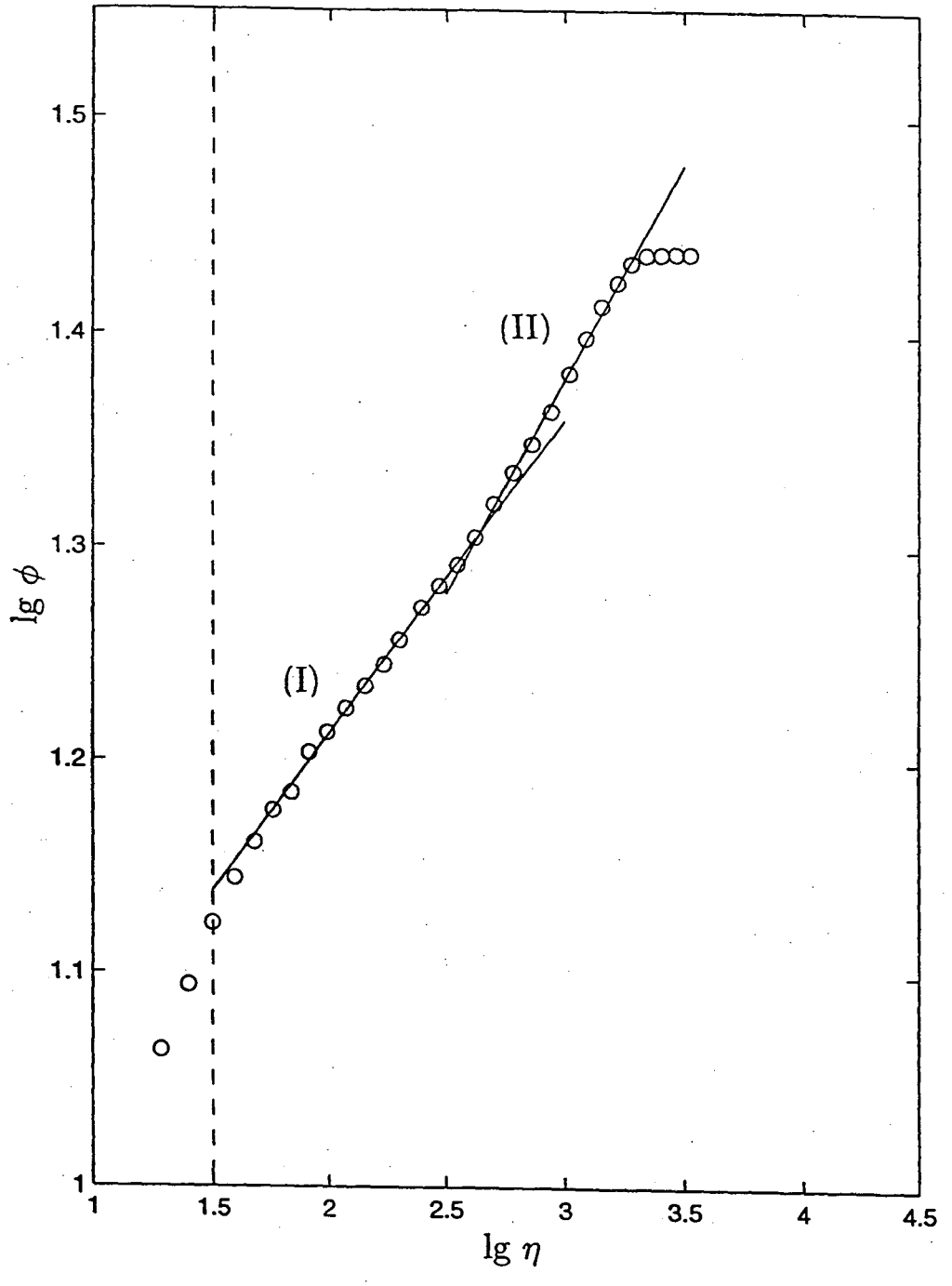

Figure 4. (b) The experiments by Naguib, (1992). $Re_\theta = 6,240$. Both self-similar intermediate regions (I) and (II) are clearly seen.

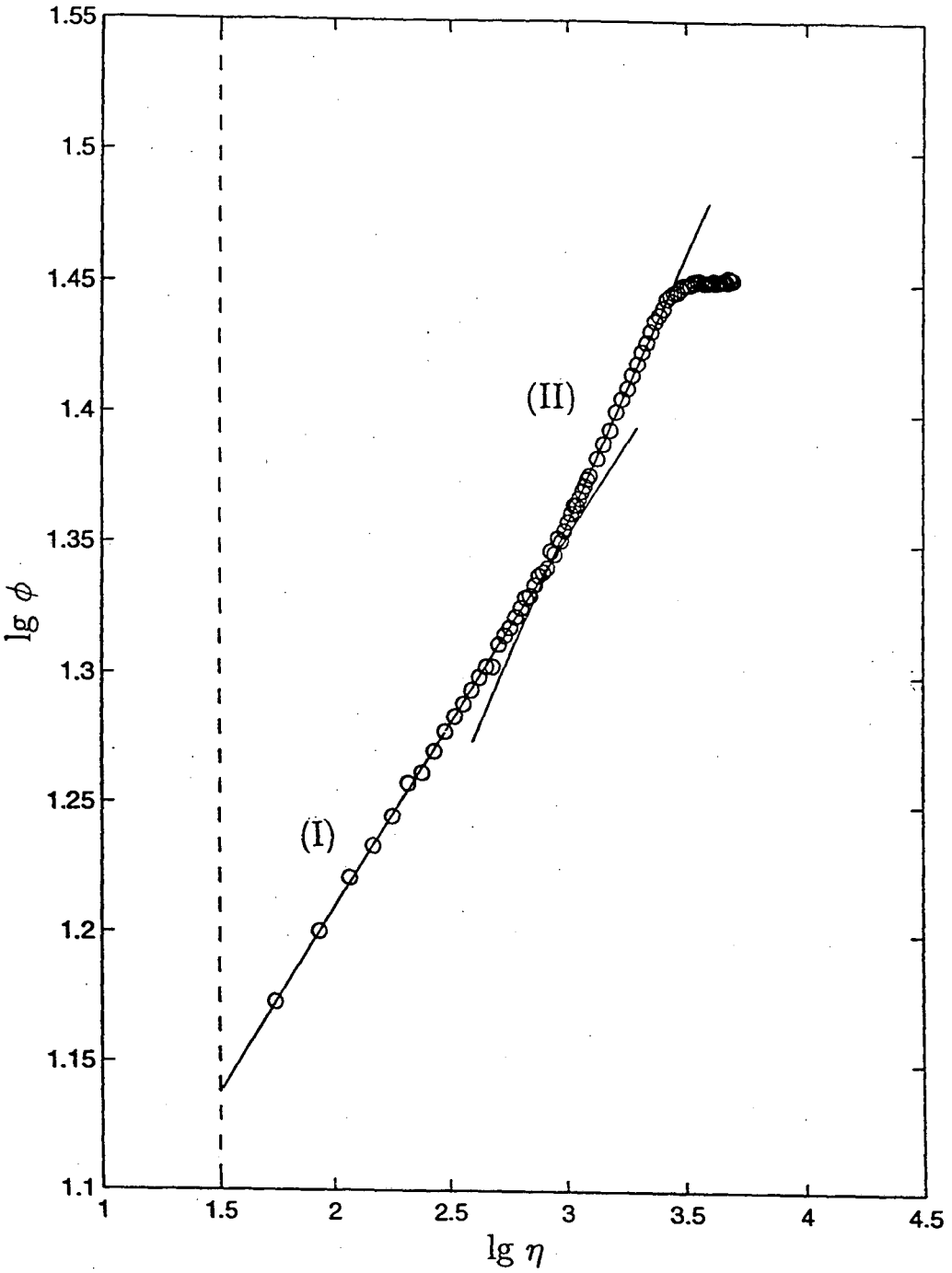

Figure 4. (c) The experiments by Hites and Nagib, (1995). $\mathrm{Re}_\theta = 9,590$. Both self-similar intermediate regions (I) and (II) are clearly seen.

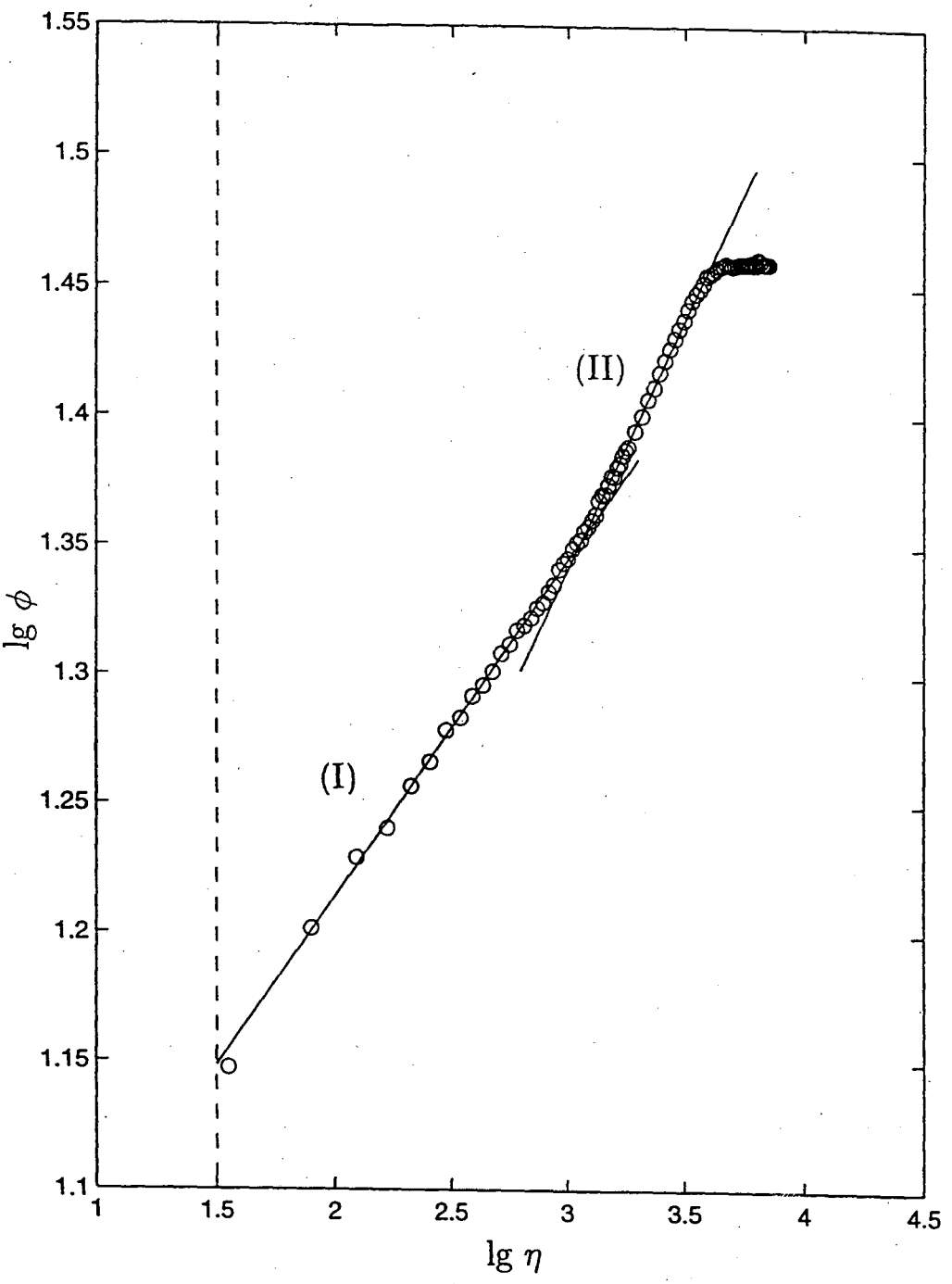

Figure 4. (d) The experiments by Nagib and Hites, (1995). $\mathrm{Re}_\theta = 13,800$. Both self-similar intermediate regions (I) and (II) are clearly seen.

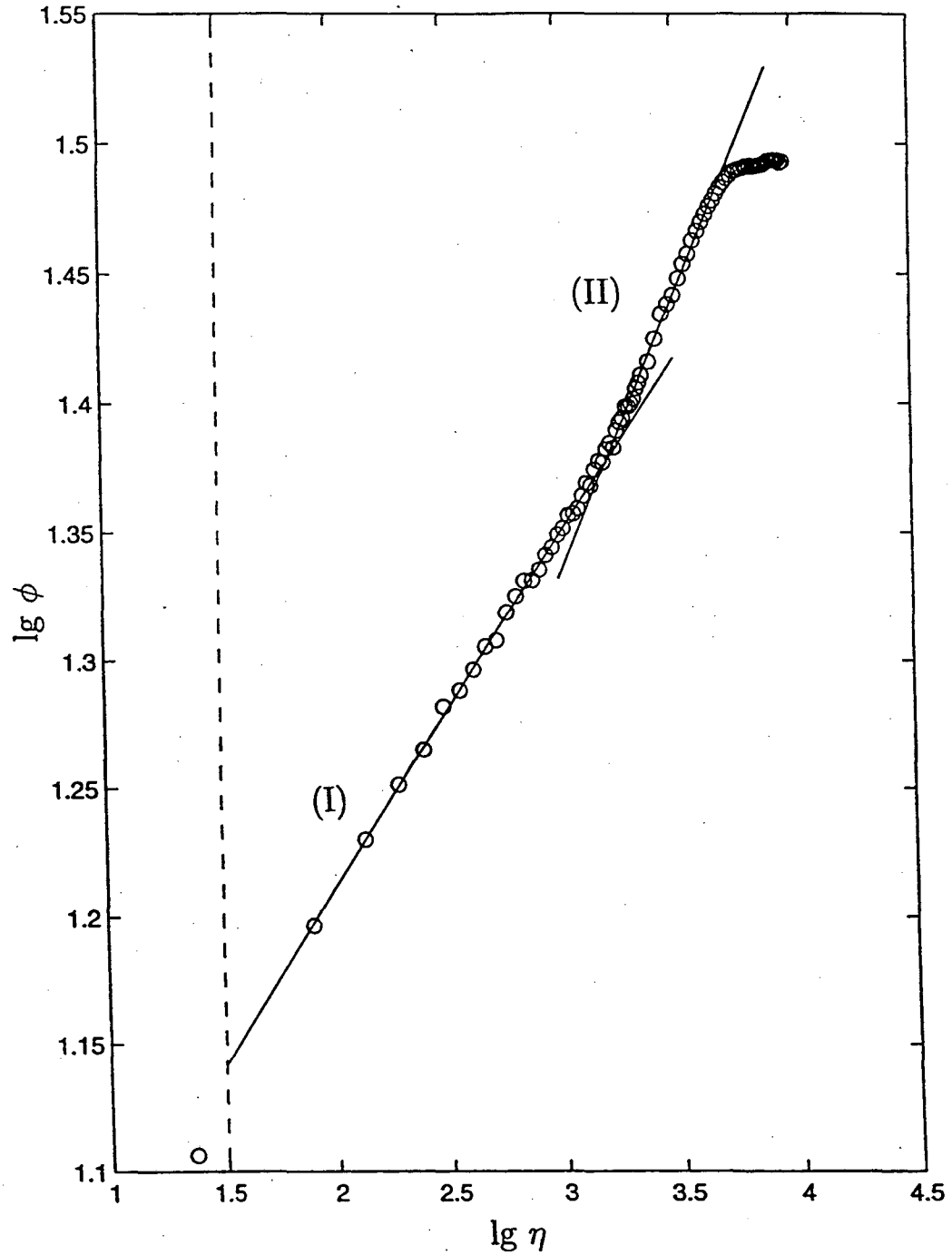

Figure 4. (e) The experiments by Hites and Nagib, (1995). $Re_\theta = 21,300$. Both self-similar intermediate regions (I) and (II) are clearly seen.

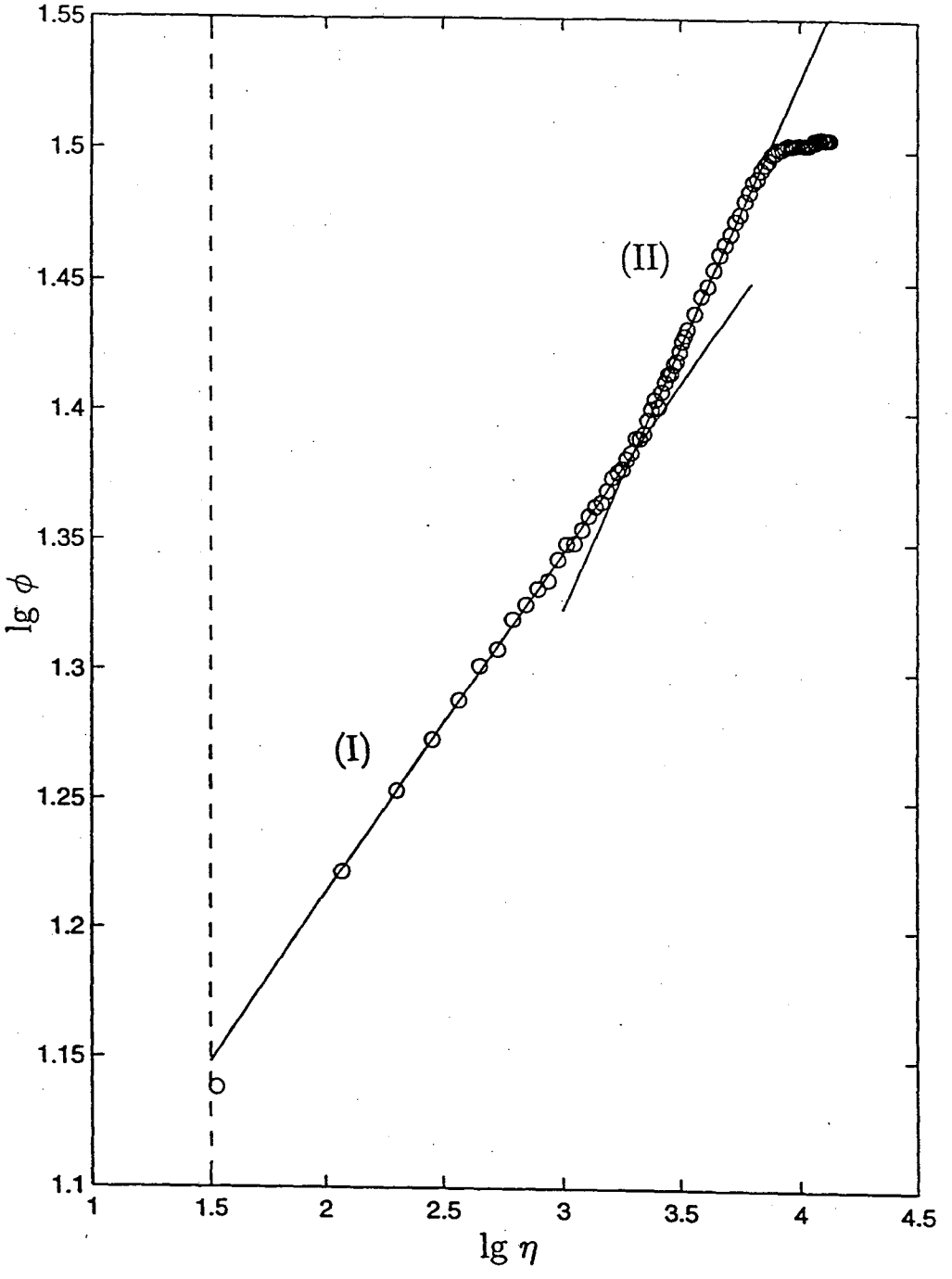

Figure 4. (f) The experiments by Hites and Nagib, (1995). $\mathrm{Re}_\theta = 29,900$. Both self-similar intermediate regions (I) and (II) are clearly seen.

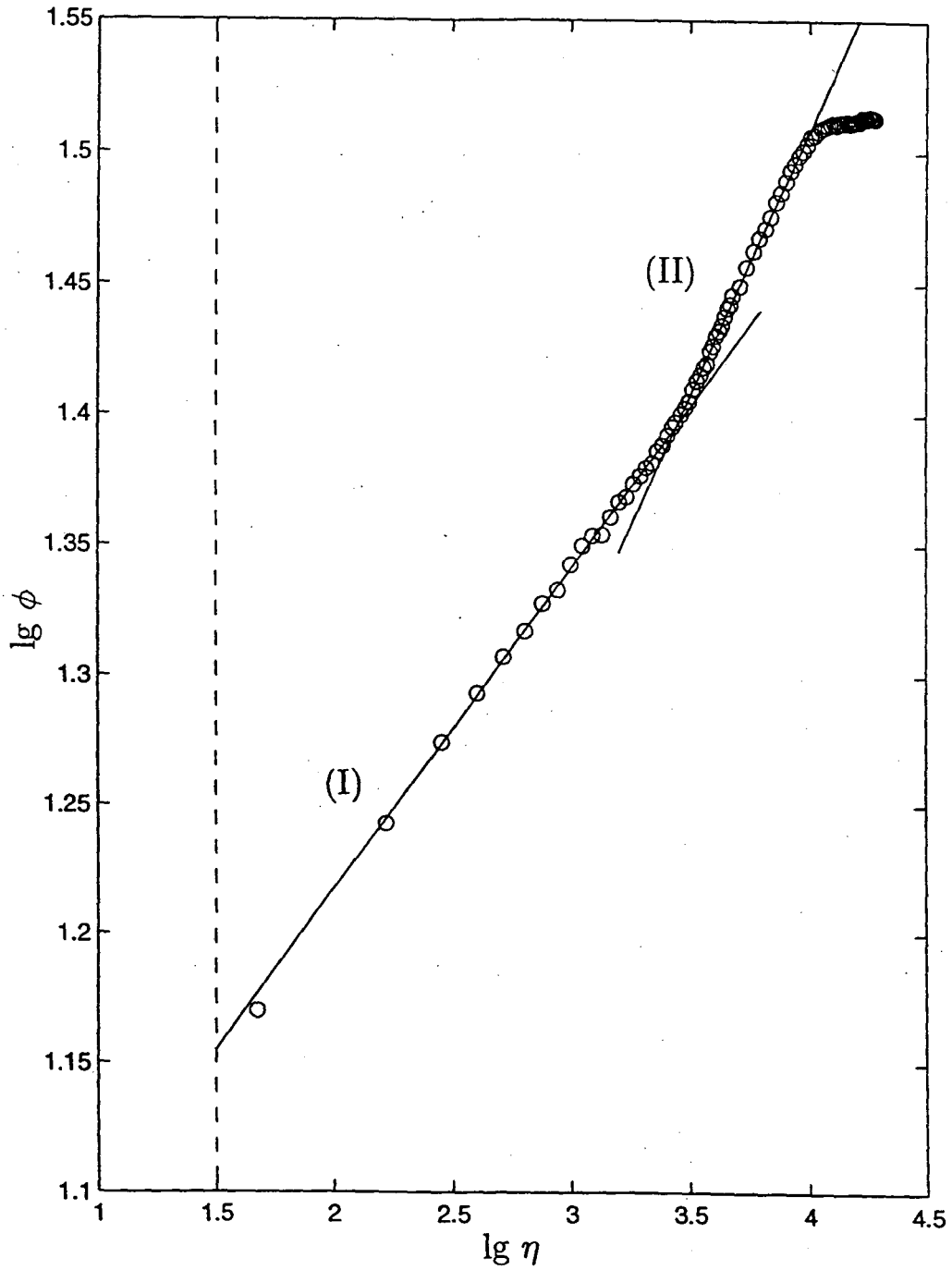

Figure 4. (g) The experiments by Nagib and Hites, (1995). $\mathrm{Re}_\theta = 41,800$. Both self-similar intermediate regions (I) and (II) are clearly seen.

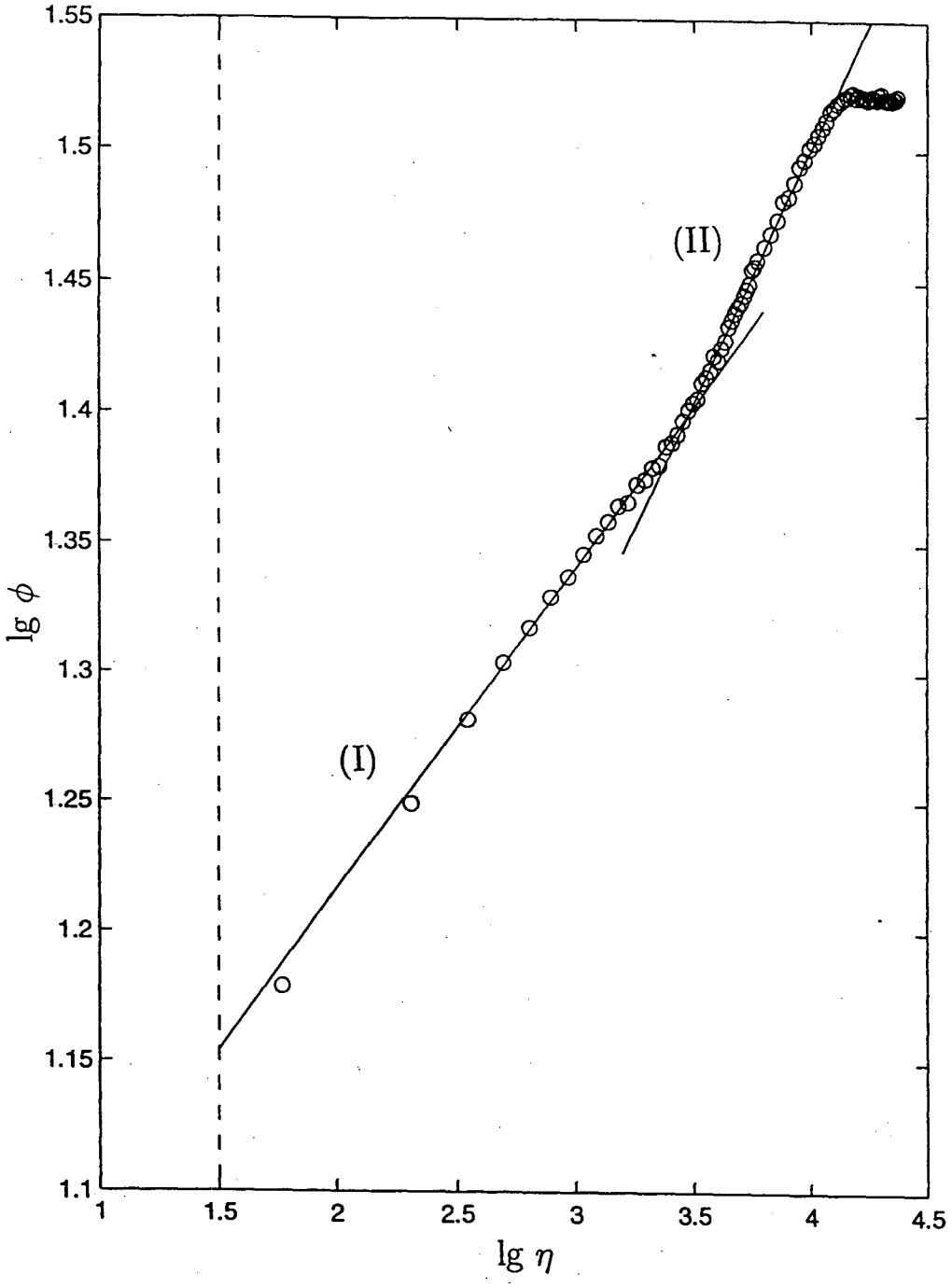

Figure 4. (h) The experiments by Nagib and Hites, (1995). $\mathrm{Re}_\theta = 48,900$. Both self-similar intermediate regions (I) and (II) are clearly seen.

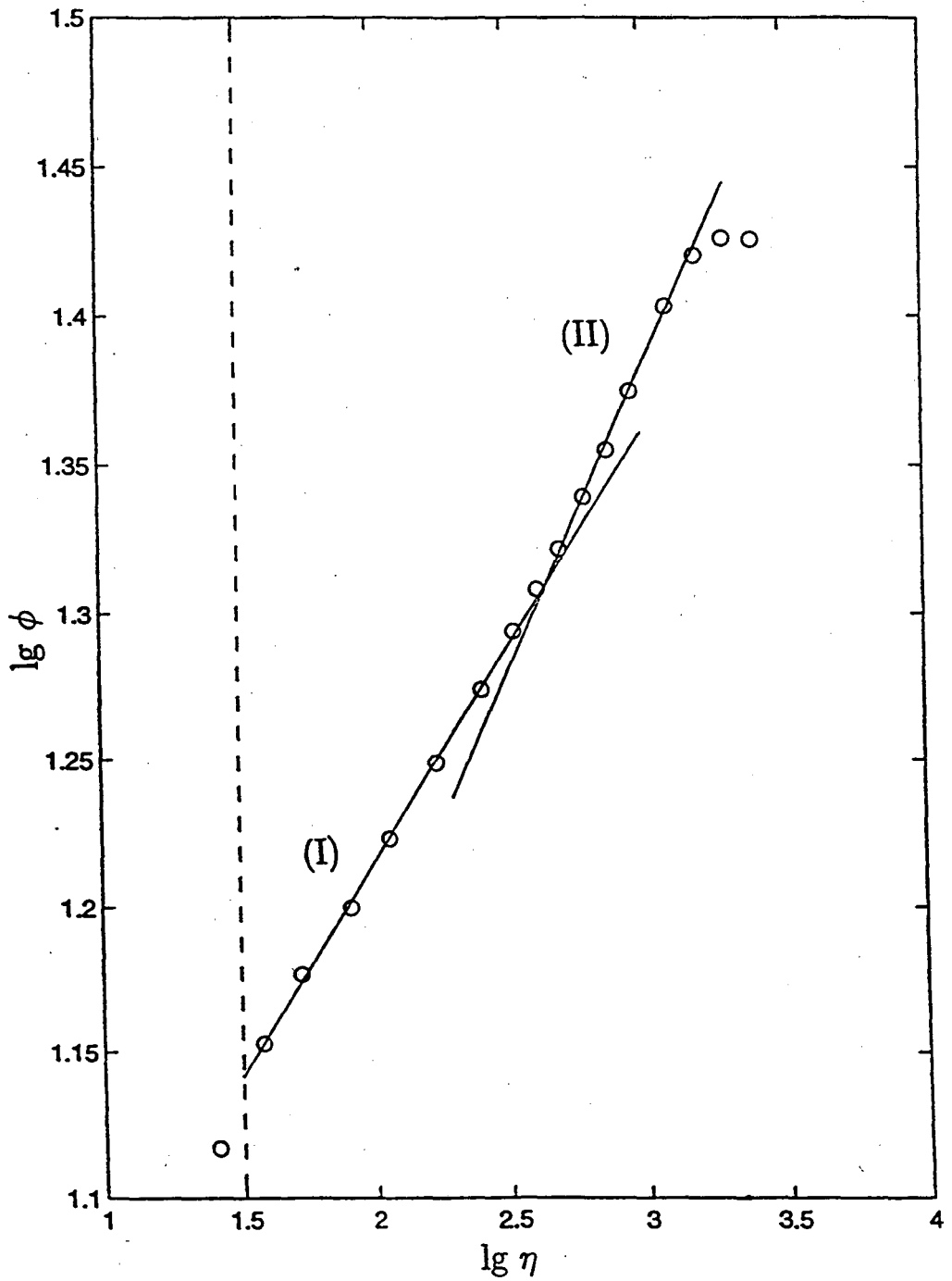

Figure 5. (a) The experiments of Smith, (1994). $\mathrm{Re}_\theta = 4,996$. The first self-similar intermediate region (I) is clearly seen, the second region (II) can be revealed.

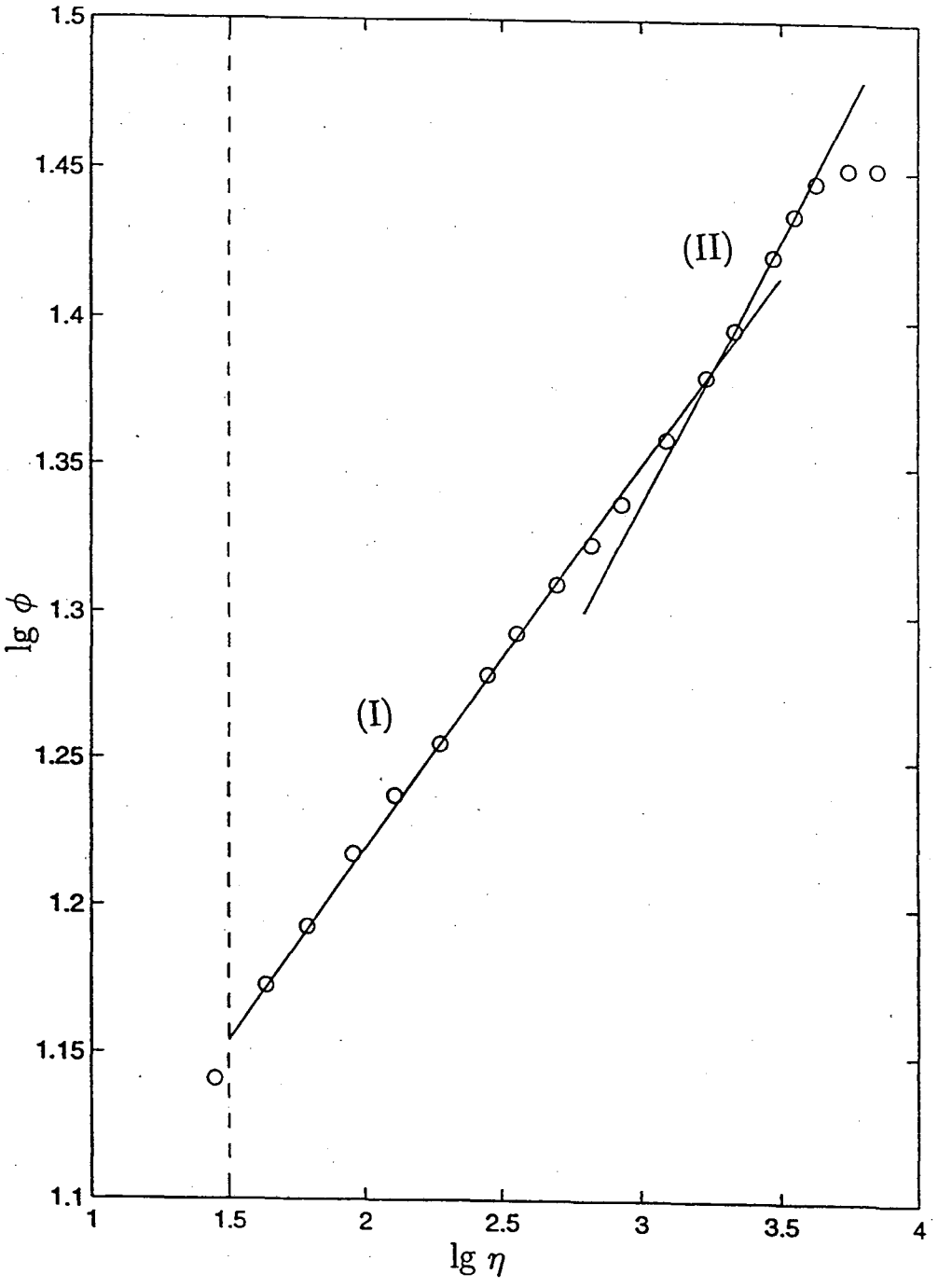

Figure 5. (b) The experiments of Smith, (1994) $\mathrm{Re}_\theta = 12,990$. The first self-similar intermediate region (I) is clearly seen, the second region (II) can be revealed.

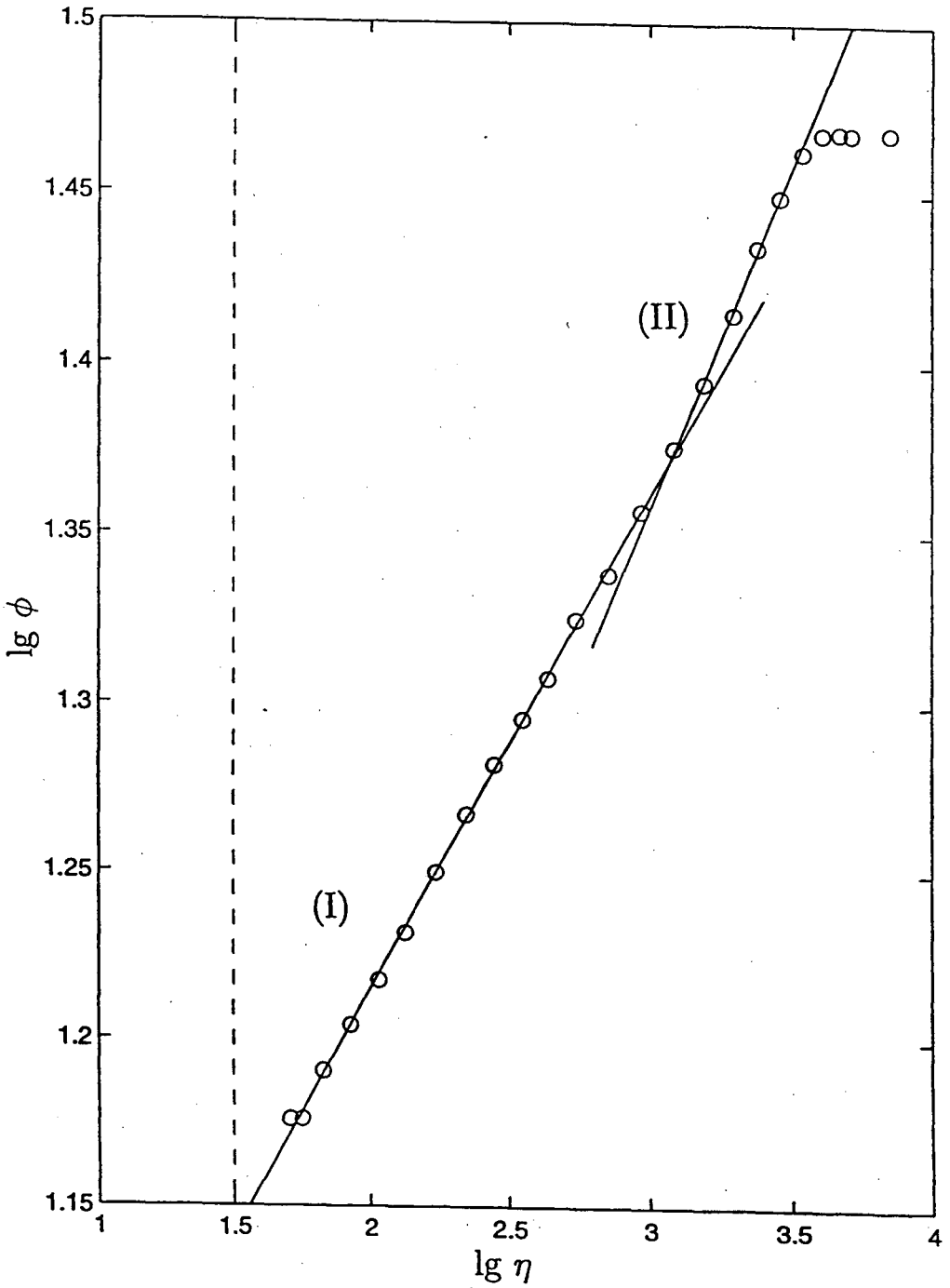

Figure 6. The experiments of Krogstad and Antonia,(1998). $\mathrm{Re}_\theta = 12,570$. Both self-similar intermediate regions (I) and (II) can be clearly seen.

3 Zero-pressure-gradient boundary layer beneath a turbulent free stream: The experiments of Hancock and Bradshaw

The experiments of Hancock and Bradshaw (1989) revealed a new feature important for our analysis. Examination of these experimental data suggested that we separate the other experiments into two groups. In the Hancock and Bradshaw experiments the free stream was turbulized by a grid in all series, except one. Thus, processing the data from these experiments we were able not only to compare the scaling law (5) with experimental data once again but also to investigate the influence of the turbulence of the external flow on the second self-similar intermediate region. The results of the processing are presented in Table 2 and Figures 7 and 8. In both Table 2 and Figures 7 and 8 the intensity of turbulence is shown by the value of u'/U, where u' is the mean square velocity fluctuation in the free stream.

Table 2

Figure	Re_θ	α	A	ln Re_1	ln Re_2	ln Re	u'/U	$\mathrm{Re}_\theta/\mathrm{Re}$	β
				Hancock, P.E. and Bradshaw, P. (1989)					
Fig.8a	4,680	0.140	8.66	10.67	10.71	10.69	0.0003	0.11	0.20
Fig.8b	2,980	0.138	8.77	10.86	10.91	10.88	0.024	0.06	0.18
Fig.8c	5,760	0.137	8.80	10.91	10.95	10.93	0.026	0.10	–
Fig.8d	4,320	0.150	8.22	9.91	10.00	9.95	0.041	0.21	–
Fig.8e	3,710	0.122	9.49	12.11	12.30	12.20	0.040	0.02	–
Fig.8f	3,100	0.128	9.13	11.48	11.70	11.59	0.058	0.03	–
Fig.8g	3,860	0.129	9.07	11.38	11.63	11.50	0.058	0.04	

First of all, our processing showed that the first self-similar intermediate layer is clearly seen in all these experiments, both in the absence of the external turbulence, and in its presence. The values of ln Re_1 and ln Re_2 are close. This means that the basic scaling law (5) is valid in the intermediate region adjacent to the viscous sublayer. At the same time, the second self-similar region is clearly observed and well-defined only when the external turbulence is weak (Figure 8a and to a lesser extent, Figure 8b) so that the external turbulence leads to a drastic reduction of the power β, and even to the deterioration of the second self-similar intermediate region so that β becomes indeterminate. We illustrate the influence of the free stream turbulence additionally by Figure 7(b).

The experiments of Hancock and Bradshaw are instructive because they suggest at least one possible reason for the destruction of the intermediate self-similar region adjacent to the external flow that is observed in the experiments of the next group.

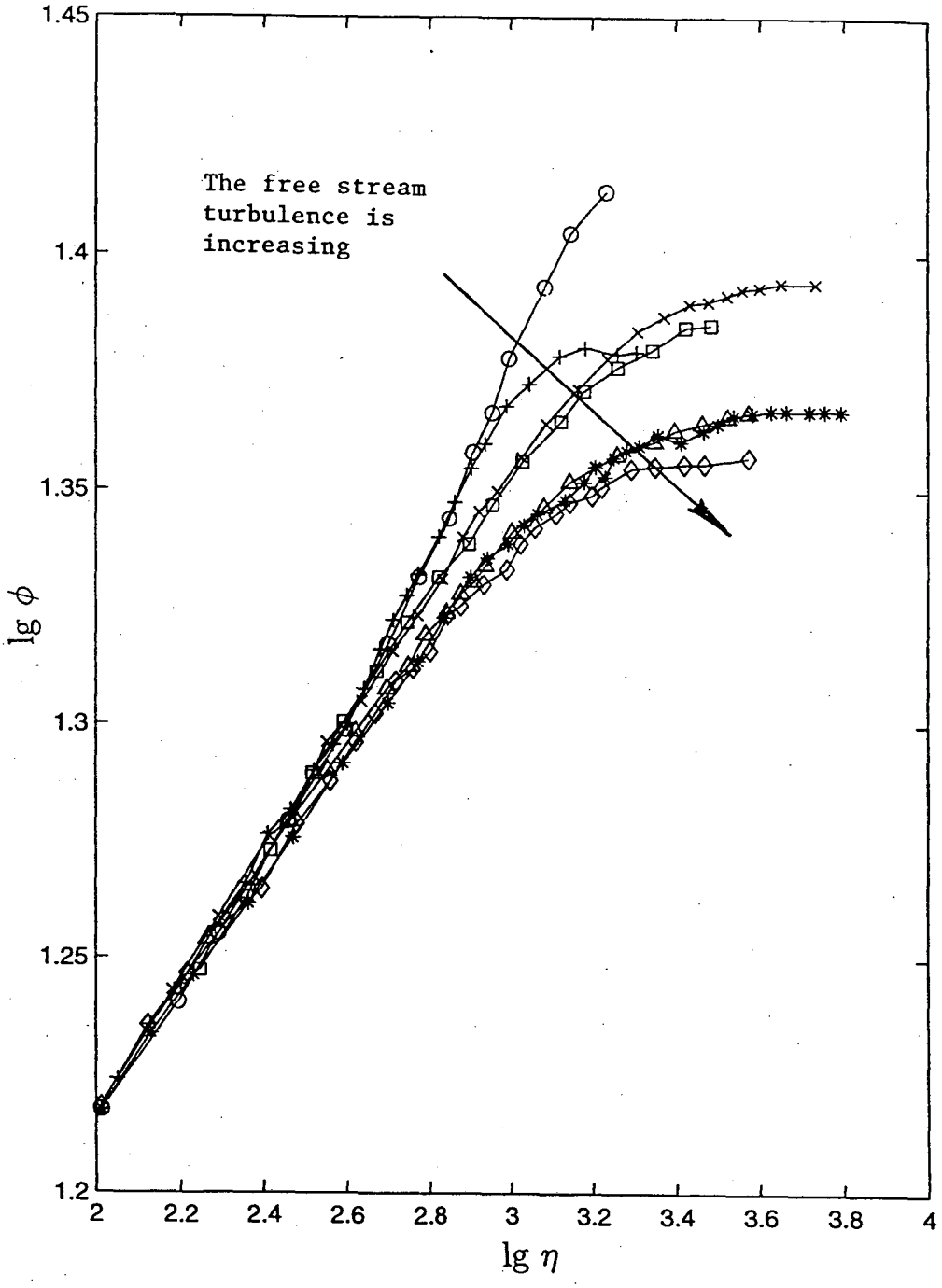

Figure 7. (a) The experiments by Hancock and Bradshaw, (1989) – a general view. $\circ$, see Figure 8(a); $+$, see Figure 8(b); $\times$, see Figure 8(c); $\square$, see Figure 8(d); Δ, see Figure 8(e); $\diamond$, see Figure 8(f); $*$, see Figure 8(g).

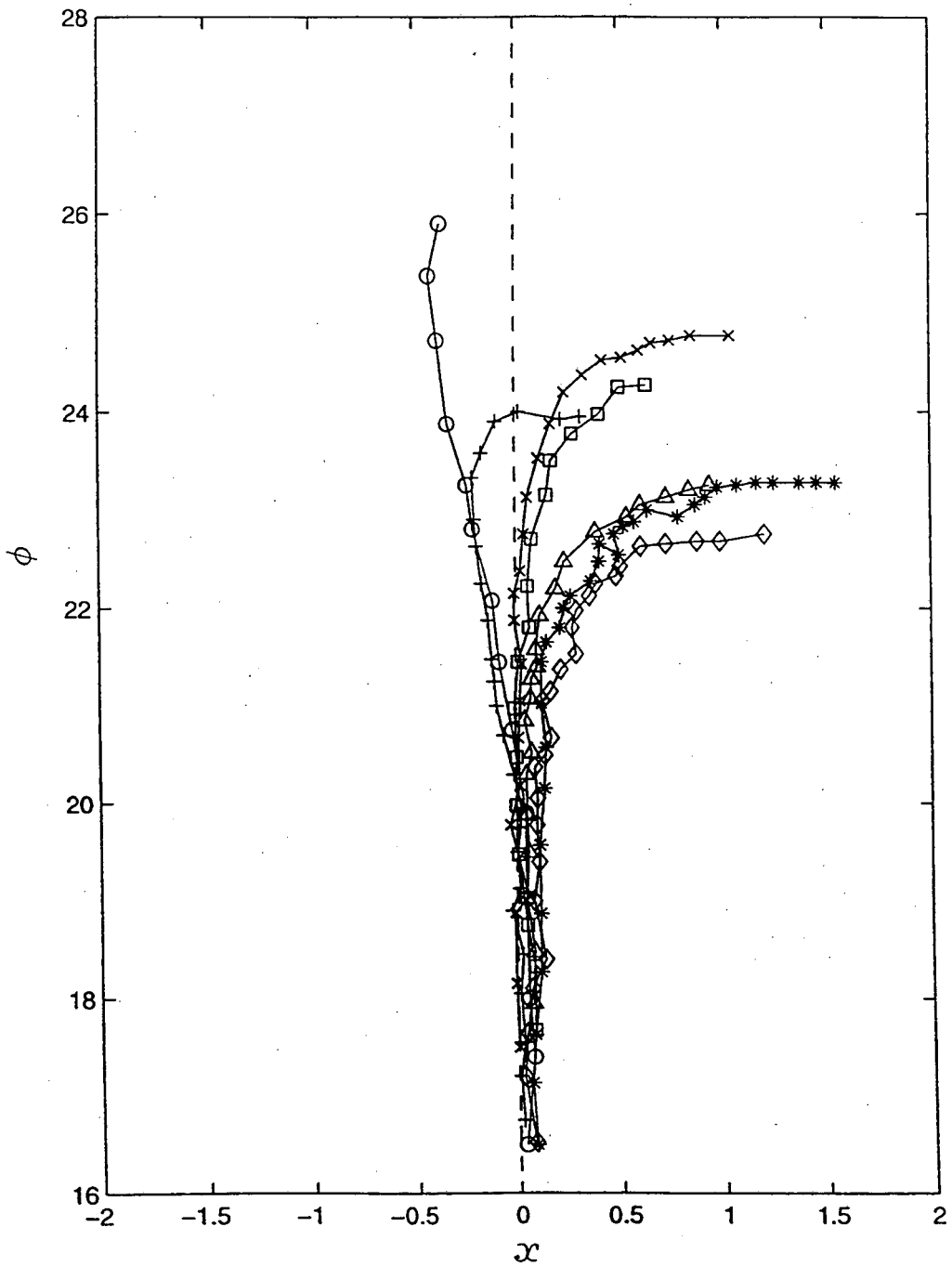

Figure 7. (b) The same data as in Figure 7(a) with the coordinates $\left(x = \ln \eta - \frac{2}{3} \ln \mathrm{Re} \left(\ln \frac{\phi}{\frac{5}{2} + \ln \mathrm{Re}/\sqrt{3}}\right), \phi\right)$. The deviations from the axis $x = 0$ reflect the influence of the turbulence of the free stream.

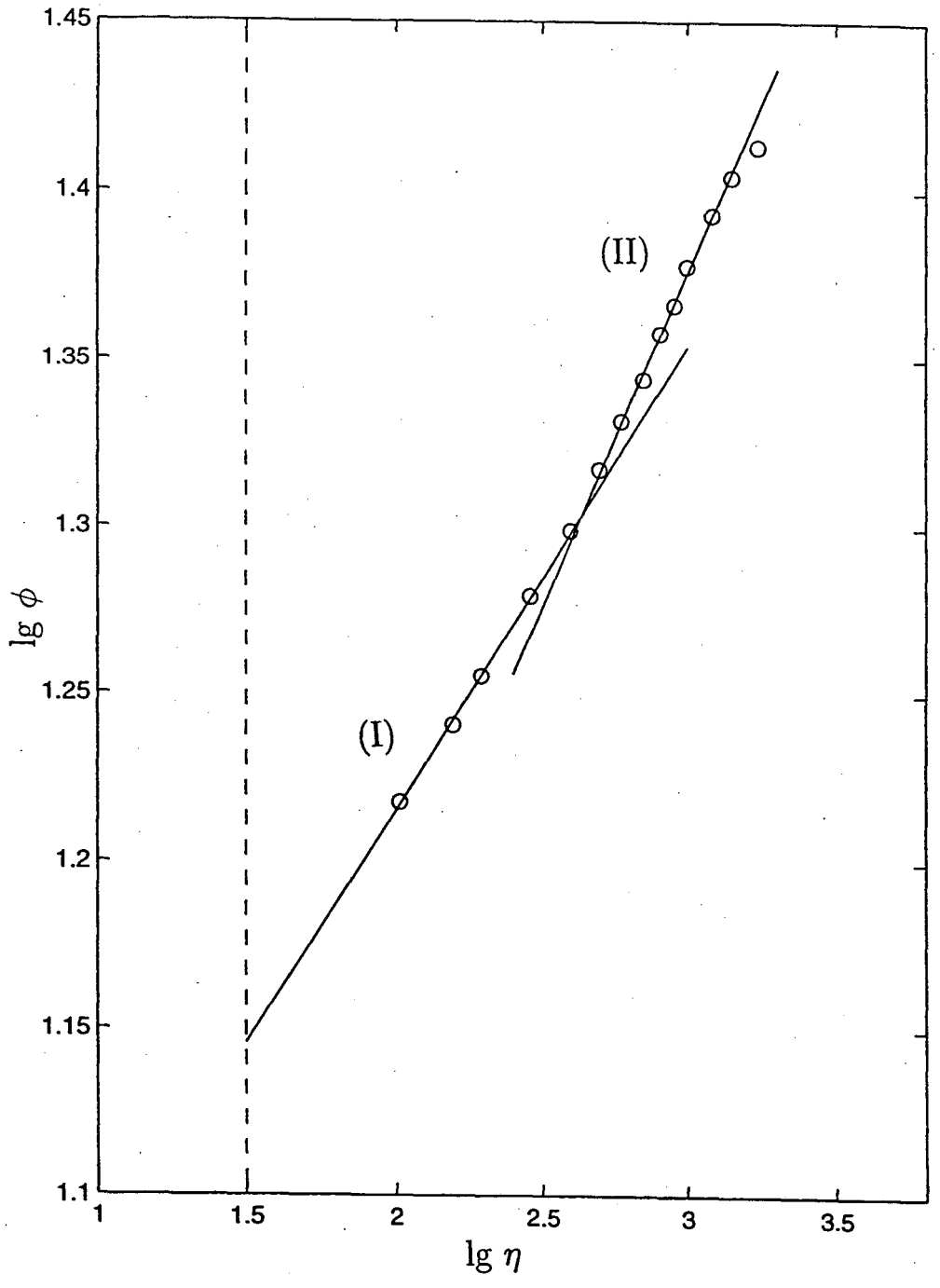

Figure 8. (a) The experiments by Hancock and Bradshaw, (1989). $\mathrm{Re}_\theta = 4,680$, $u'/U = 0.0003$. Both self-similar intermediate regions are clearly seen.

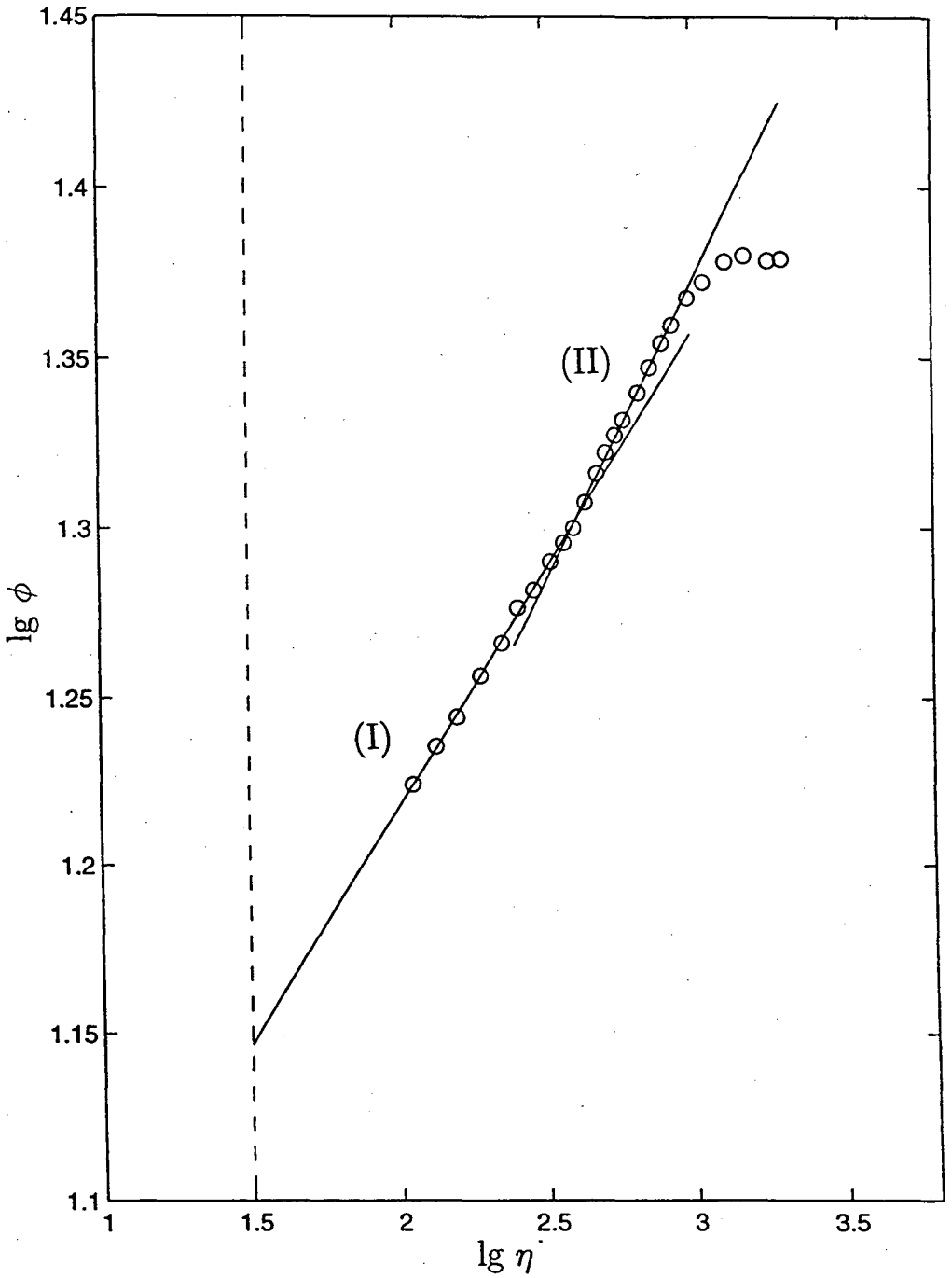

Figure 8. (b) The experiments by Hancock and Bradshaw, (1989). $\mathrm{Re}_\theta = 2,980$, $u'/U = 0.024$. Both self-similar intermediate structures (I) and (II) are clearly seen.

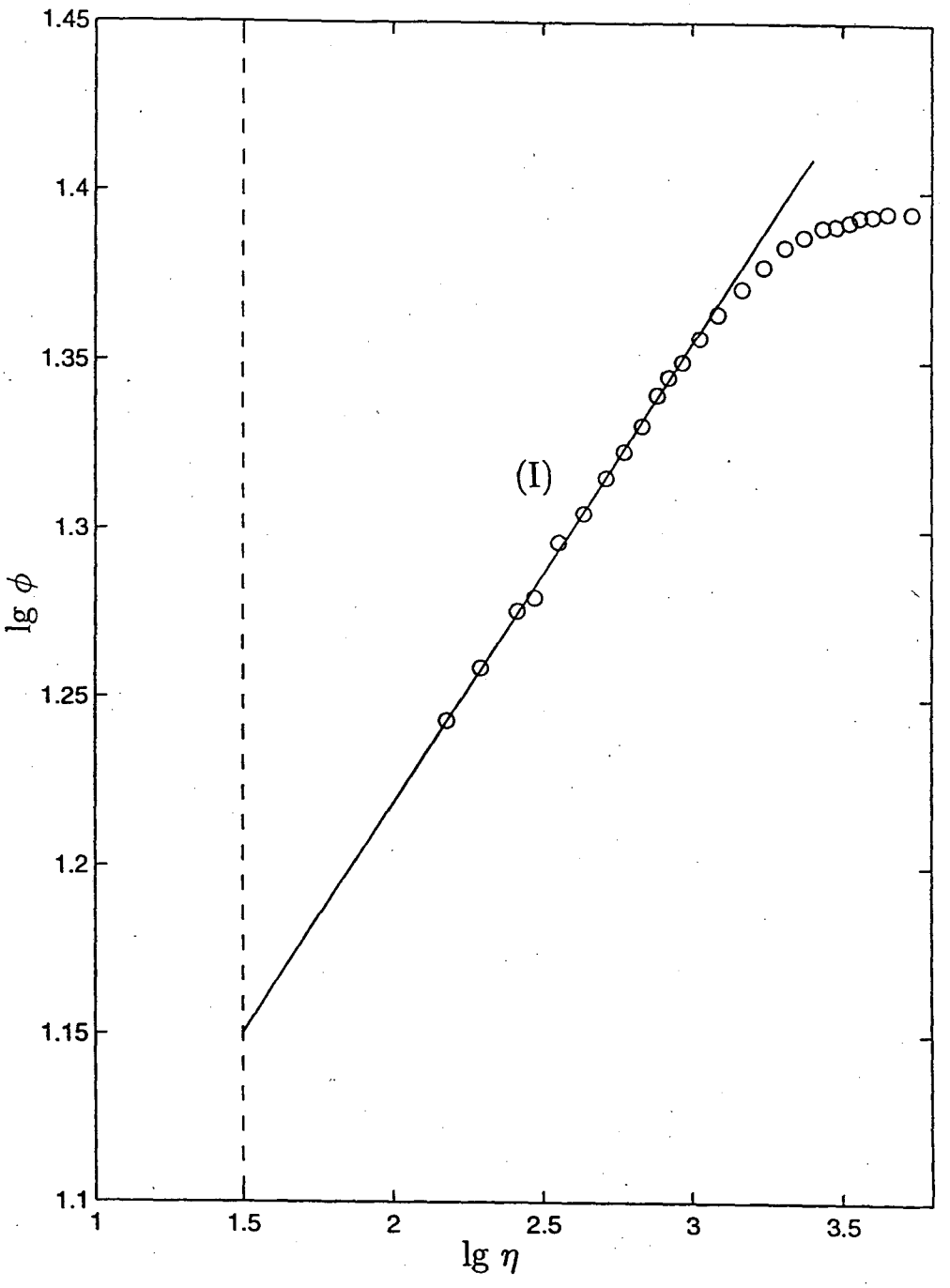

Figure 8. (c) The experiments by Hancock and Bradshaw, (1989). $\mathrm{Re}_\theta = 5,760$, $u'/U = 0.026$. The first self-similar intermediate region (I) is clearly seen, the second is not revealed.

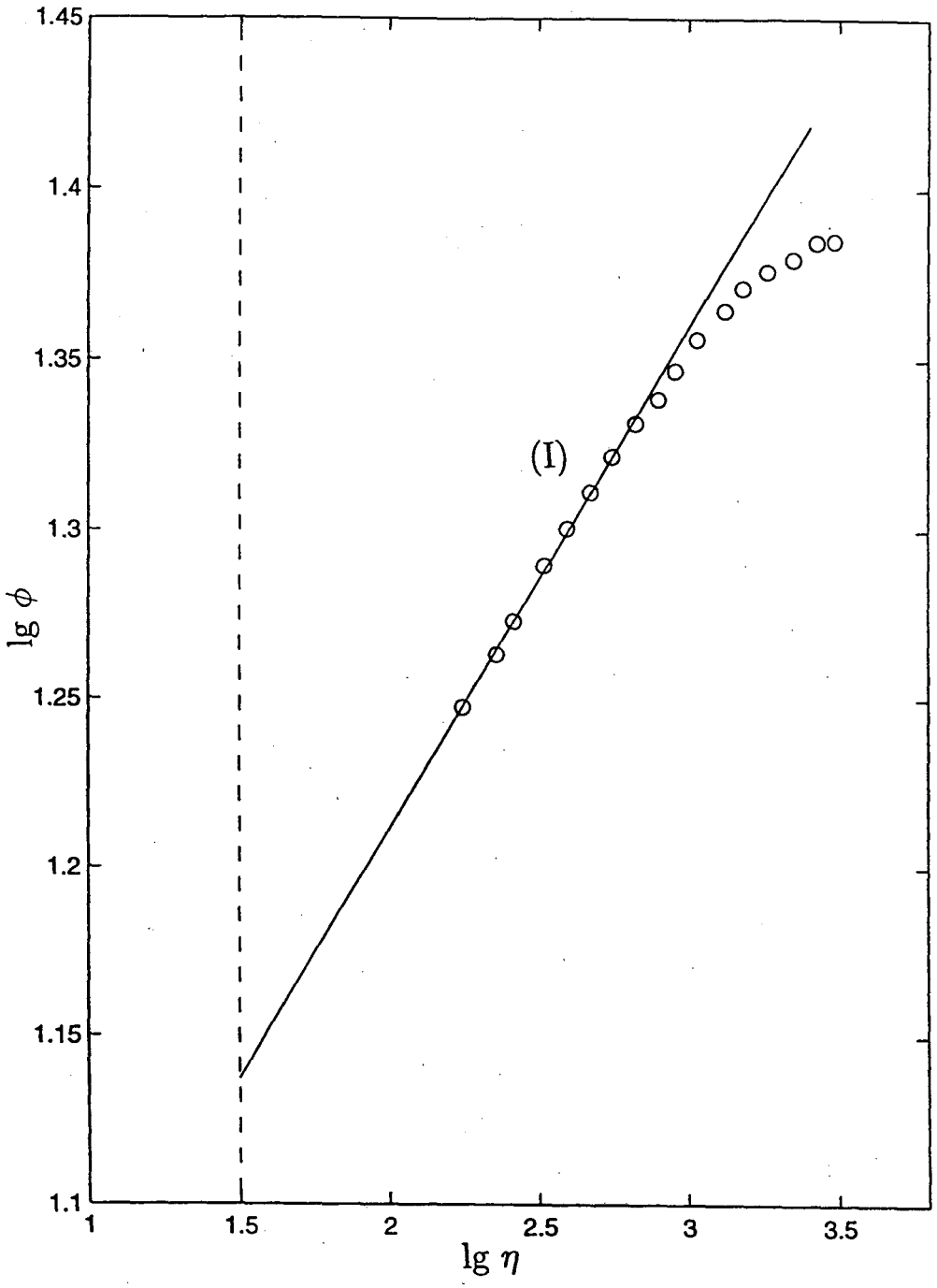

Figure 8. (d) The experiments by Hancock and Bradshaw, (1989). $\mathrm{Re}_\theta = 4,320$, $u'/U = 0.041$. The first self-similar intermediate region (I) is clearly seen, the second is not revealed.

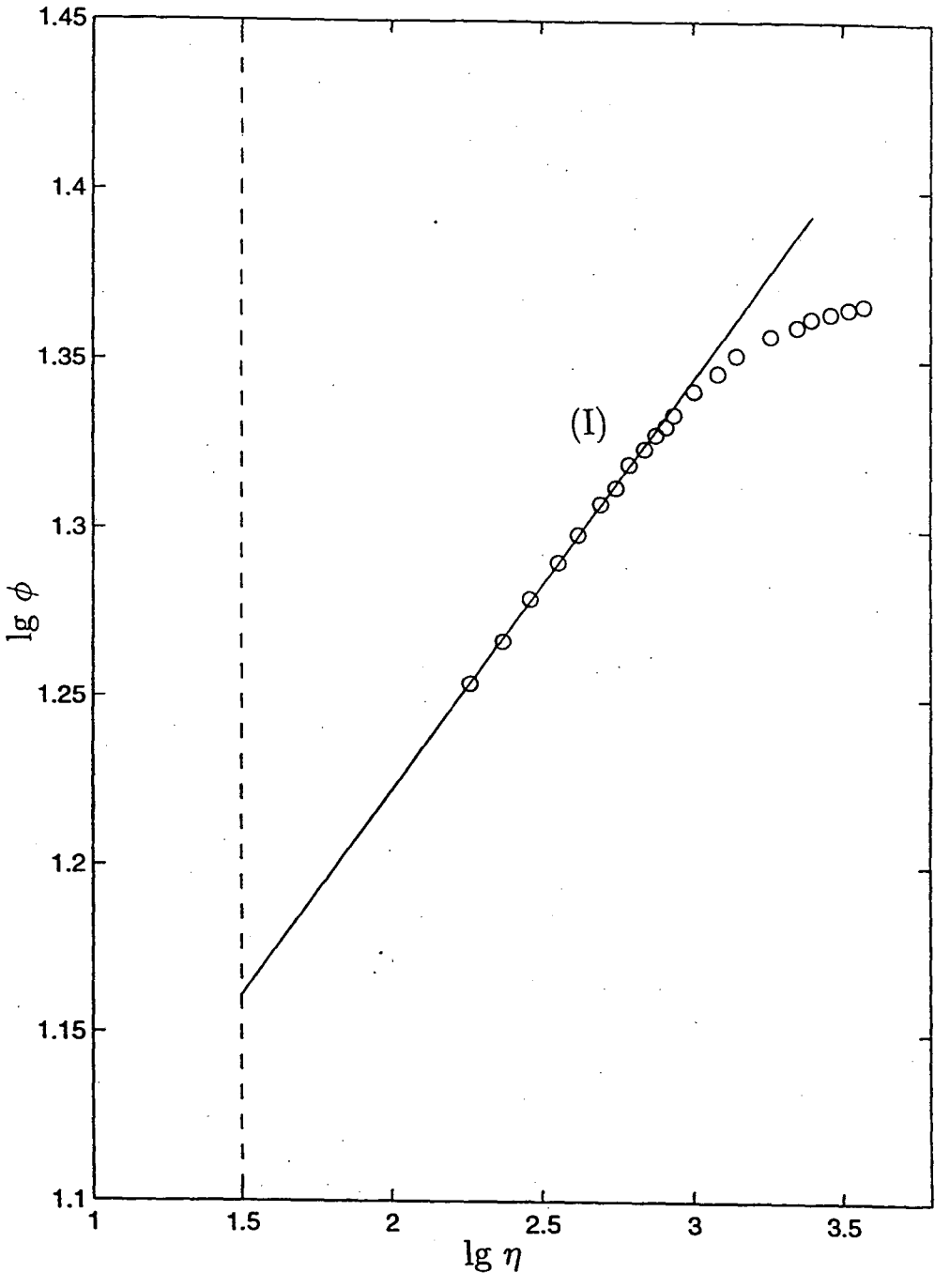

Figure 8. (e) The experiments by Hancock and Bradshaw, (1989). $\mathrm{Re}_\theta = 3,710$, $u'/U = 0.040$. The first self-similar intermediate region (I) is clearly seen, the second is not revealed.

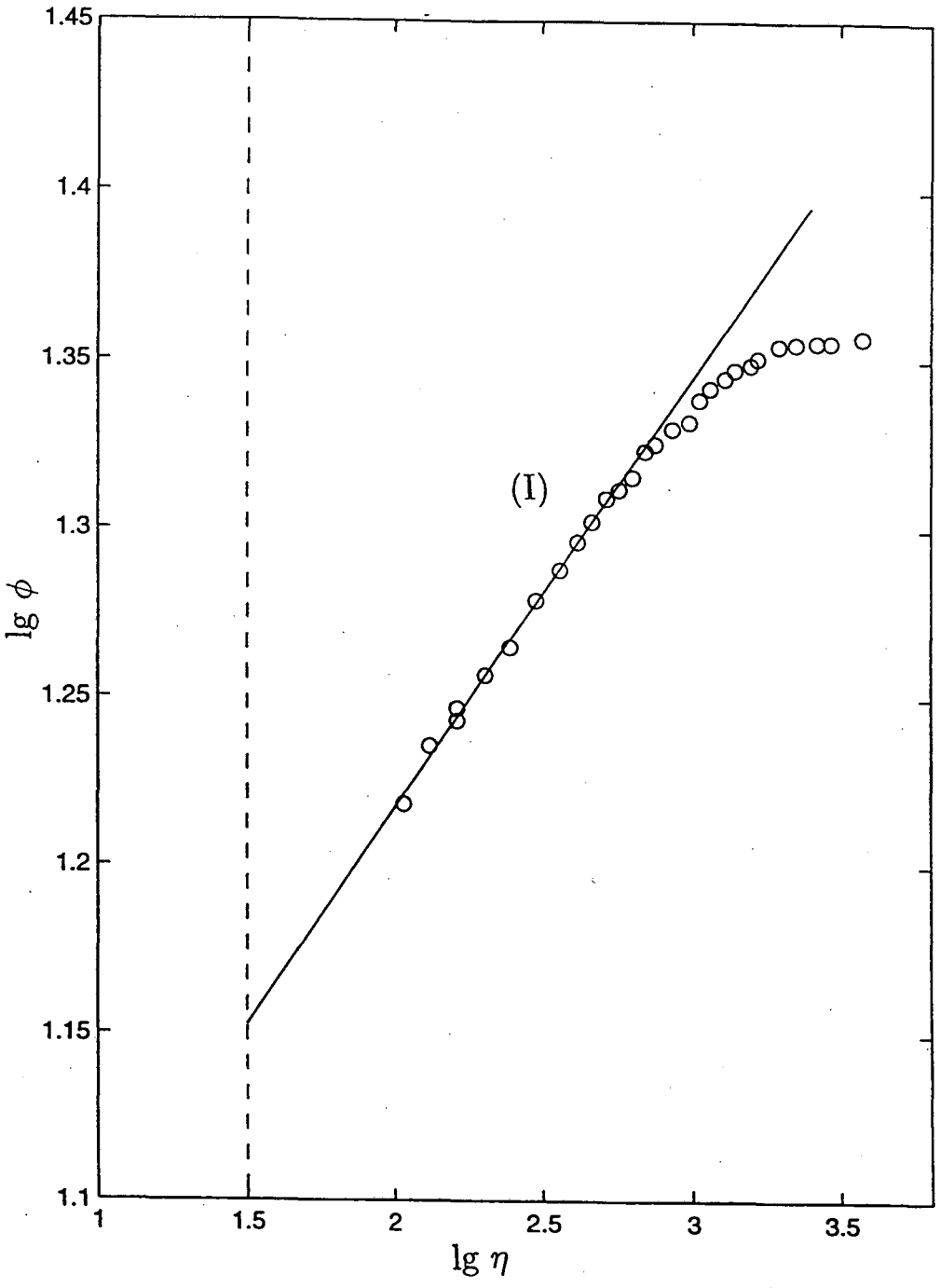

Figure 8. (f) The experiments by Hancock and Bradshaw, (1989). $\mathrm{Re}_\theta = 3,100$, $u'/U = 0.058$. The first self-similar intermediate region (I) is seen, although with a larger scatter. The second is not revealed.

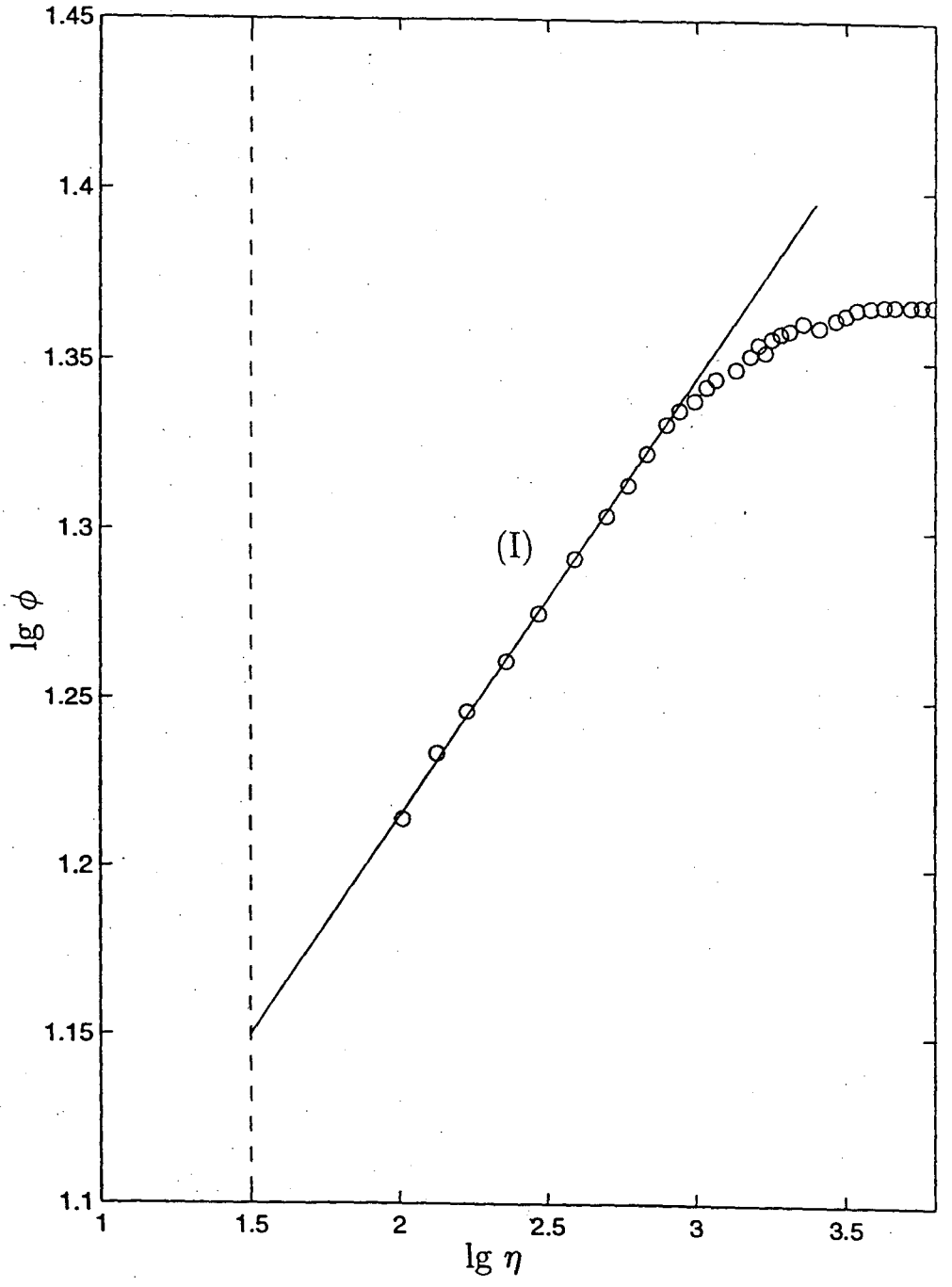

Figure 8. (g) The experiments of Hancock and Bradshaw, (1989). $\mathrm{Re}_\theta = 3,860$, $u'/U = 0.058$. The first self-similar intermediate region (I) is seen, although with a larger scatter. The second is not revealed.

4 The remaining group of zero-pressure-gradient boundary layer experiments

In this section the results of the processing are presented for all the remaining series of experiments. For all of them we used the data presented in the form of graphs in the review of Fernholz and Finley (1996). The results of the processing are presented in Table 3 and in Figures 9–15.

All the data reveal the self-similar structure in the first intermediate region adjacent to the viscous sublayer. The scaling laws obtained for this region give values of ln Re_1 and ln Re_2, close to each other, although the difference between ln Re_1 and ln Re_2 is sometimes larger than in the experiments of the first group. The scaling law (5) is confirmed by all these experiments. At the same time, for this group of experiments the second self-similar structure adjacent to the free stream turns out to be less clear-cut, if it is there at all. Therefore, for this group of experiments, we did not present the estimates for the values of β. Nevertheless we note that when it was possible to obtain estimates of β they always gave a β less than 0.2. Note also that for all these experiments the number of experimental points belonging to the region adjacent to the free stream was less than for the experiments of the first group: this was an additional argument for our reluctance to show here the second self-similar layer. As explained in Section 3, we suggest that the turbulence of the external flow in the experiments of this remaining group was more significant.

Table 3.

Figure	Re_θ	α	A	$\ln Re_1$	$\ln Re_2$	$\ln Re$	Re_θ/Re
			Winter K.G., Gaudet L., (1973)				
Fig. 9 (a)	32,150	0.133	8.86	11.02	11.32	11.17	0.45
Fig. 9 (b)	42,230	0.122	9.37	11.90	12.30	12.10	0.24
Fig. 9 (c)	77,010	0.115	10.30	13.51	13.04	13.27	0.13
Fig. 9 (d)	96,280	0.107	10.56	13.96	14.02	13.99	0.08
Fig. 9 (f)	136,600	0.101	10.99	14.71	14.85	14.78	0.05
Fig. 9 (e)	167,600	0.096	11.65	15.85	15.63	15.74	0.02
Fig. 9 (g)	210,600	0.096	11.30	15.24	15.63	15.43	0.04
	Purtell L.P., Klebanov P.S., Buckley F.T. (1981)						
Fig. 10 (a)	1,002	0.170	7.39	8.47	8.82	8.64	0.18
Fig. 10 (b)	1,837	0.164	7.62	8.87	9.15	9.01	0.23
Fig. 10 (c)	5,122	0.149	8.11	9.72	10.07	9.89	0.26
			Erm L.P. (1988)				
Fig. 11 (a)	2,244	0.155	8.04	9.60	9.68	9.64	0.15
Fig. 11 (b)	2,777	0.157	7.99	9.51	9.55	9.53	0.20
	Petrie H.L., Fontaine A.A., Sommer S.T., Brungart T.A. (1990)						
Fig. 12	35,530	0.119	9.76	12.57	12.61	12.59	0.12
	Bruns J., Dengel P., Fernholz H.H. (1992) and Fernholz H.H., Krause E., Nockemann M., Schober M. (1995)						
Fig. 13 (a)	2,573	0.151	8.46	10.32	9.93	10.13	0.10
Fig. 13 (b)	5,023	0.144	8.85	11.00	10.42	10.70	0.11
Fig. 13 (c)	7,139	0.148	8.49	10.37	10.14	10.25	0.25
Fig. 13 (d)	16,080	0.142	8.45	10.31	10.56	10.43	0.47
Fig. 13 (e)	20,920	0.137	8.51	10.41	10.95	10.68	0.48
Fig. 13 (f)	41,260	0.132	8.63	10.62	11.36	10.98	0.70
Fig. 13 (g)	57,720	0.130	8.71	10.76	11.54	11.14	0.84
			Djenidi L. & Antonia R.A. (1993)				
Fig. 14 a	1,033	0.163	7.88	9.32	9.19	9.25	0.10
Fig. 14 b	1,320	0.152	8.32	10.08	9.87	9.97	0.06
			Warnack D.(1994)				
Fig. 15 (a)	2,552	0.152	8.29	10.03	9.87	9.95	0.12
Fig. 15 (b)	4,736	0.149	8.20	9.87	10.07	9.97	0.22

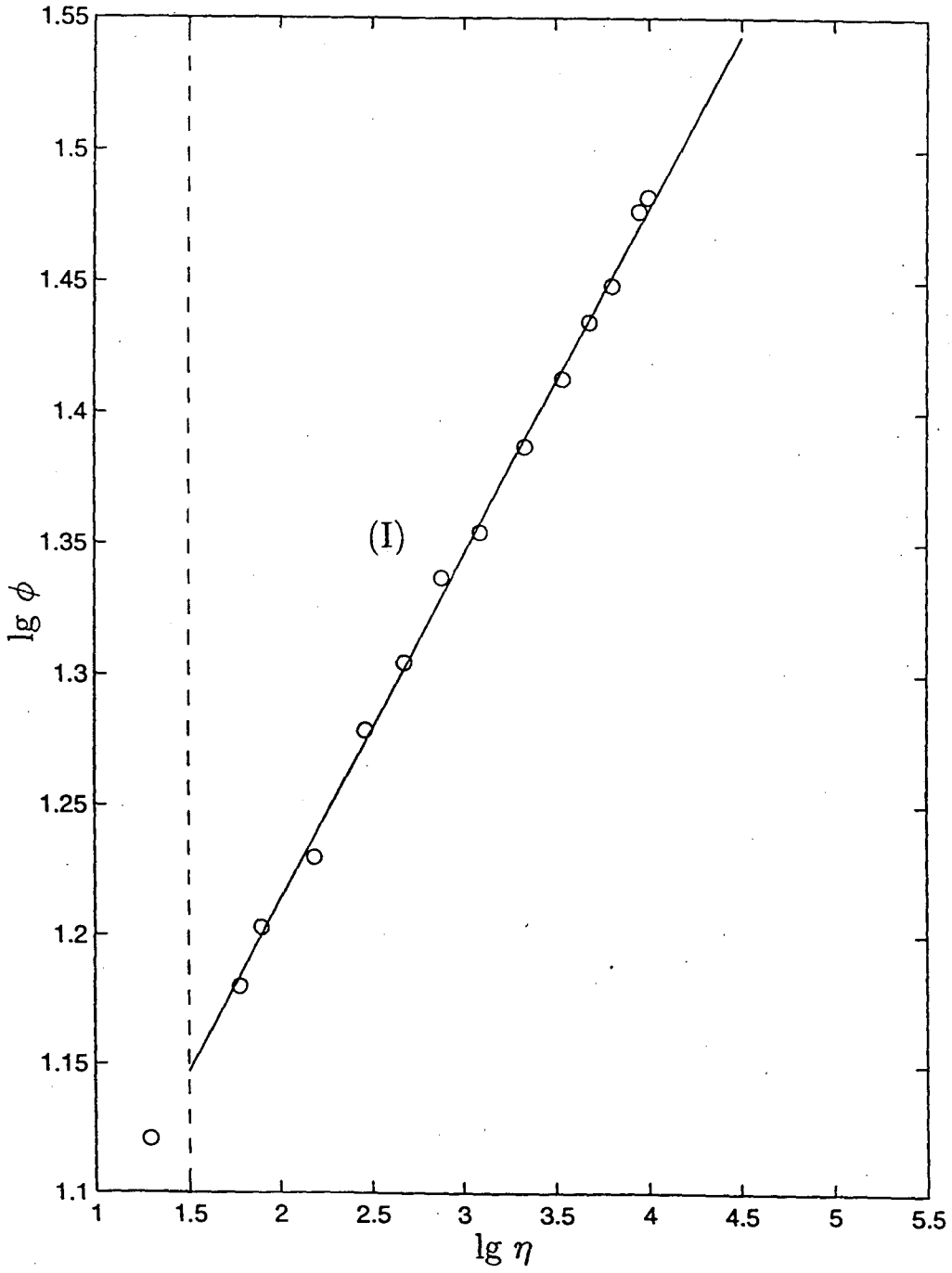

Figure 9. (a) The experiments of Winter and Gaudet, (1973). $\mathrm{Re}_\theta = 32,150$. The first self-similar intermediate region (I) is seen, although with a larger scatter. The second is not revealed.

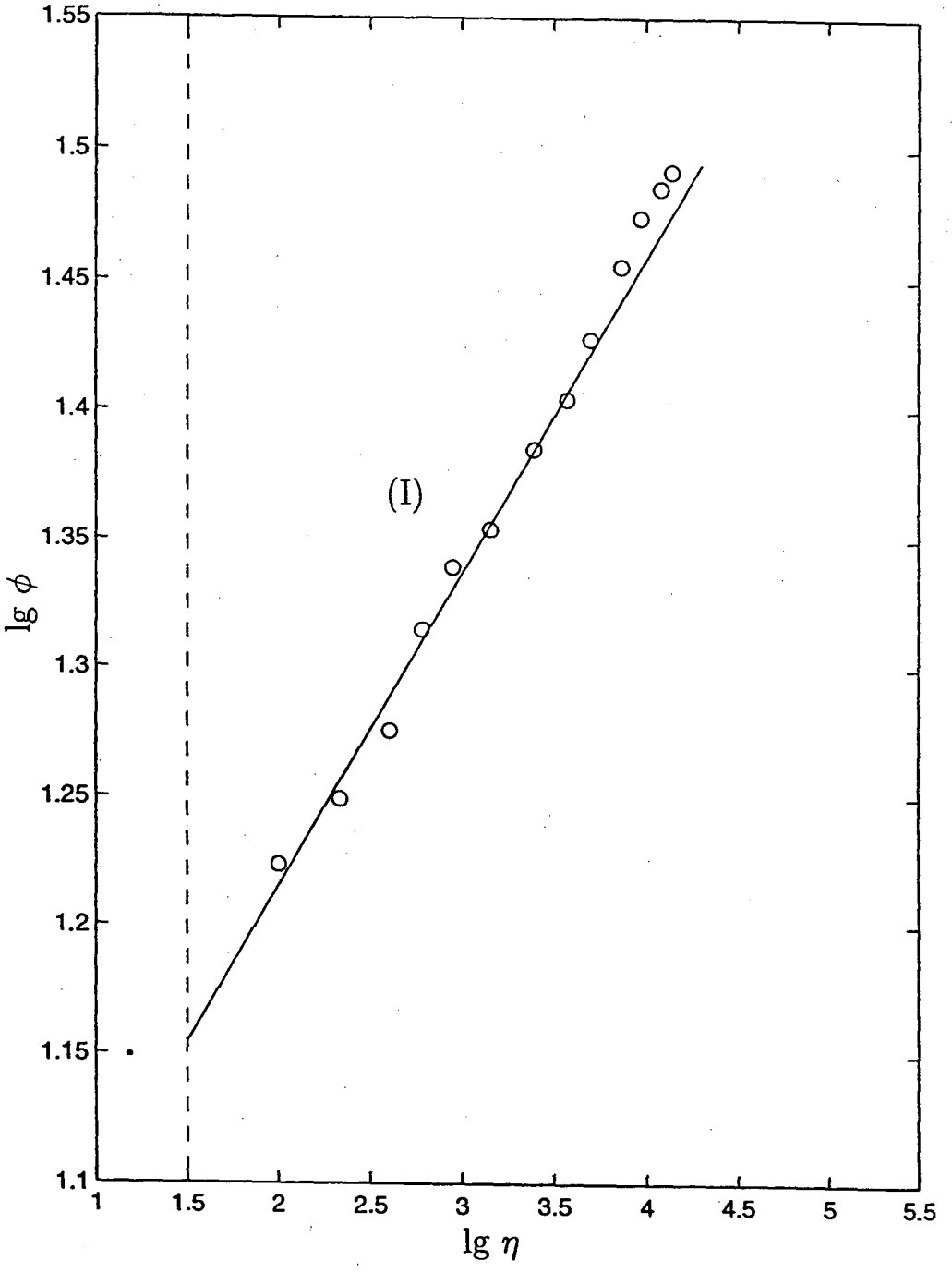

Figure 9. (b) The experiments of Winter and Gaudet, (1973). $\mathrm{Re}_\theta = 42,230$. The first self-similar intermediate region (I) is seen, although with a larger scatter. The second is not revealed.

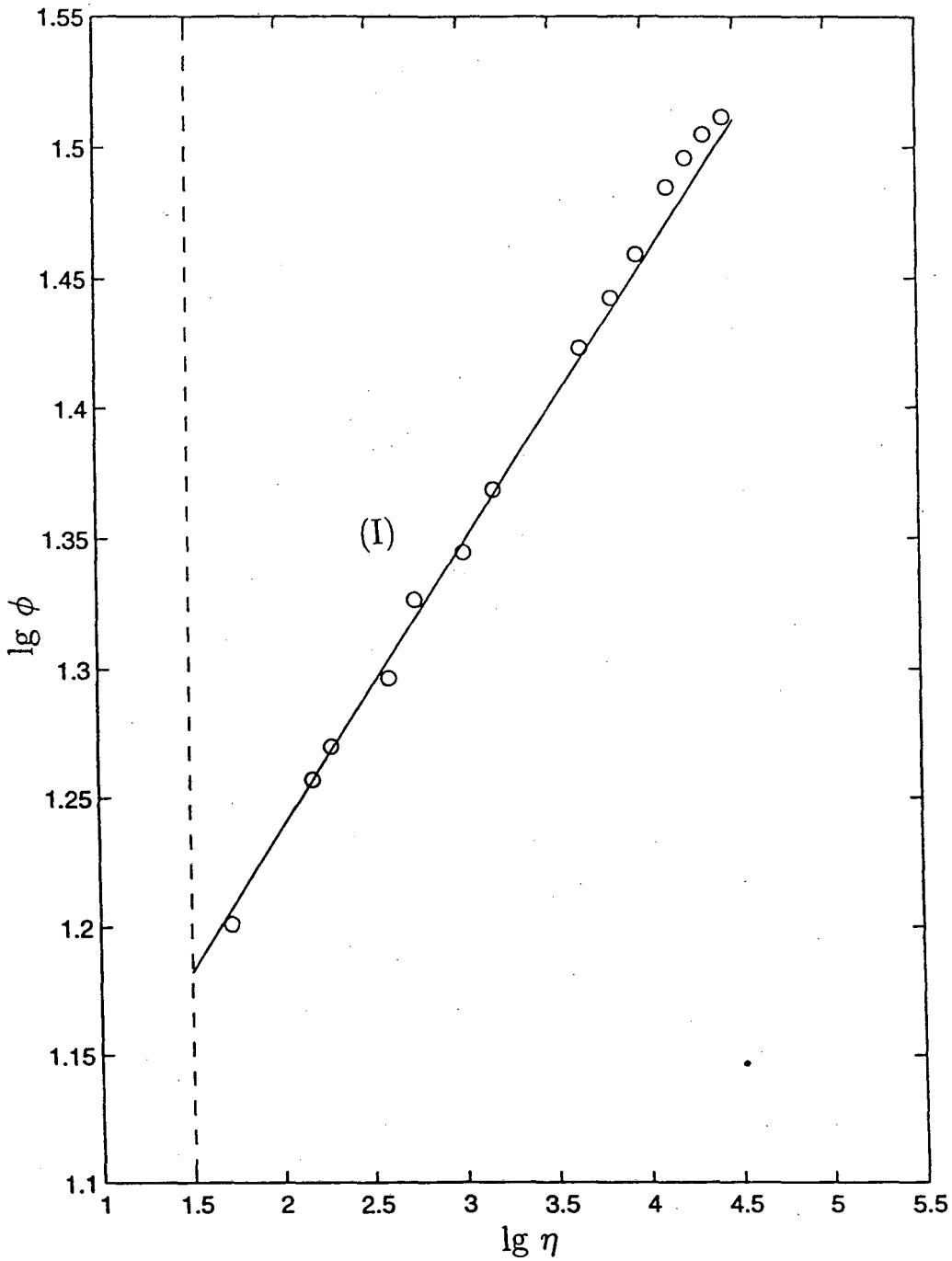

Figure 9. (c) The experiments of Winter and Gaudet, (1973). $Re_\theta = 77,010$. The first self-similar intermediate region (I) is seen, although with a larger scatter. The second is not revealed.

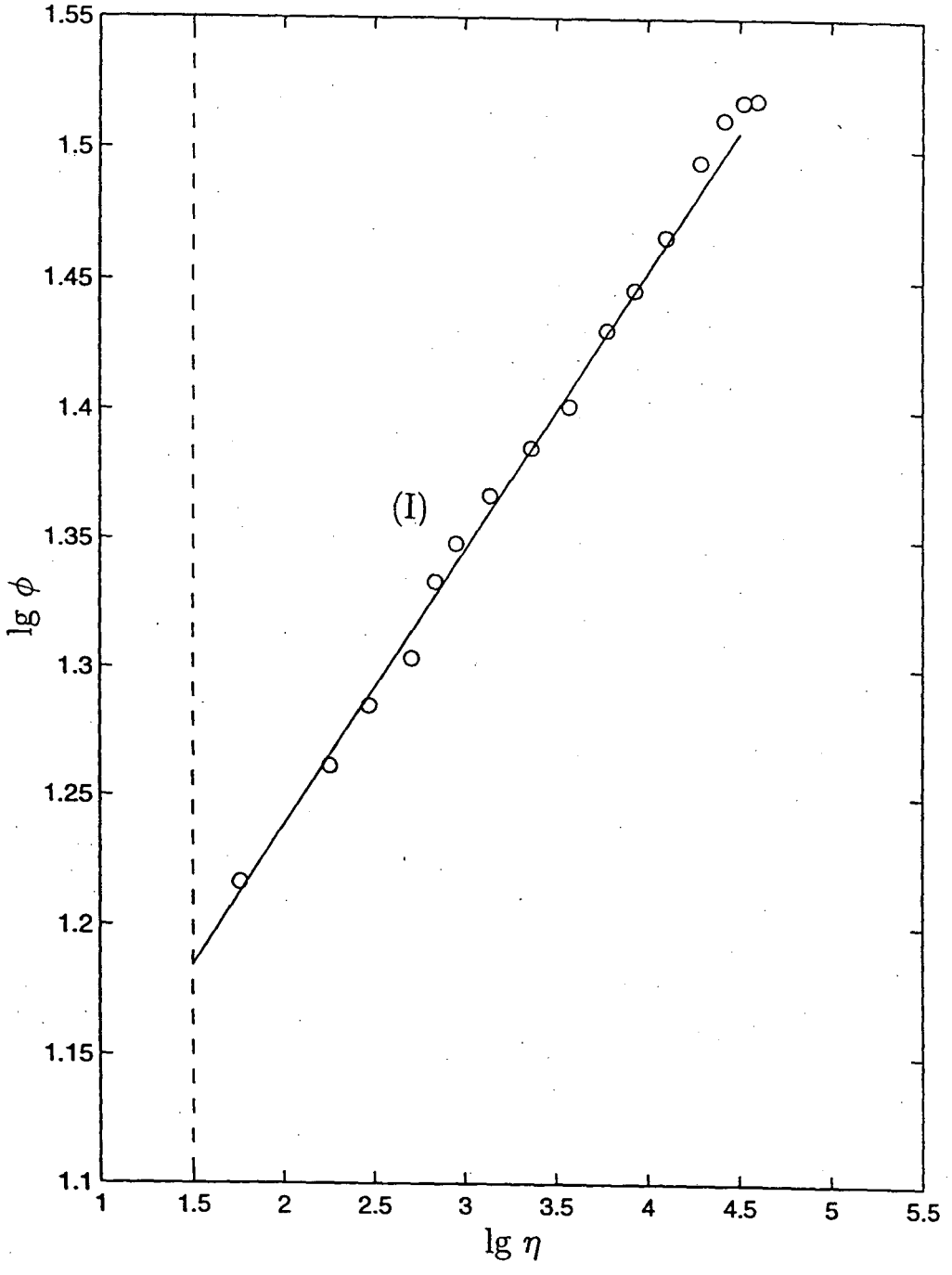

Figure 9. (d) The experiments of Winter and Gaudet, (1973). $Re_\theta = 96,280$. The first self-similar intermediate region (I) is seen, although with a larger scatter. The second is not revealed.

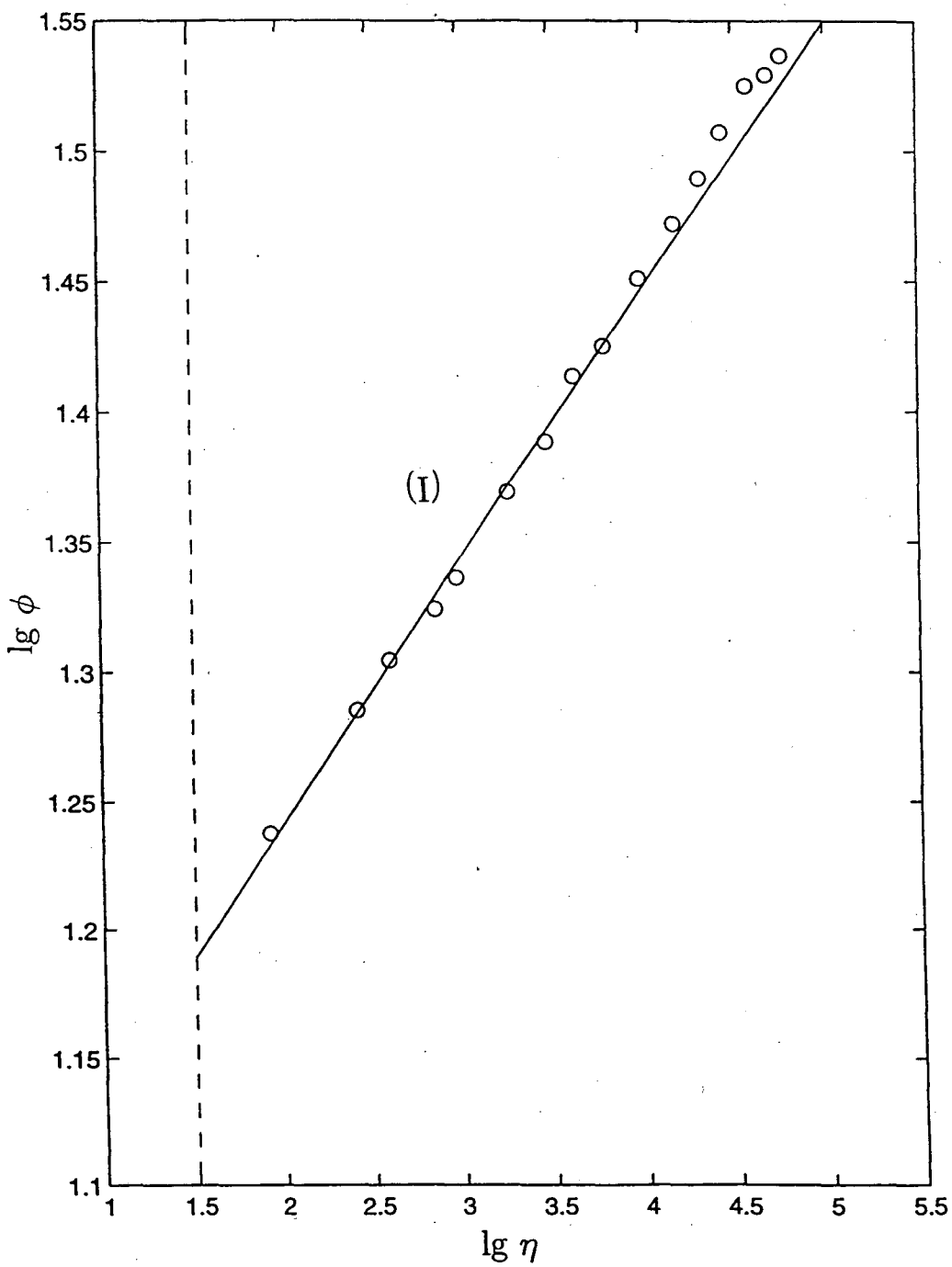

Figure 9. (e) The experiments of Winter and Gaudet, (1973). $Re_\theta = 136,600$. The first self-similar intermediate region (I) is seen, although with a larger scatter. The number of points is not enough to make a definite estimate for the second region, but the slope β is less than 0.2.

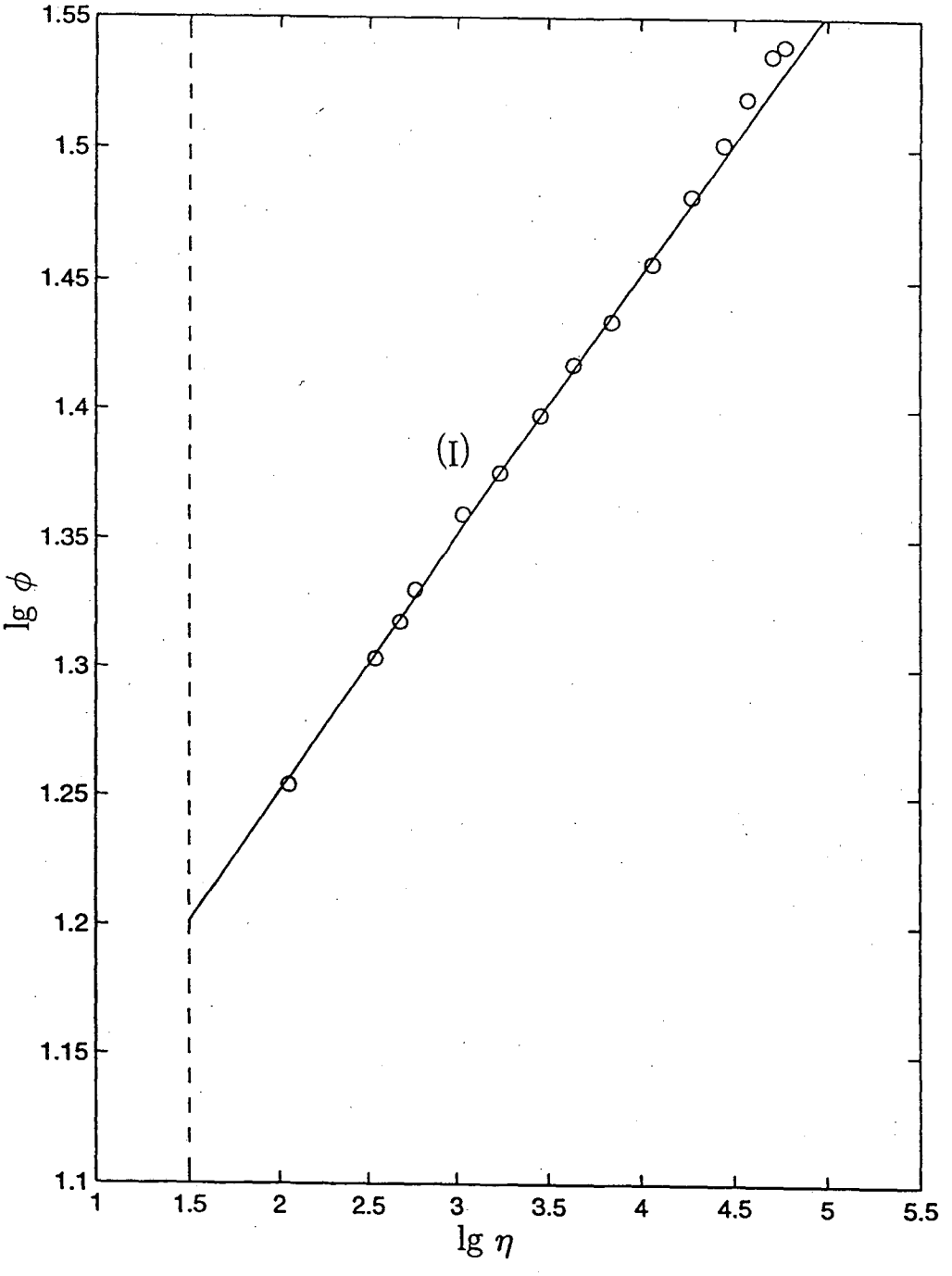

Figure 9. (f) The experiments of Winter and Gaudet, (1973). $\mathrm{Re}_\theta = 167,600$. The first self-similar intermediate region (I) is seen, although with a larger scatter. The second is not revealed.

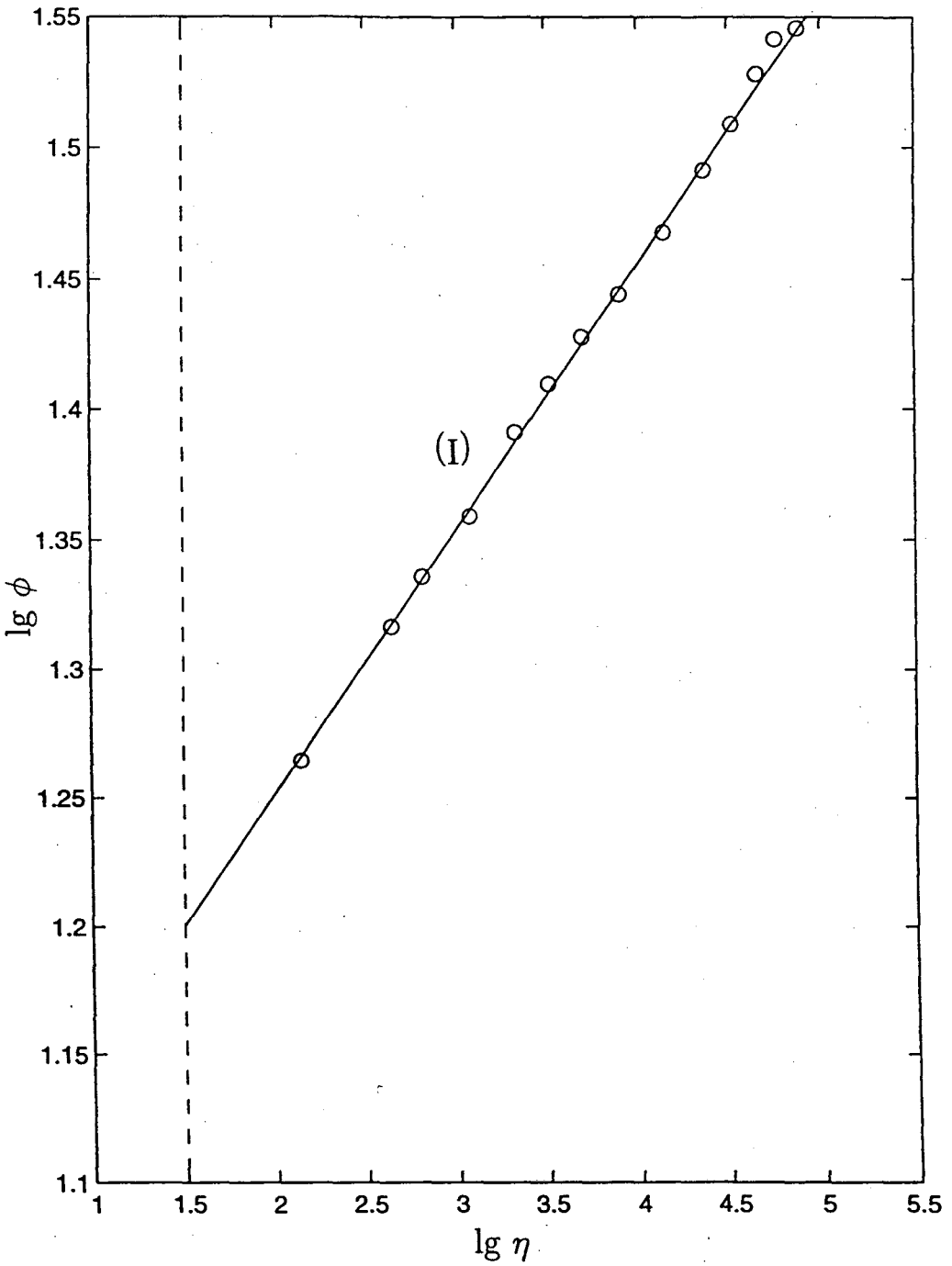

Figure 9. (g) The experiments of Winter and Gaudet, (1973). $\mathrm{Re}_\theta = 210,600$. The first self-similar intermediate region (I) is seen, although with a larger scatter. The second is not revealed.

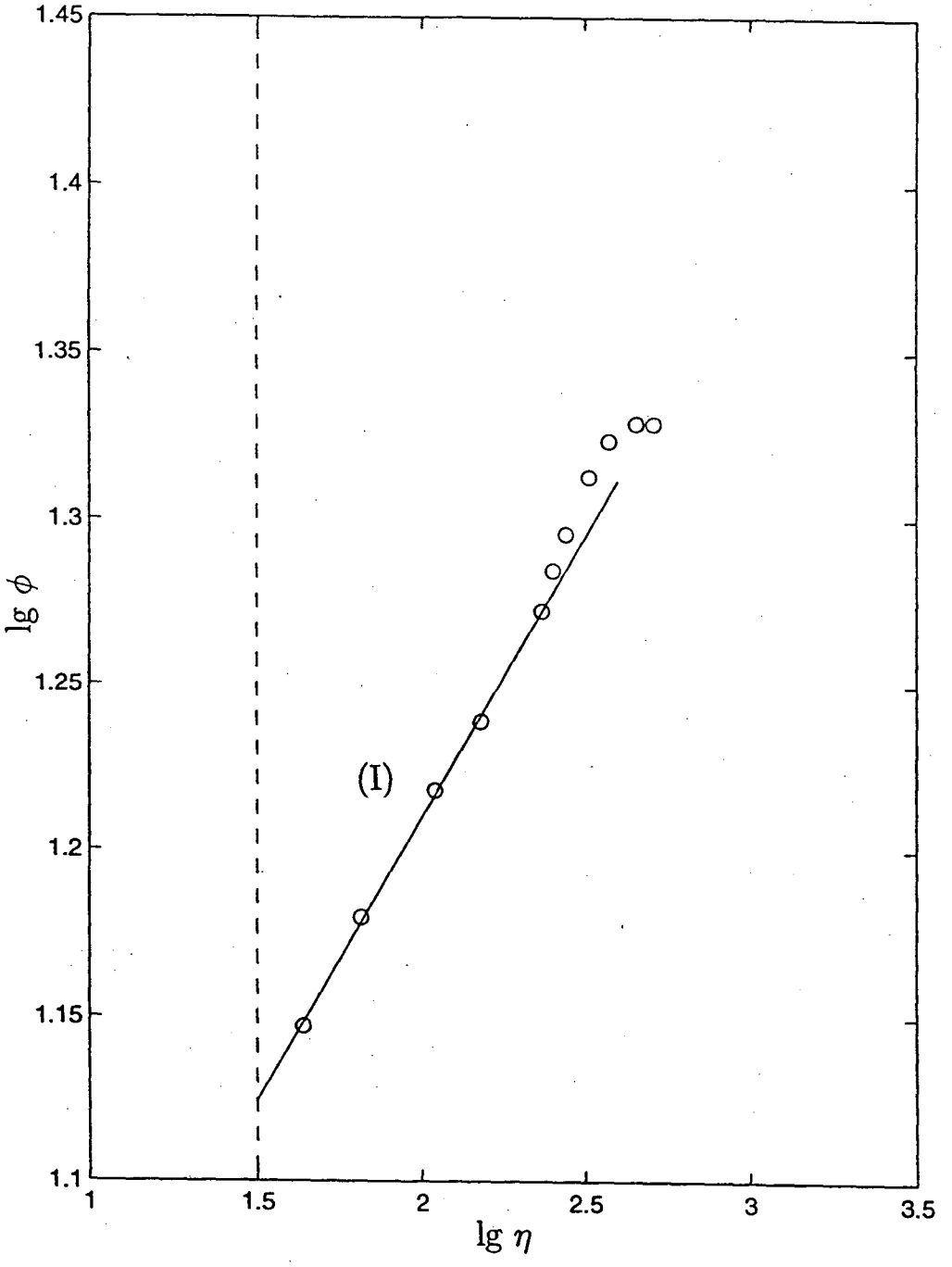

Figure 10. (a) The experiments of Purtell, Klebanov and Buckley, (1981). $\mathrm{Re}_\theta = 1,002$. The first self-similar region (I) is revealed in spite of the small number of points. The second self-similar region is not revealed.

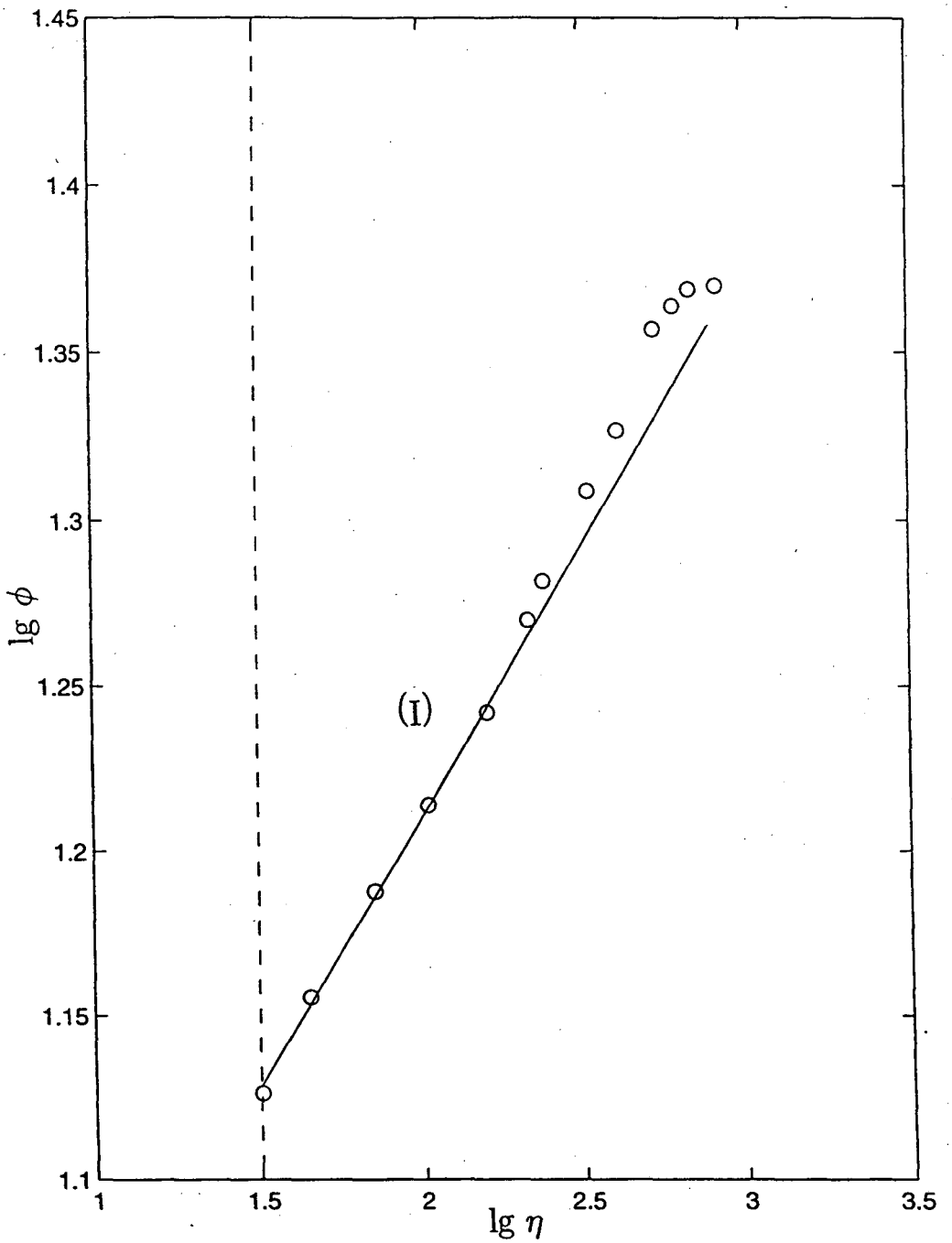

Figure 10. (b) The experiments of Purtell, Klebanov and Buckley, (1981). $\mathrm{Re}_\theta = 1,837$. The first self-similar region (I) is revealed in spite of the small number of points. The second self-similar region is revealed.

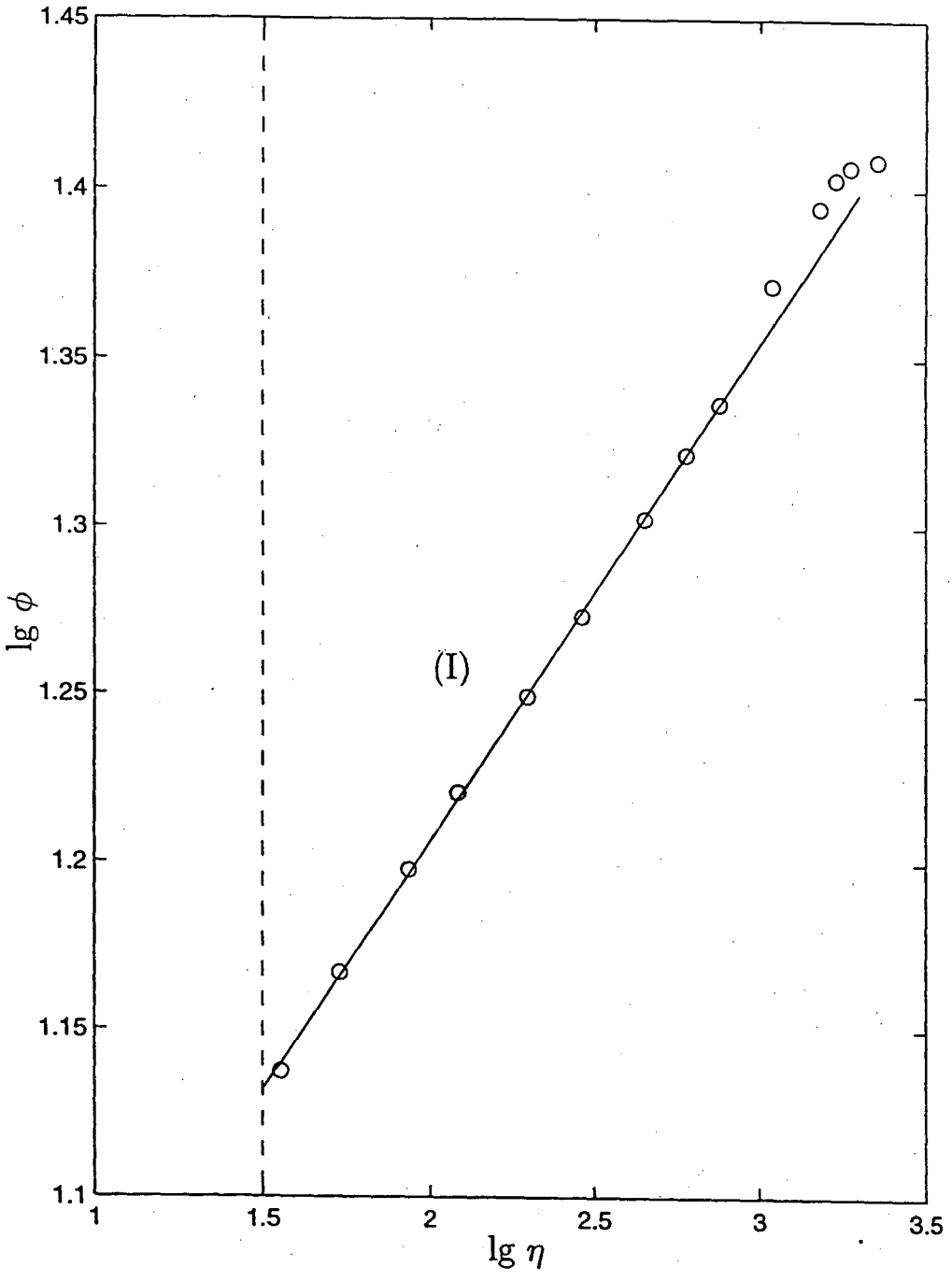

Figure 10. (c) The experiments of Purtell, Klebanov and Buckley, (1981). $\mathrm{Re}_\theta = 5,122$. The first self-similar region (I) is revealed. The second self-similar region is not revealed.

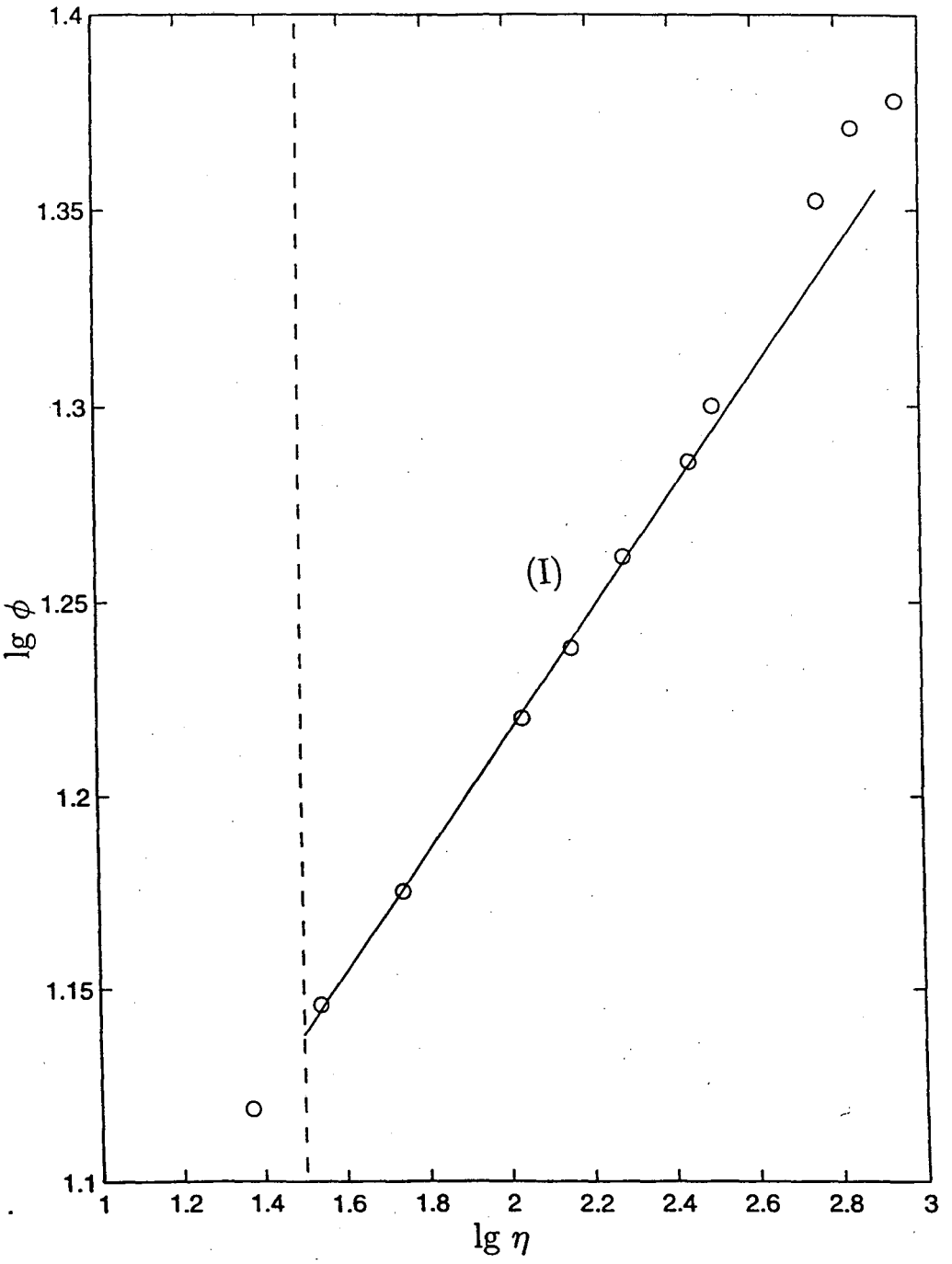

Figure 11. (a) The experiments of Erm, (1988). $\mathrm{Re}_\theta = 2,244$. The first self-similar region (I) is revealed. The second self-similar region is not revealed.

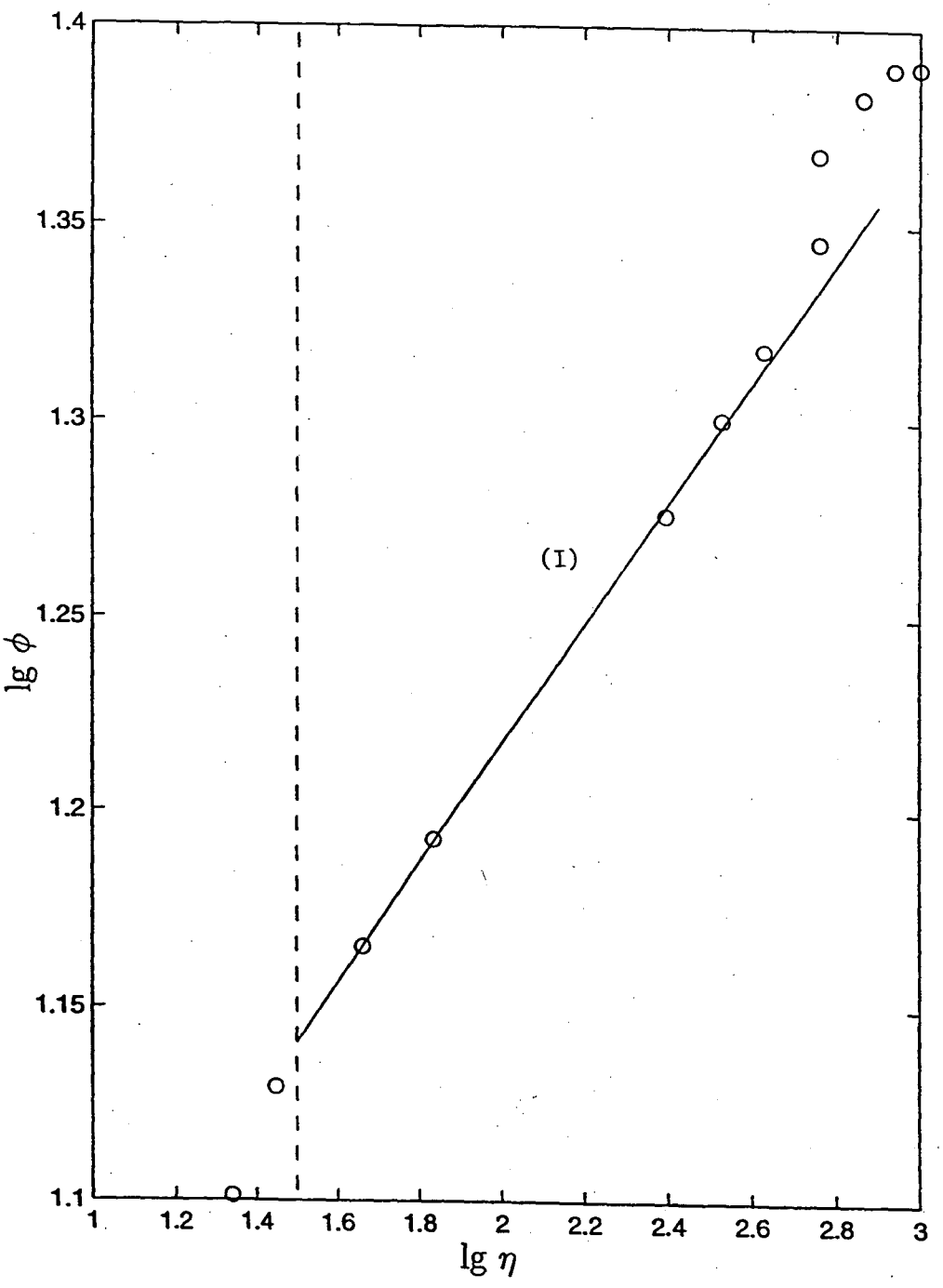

Figure 11. (b) The experiments of Erm,(1988). $Re_\theta = 2,777$. The first self-similar region (I) is revealed. The second self-similar region is not revealed.

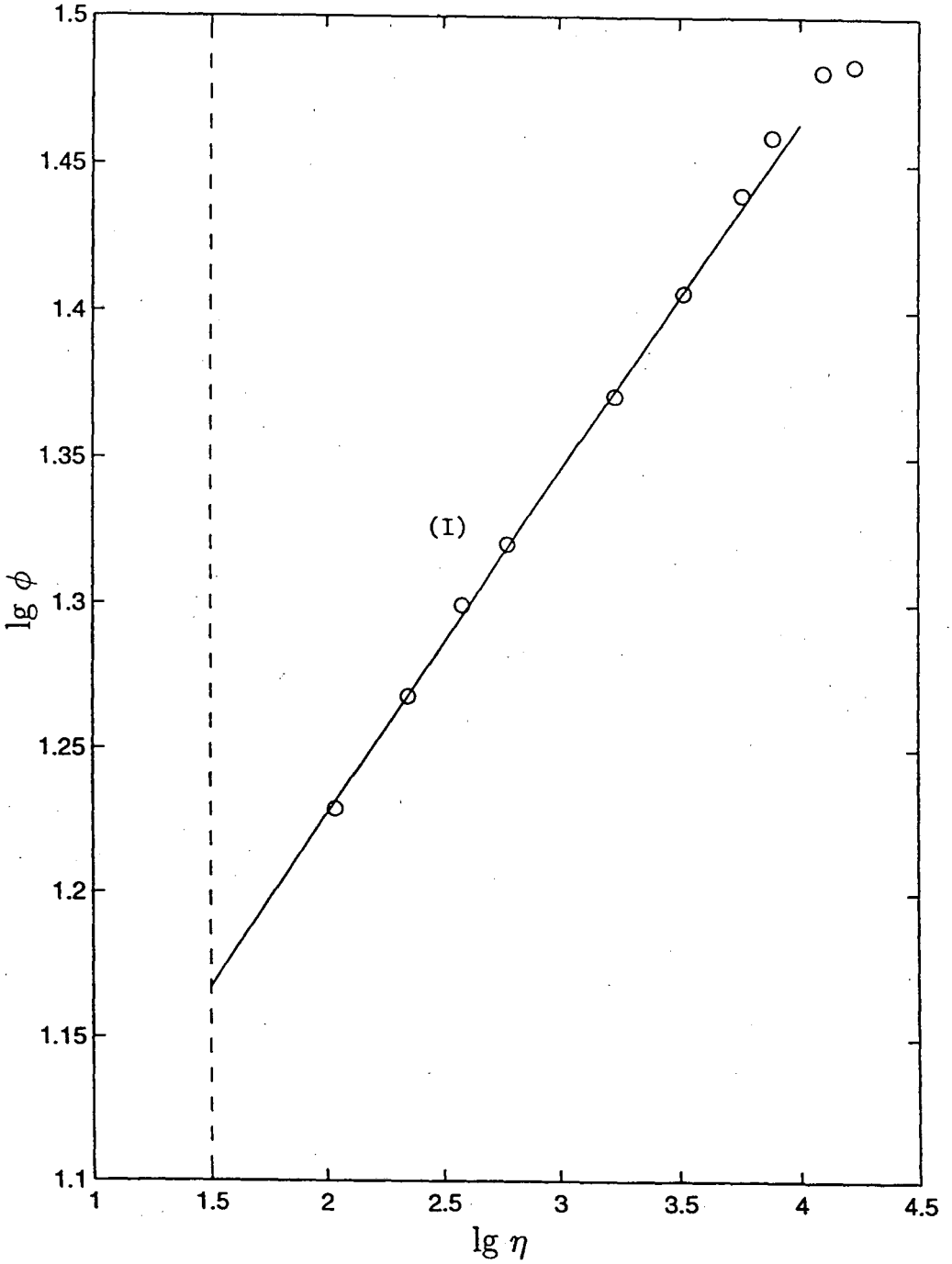

Figure 12. The experiments of Petrie, Fontaine, Sommer and Brungart, (1990). $Re_\theta = 35,530$. The first self-similar region (I) is revealed. The second self-similar region is not revealed.

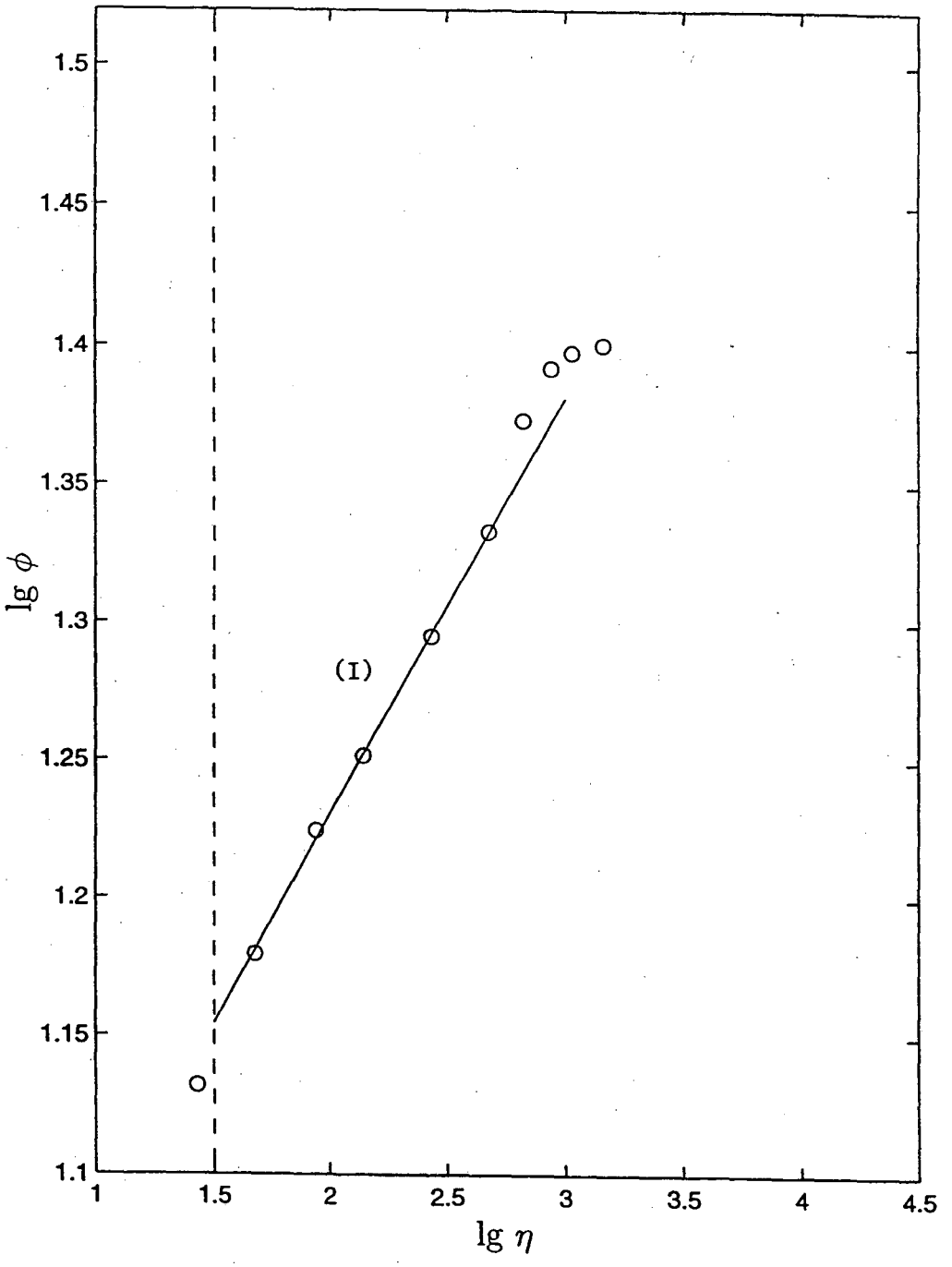

Figure 13. (a) The experiments of Bruns et al., (1992), and Fernholz et al., (1995). $Re_\theta = 2,573$. The first self-similar region (I) is revealed. The second self-similar region is not revealed.

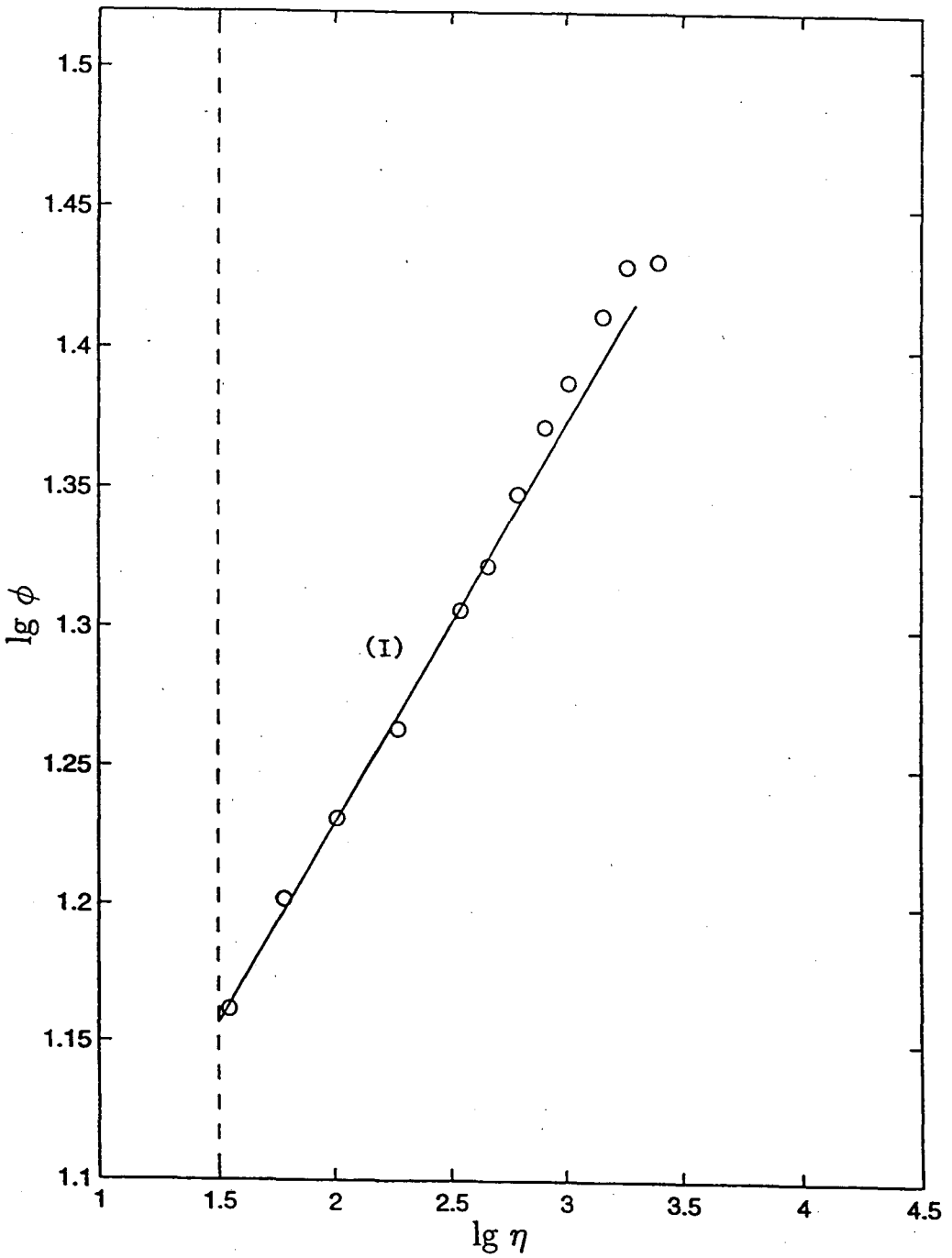

Figure 13. (b) The experiments of Bruns et al.,(1992) and Fernholz et al.,(1995). $Re_\theta = 5,023$. The first self-similar region (I) is revealed. The second self-similar region is not revealed.

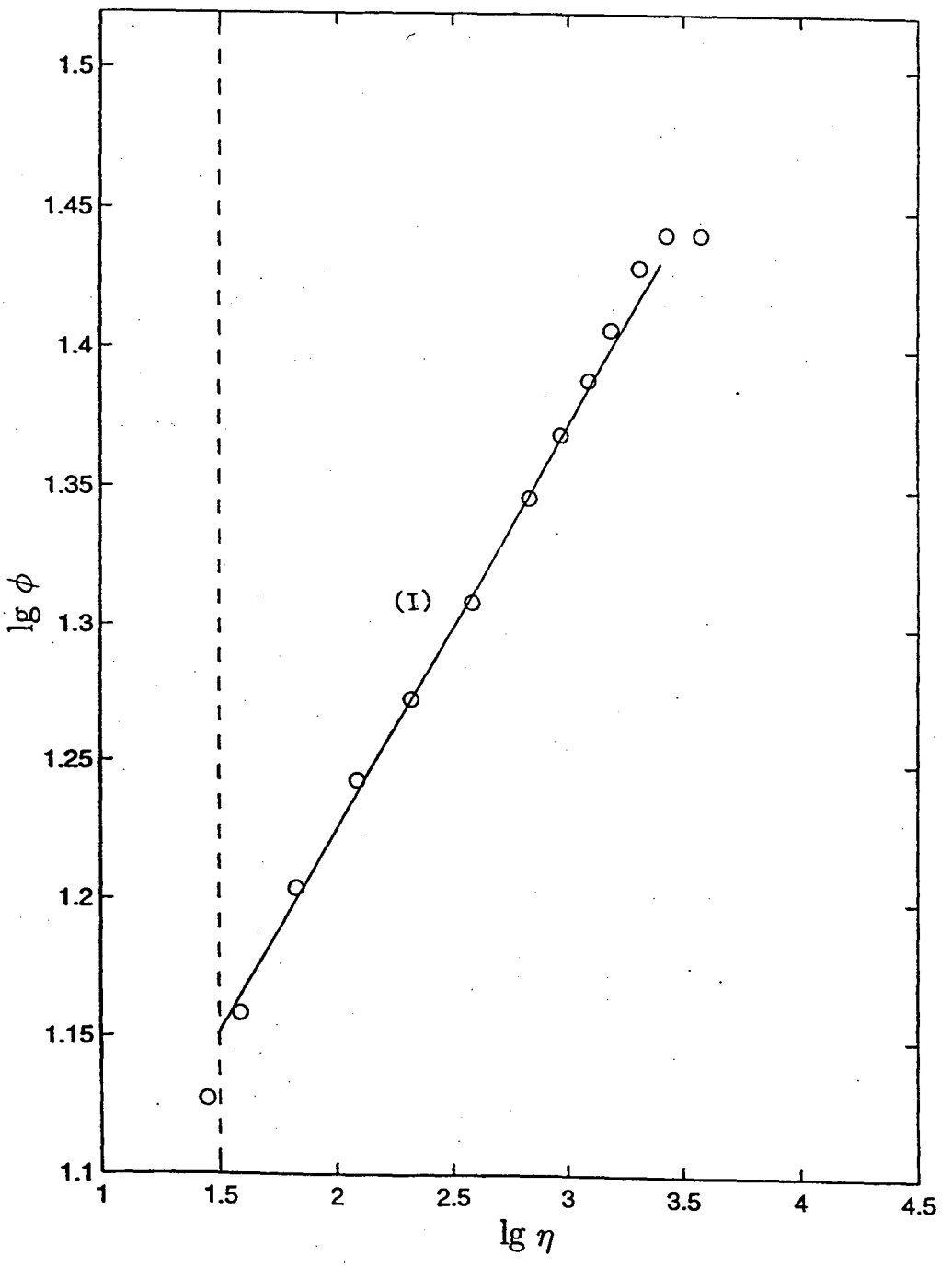

Figure 13. (c) The experiments of Bruns et al.,(1992) and Fernholz et al.,(1995).$Re_\theta = 7,139$. The first self-similar region (I) is revealed. The second self-similar region is not revealed.

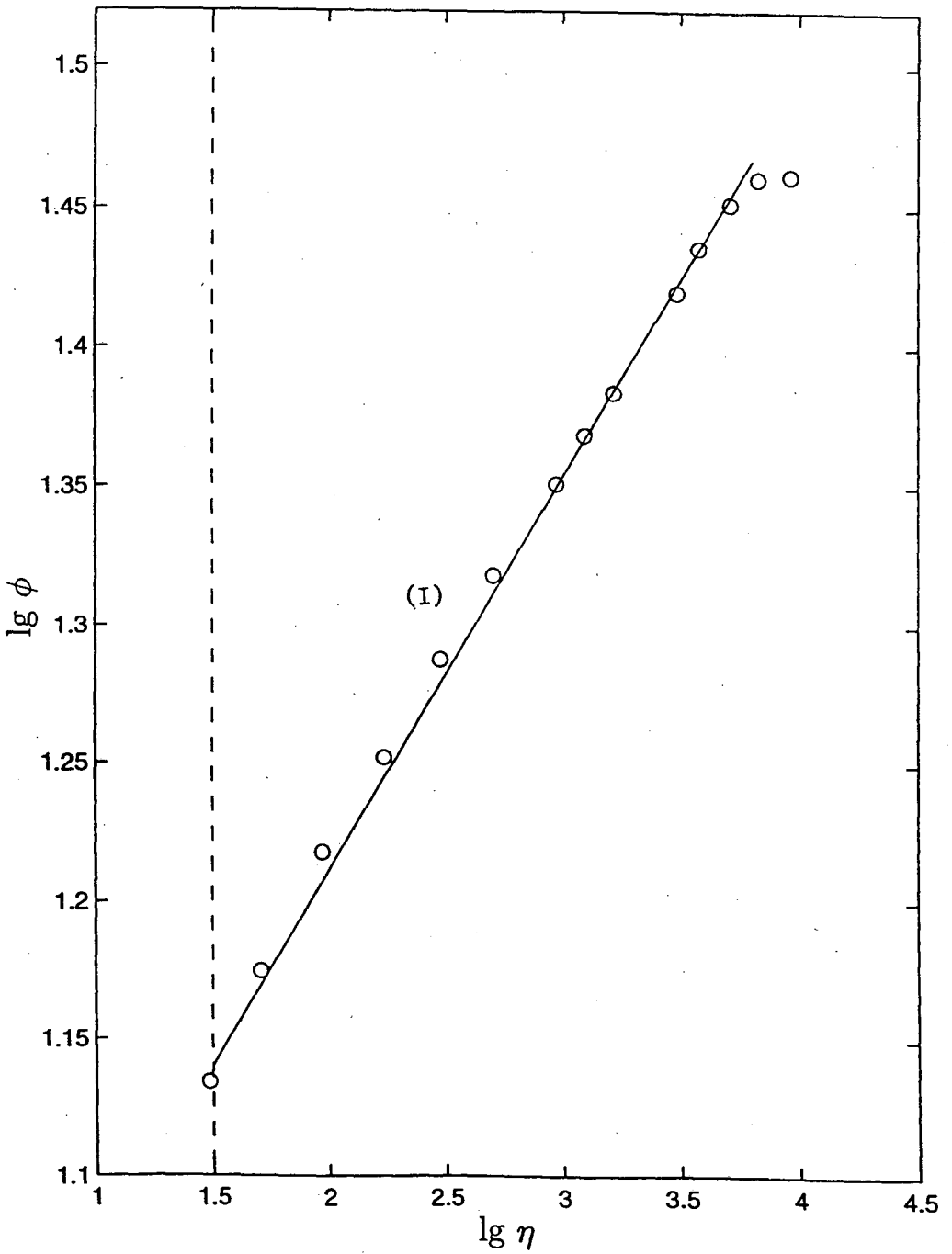

Figure 13. (d) The experiments of Bruns et al., (1992), and Fernholz et al., (1995). $Re_\theta = 16,080$. The first self-similar region (I) is revealed. The second self-similar region is not revealed.

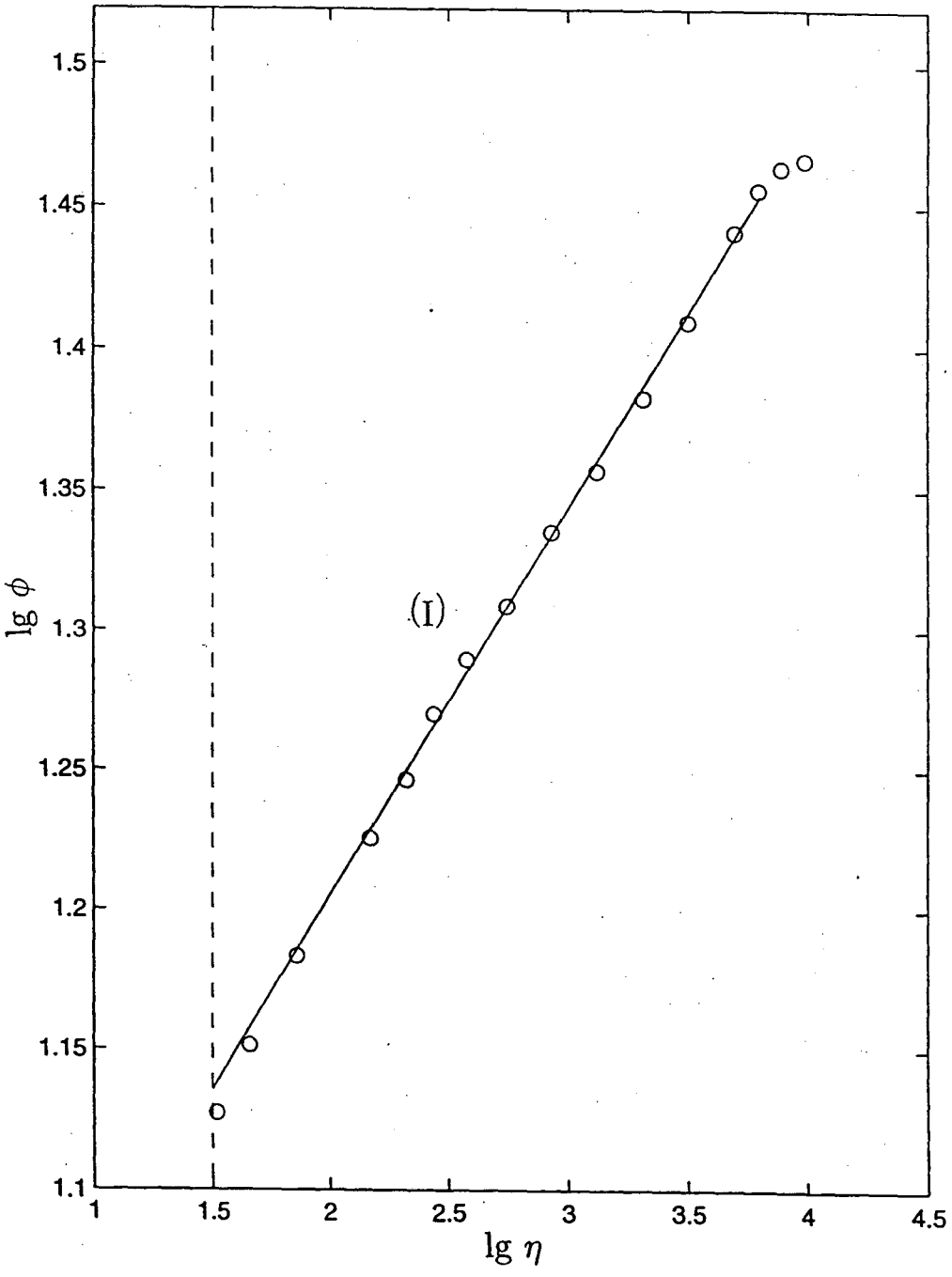

Figure 13. (e) The experiments of Bruns et al., (1992), and Fernholz et al., (1995). $Re_\theta = 20,920$. The first self-similar region (I) is revealed. The second self-similar region is not revealed.

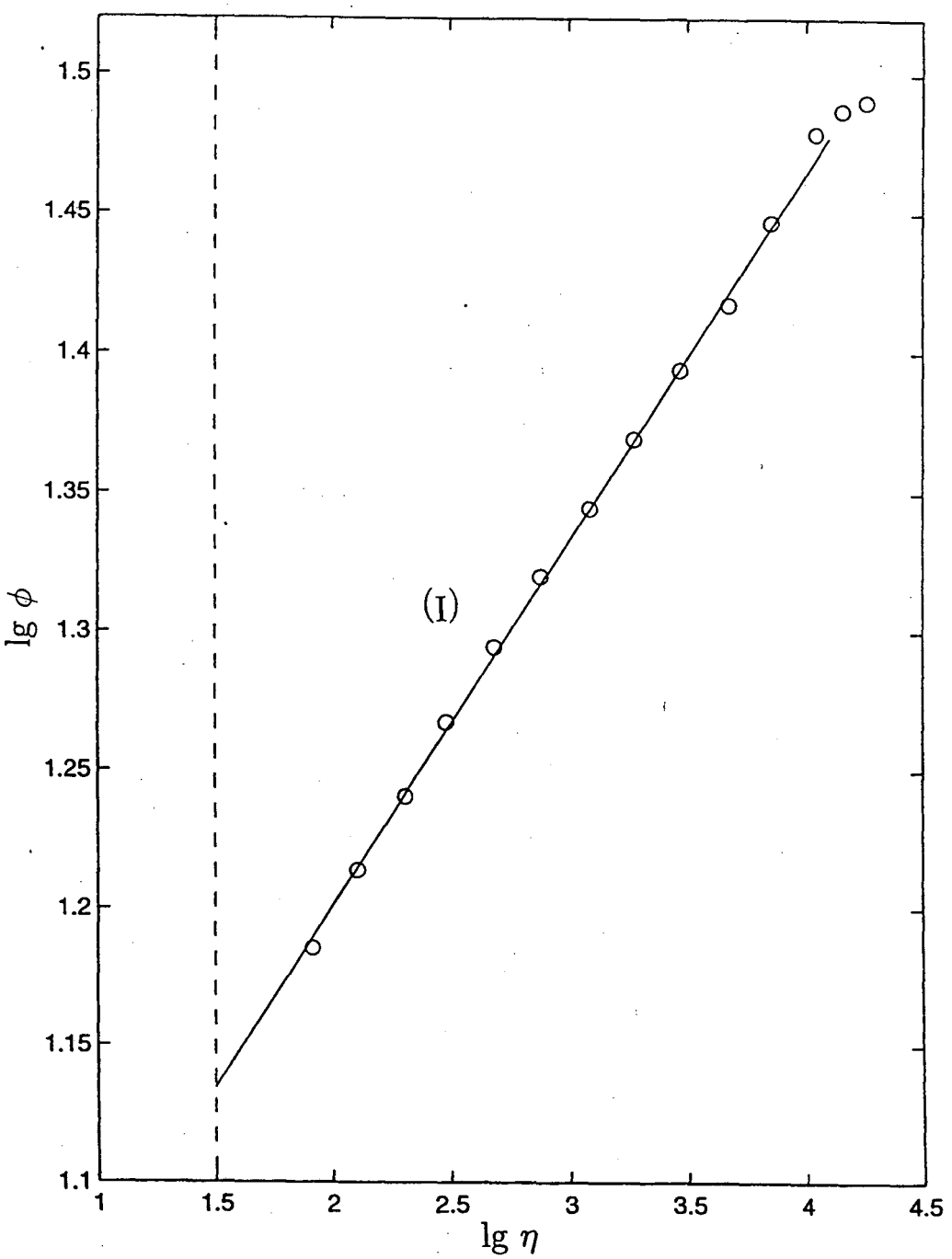

Figure 13. (f) The experiments of Bruns et al., (1992), and Fernholz et al., (1995). $Re_\theta = 41,260$. The first self-similar region (I) is revealed. The second self-similar region is not revealed.

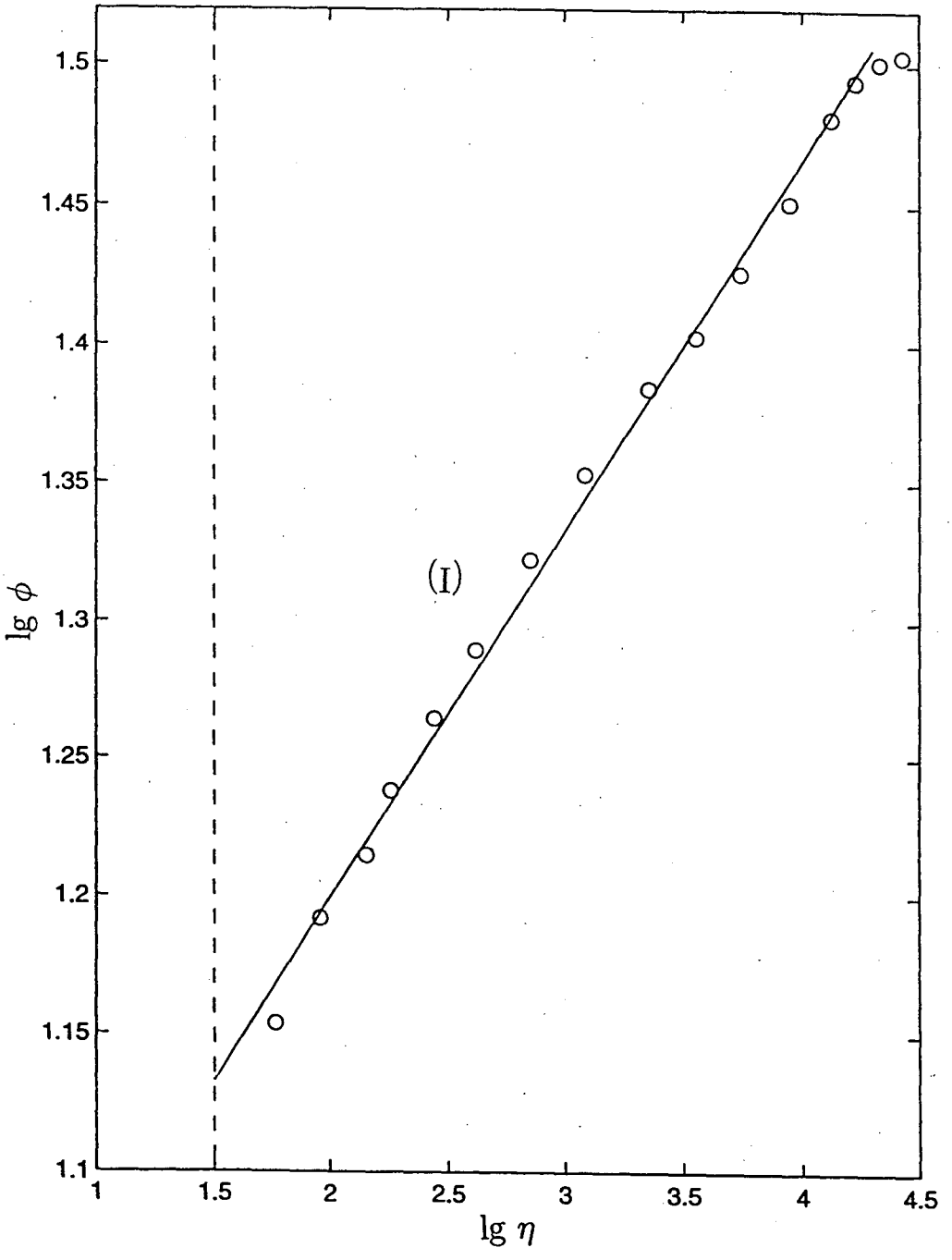

Figure 13. (g) The experiments of Bruns et al., (1992), and Fernholz et al., (1995). $Re_\theta = 57,720$. The first self-similar region (I) is revealed. The second self-similar region is not revealed.

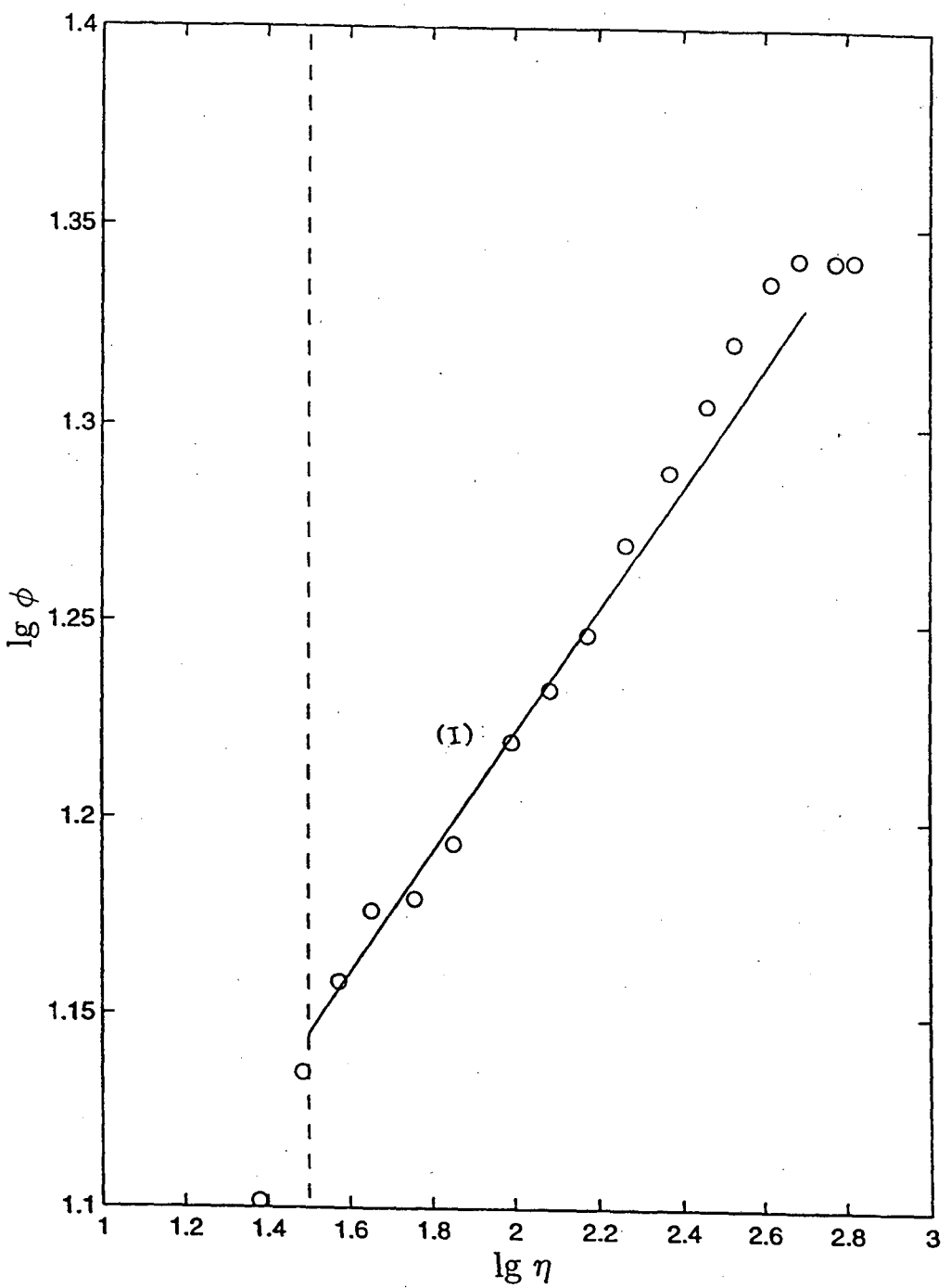

Figure 14. (a) The experiments of Djenidi and Antonia, (1993). $\mathrm{Re}_\theta = 1,033$. The first self-similar region (I) is revealed although with a larger scatter. The second self-similar region can be traced.

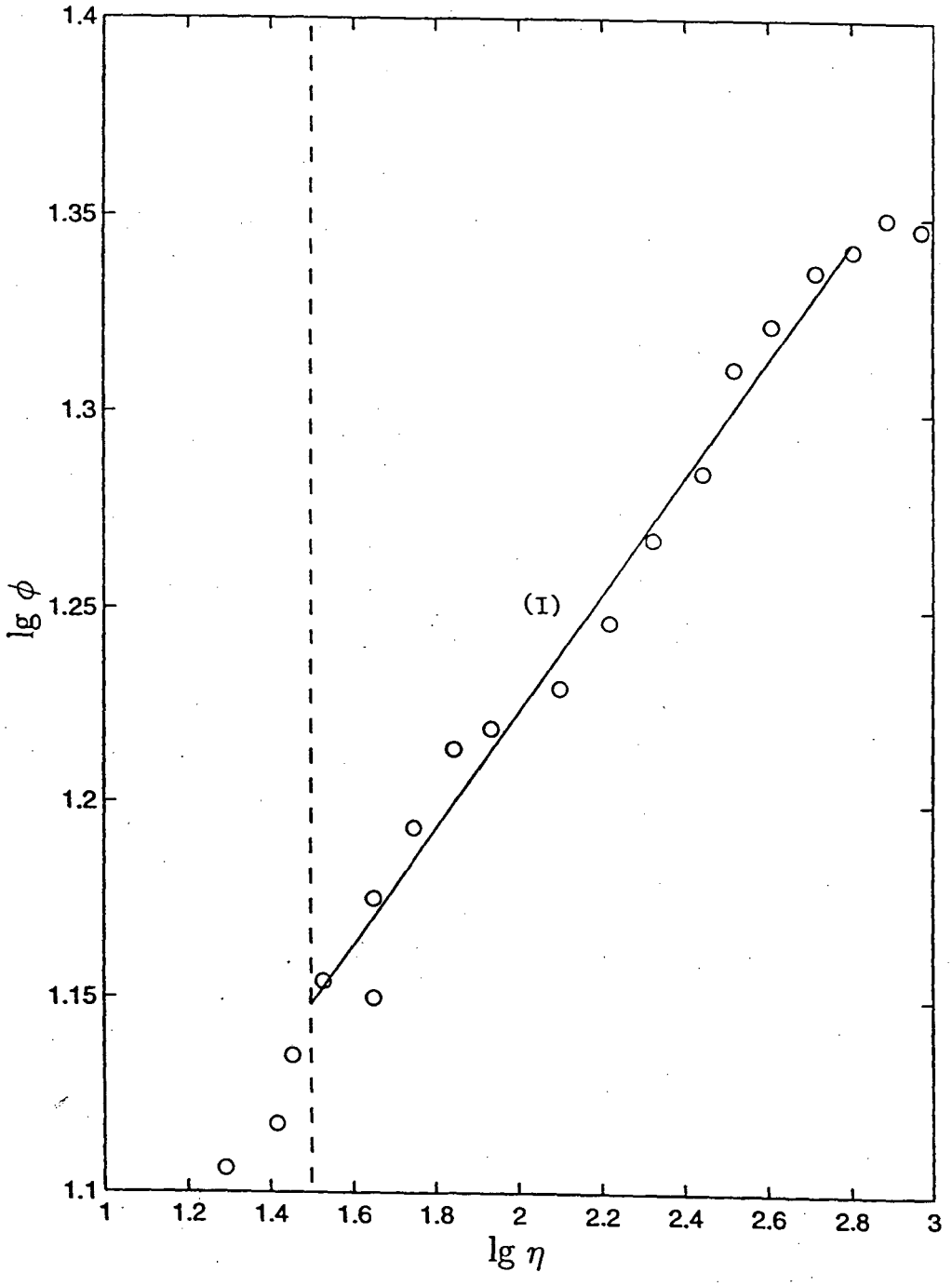

Figure 14. (b) The experiments of Djenidi and Antonia, (1993). $Re_\theta = 1,320$. The first self-similar region (I) can be revealed although with a larger scatter. The second self-similar region is not revealed.

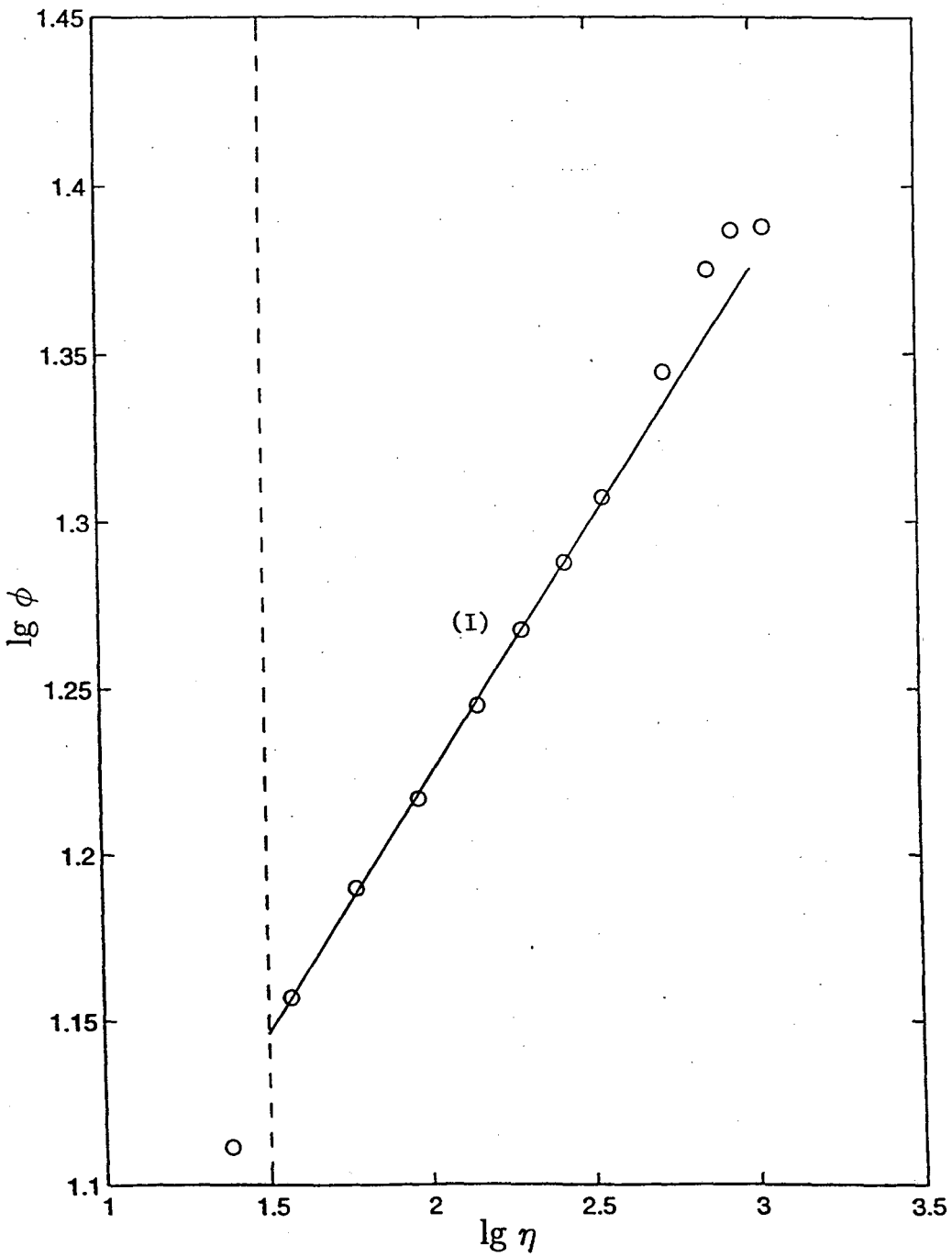

Figure 15. (a) The experiments of Warnack, (1994). $\mathrm{Re}_\theta = 2,552$. The first self-similar region (I) is clearly seen. The second self-similar region can be traced.

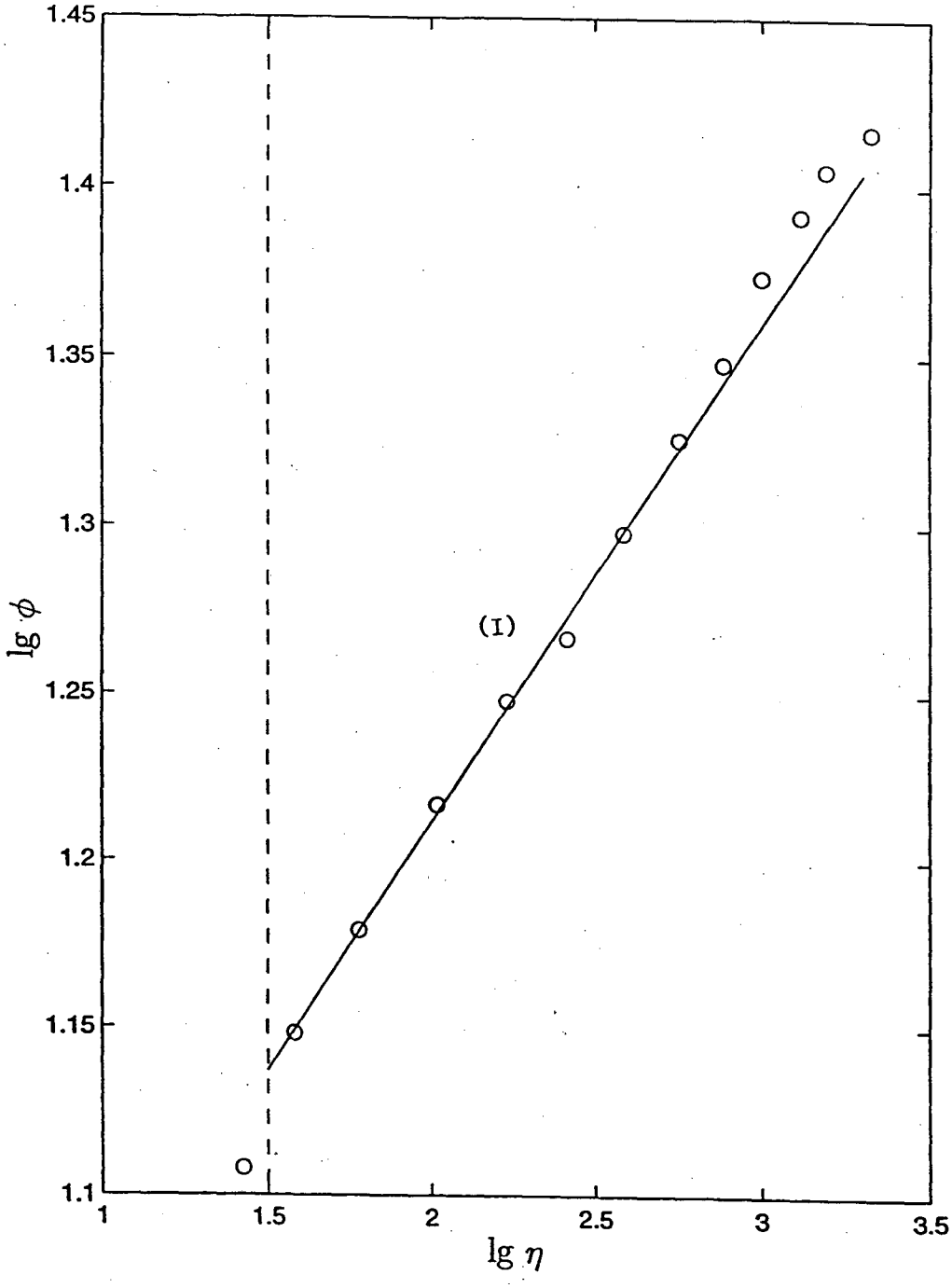

Figure 15. (b) The experiments of Warnack,(1994). $\mathrm{Re}_\theta = 4,736$. The first self-similar region (I) is clearly seen. The second self-similar region can be traced.

5 Checking universality

The universal form of the scaling law

$$\psi = \frac{1}{\alpha}\ln\left(\frac{2\alpha\phi}{\sqrt{3}+5\alpha}\right) = \ln\eta \tag{14}$$

gives another way to demonstrate clearly the applicability of the scaling law (5) to the first intermediate region of the flow adjacent to the viscous sublayer. According to relation (??), in the coordinates $(\ln\eta, \psi)$, all experimental points should collapse onto the bisectrix of the first quadrant. In Figure 16a are represented the data of Erm and Joubert (1991), Smith (1994), and Krogstad and Antonia (1998). It is seen that the data collapse on the bisectrix with sufficient accuracy to confirm the scaling law (5). The parameter α was calculated according to the formula $\alpha = (3/2\ln \mathrm{Re})$, $\ln \mathrm{Re}$ was taken here to be $(\ln \mathrm{Re}_1 + \ln \mathrm{Re}_2)/2$ (see Tables 1 and 3).

In Figure 16b the results of the experiments of Winter and Gaudet (1973), are presented. These experiments are specially interesting because they cover a large range of Reynolds numbers (see Table 3). The collapse onto the bisectrix, although with a larger scatter than for the data presented in Figure 16a, is clearly demonstrated.

In Figure 16c we present the results of the experiments of Bruns et al (1992), and Fernholz et al. (1995). Basically they also collapse onto the bisectrix, although with yet larger scatter, and some systematic deviation at large η. This deviation can be explained, at least partially, by the absence of a sharp outer boundary of the first intermediate region, unlike the situation in the experiments of the first group.

In Figure 16d are presented the results of all the experiments except those by Naguib (1992); Naguib and Hites (1995), which will be discussed later, and the experiments by Winter and Gaudet and Bruns et al. and Fernholz et al. presented separately in Figures 16b and 16c. As is seen, the correspondence to the universal form (??) of the scaling law (5) is reasonable. By contrast, Figure 16e,(a) representing the experiments by Naguib (1992), and Nagib and Hites (1995), shows a systematic deviation, in fact a parallel shift, from the bisectrix of the first quadrant. We have already seen such a shift, in the analysis of the pipe experiments of the Princeton group (Zagarola et al. (1996)); in our papers on pipe flow (Barenblatt, Chorin, and Prostokishin (1997a, 1997b)) we concluded that the shift was due to the effects of wall roughness, which increases the effective viscosity. To understand the shift better, we analyzed also the data in the paper of Krogstad and Antonia (1998) where a rough wall was used deliberately, albeit for a very large roughness. Indeed, we found that

in these experiments the experimental points lie much below the bisectrix. Furthermore, in these experiments ln Re_1 and ln Re_2 differed significantly, and we therefore picked the value of α that corresponds to ln Re_1. The result is a pair of lines parallel to the bisectrix but far below it (Figure 16e,(b)).

More generally, it is very likely that any outside cause that increases the level of turbulence should also increase the effective viscosity, and thus shift the points in the $(\ln \eta, \psi)$ plane downwards. A case in point is the set of experiments of Hancock and Bradshaw (1989) discussed above, where turbulence was created by a grid in the free stream. The parallel downward shift is indeed observed (Figure 16f), and it is of the same order of magnitude as the shift in the experiments of Nagib et al. Note that in the experiments of Nagib et al. the second intermediate region is intact, and it is therefore likely that the shift in the universal description of the first intermediate region is due to the disturbance close to the wall, i.e., to roughness, just as in the experiment of Zagarola et al. (1996).

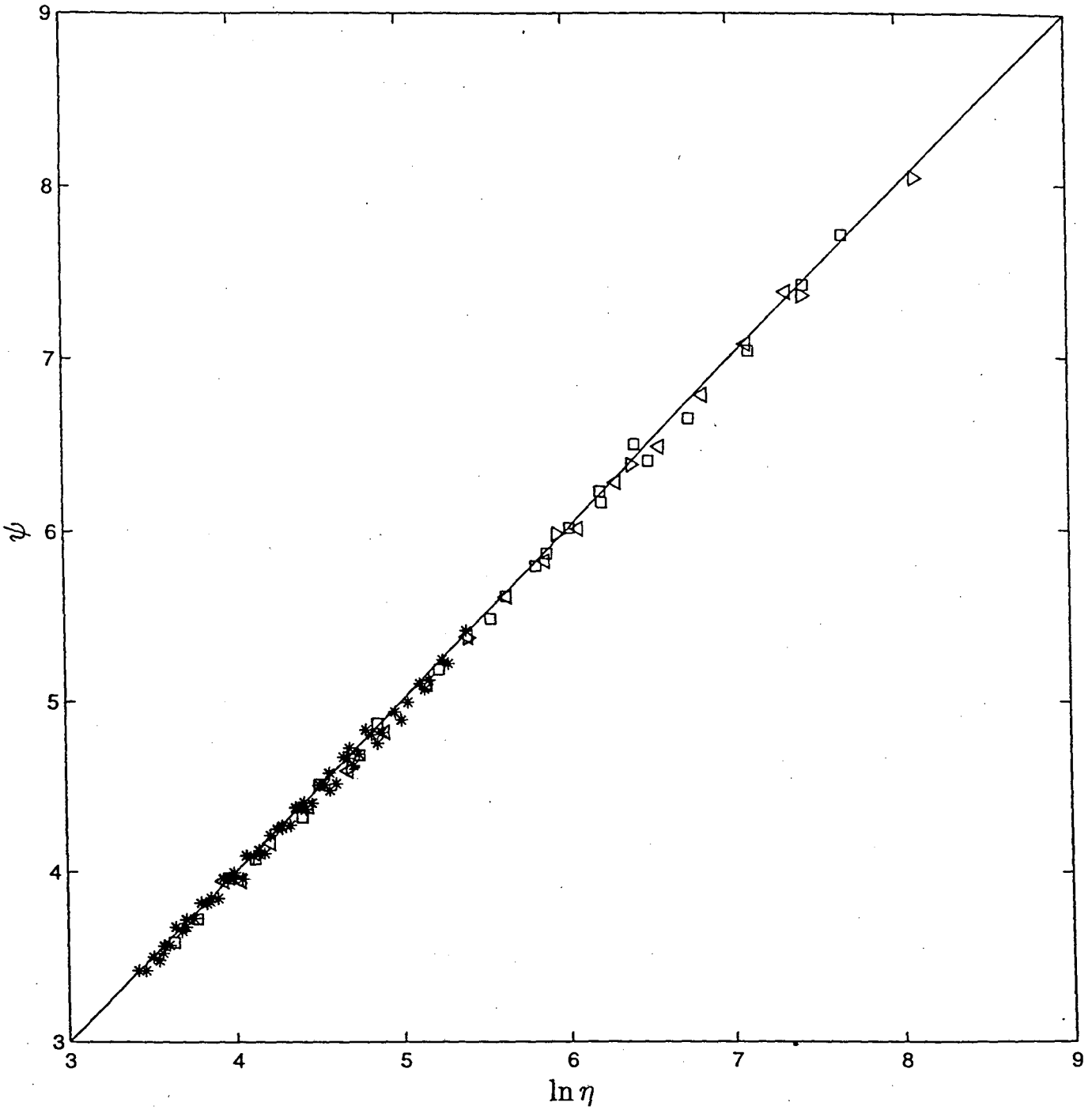

Figure 16. (a) The experiments of Erm and Joubert, (1991) (*); Smith, (1994) (□) and Krogstad and Antonia, (1998) (◁); and Petrie et al., (1990) (▷) collapse on the bisectrix of the first quadrant in accordance with the universal form (14) of the scaling law (5).

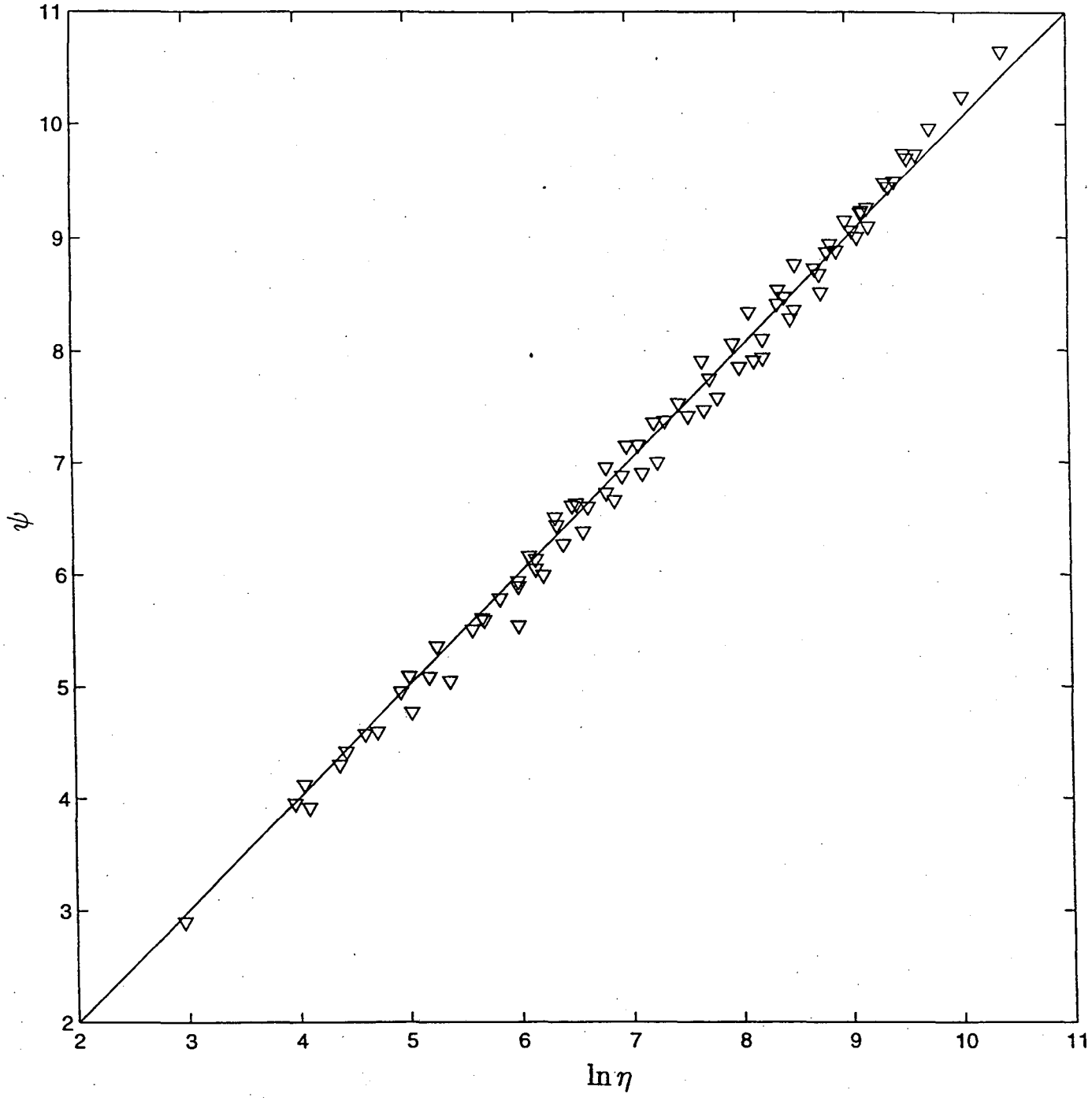

Figure 16. (b) The data of Winter and Gaudet, (1973), (∇) collapse on the bisectrix of the first quadrant in accordance with the universal form (14) of the scaling law (5).

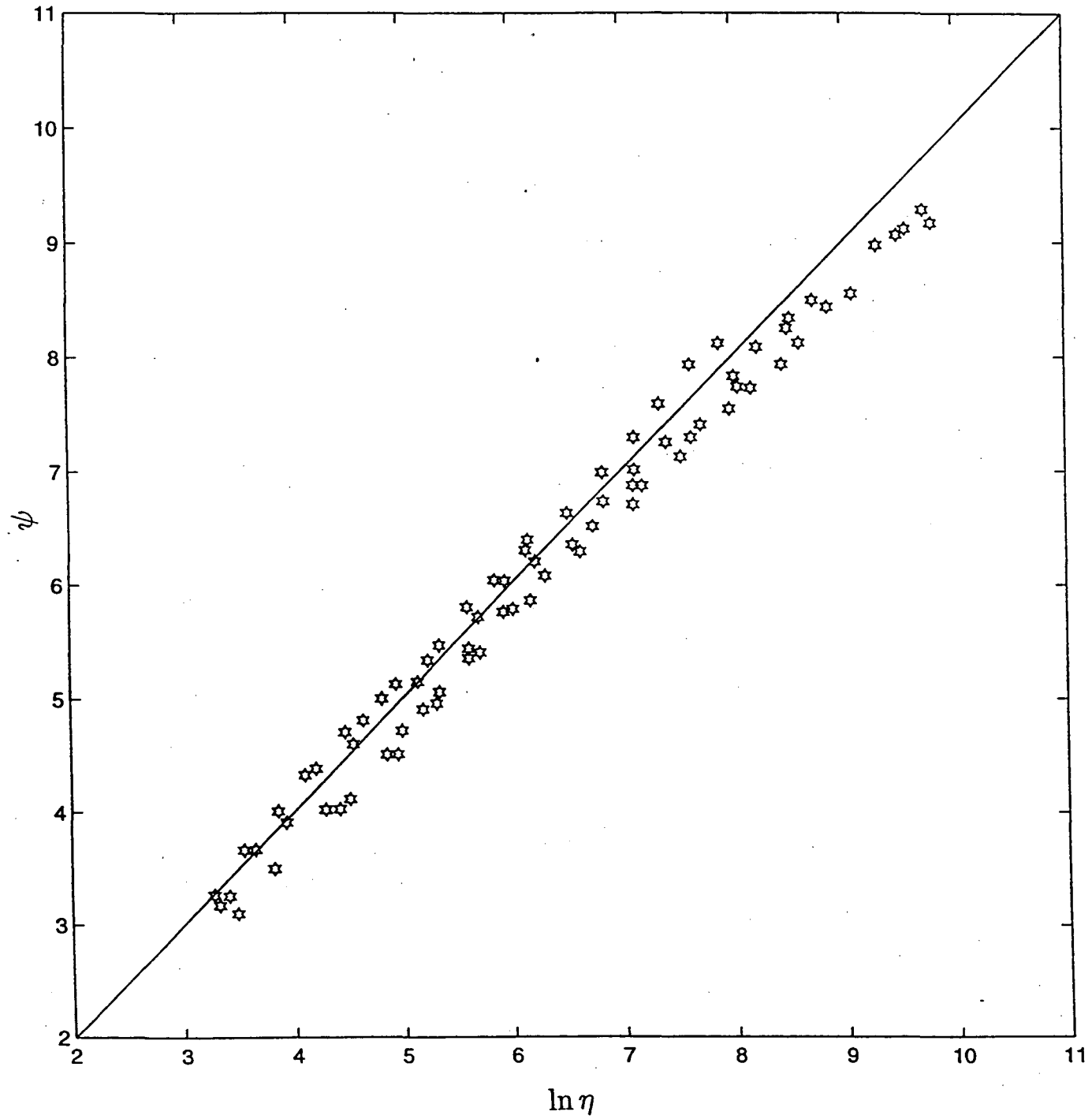

Figure 16. (c) The data of Bruns et al, 1973, and Fernholz et al, 1995 (✡) basically collapse on the bisectrix of the first quadrant in accordance with the quasi-universal form (14) of the scaling law (5).

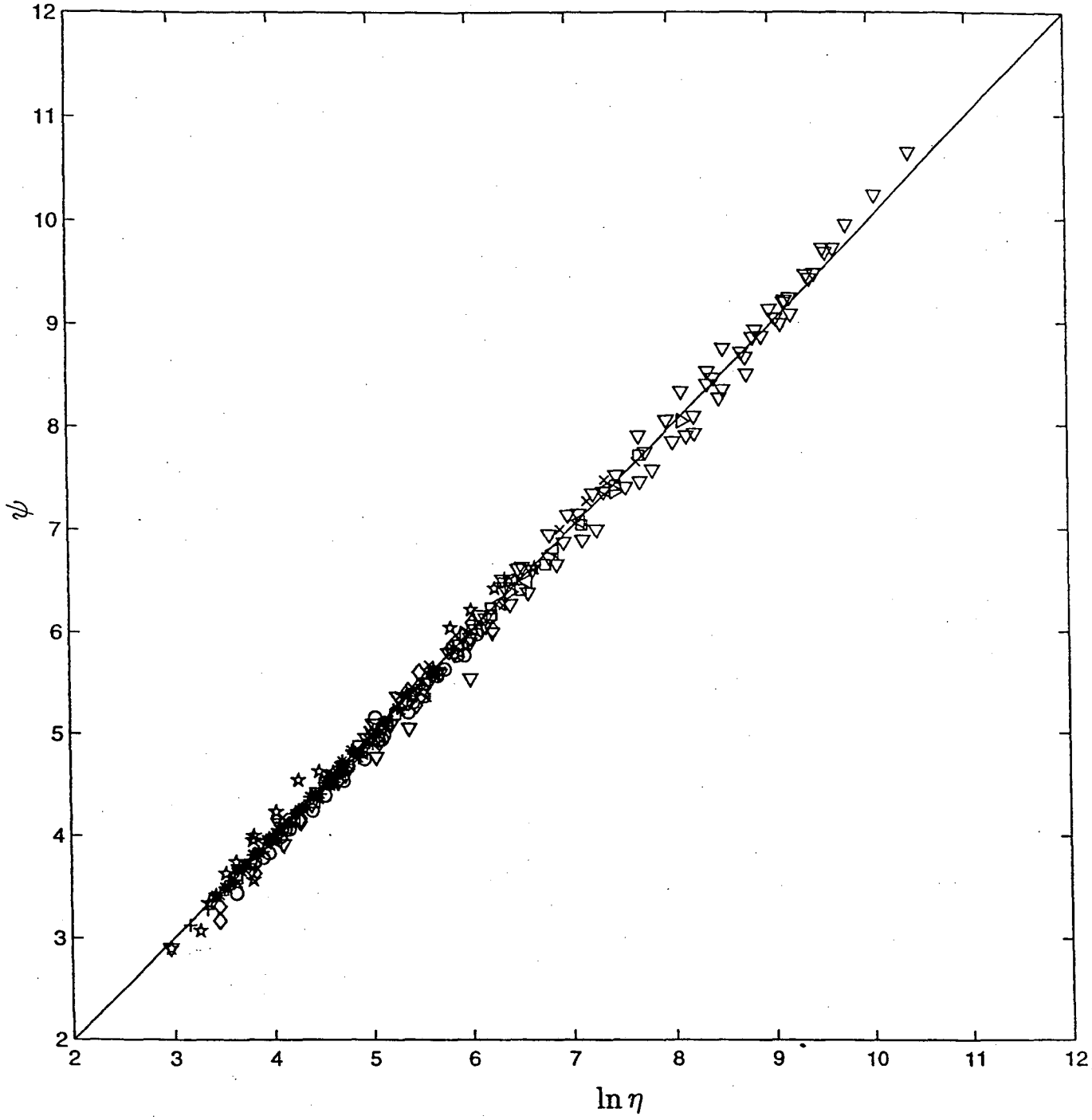

Figure 16. (d) The data of all experiments except of those by Naguib, (1992), and Nagib and Hites, (1995); Bruns et al., (1992), and Fernholz et al., (1995), collapse on the bisectrix of the first quadrant in accordance with the universal form (14) of the scaling law (5): ($\circ$) Collins et al., (1978); ($\triangleright$) Petrie et al., (1990); (+) Erm, (1988); ($\diamond$) Putell et al., (1981); ($\star$) Djenidi and Antonia, (1993); ($\times$) Warnack, (1994); ($\triangleleft$) Krogstad and Antonia, (1998); (∇) Winter and Gaudet, (1973).

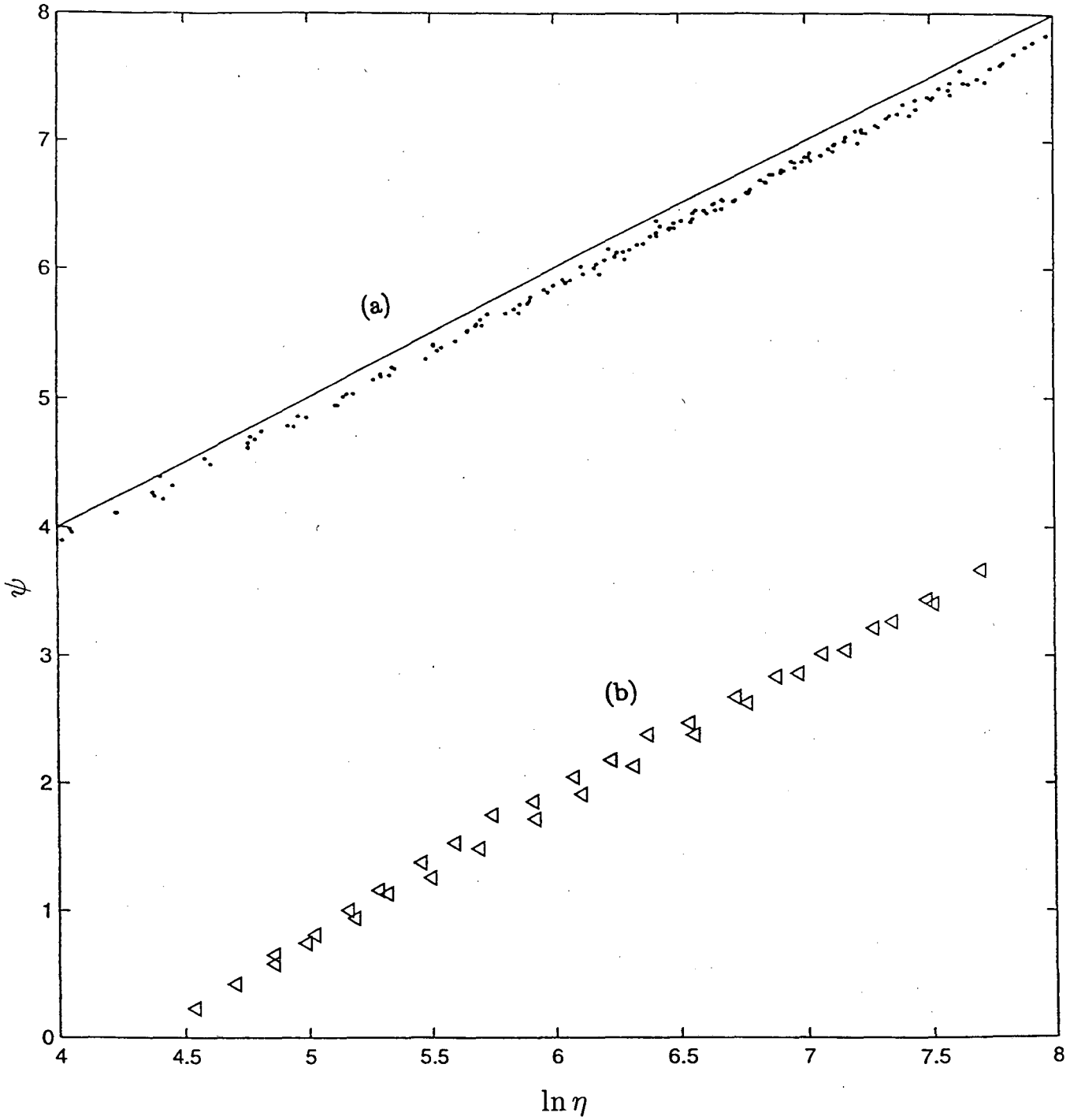

Figure 16. (e) (a) The data of Naguib, (1992), and Nagib and Hites, (1995), show a systematic deviation from the bisectric of the first quadrant.

(b) The data of Krogstad an Antonia, (1998), related to rough walls. The experimental points lie much lower than bisectric. For the evaluation of ψ the value $\alpha = 3/2 \ln \mathrm{Re}_1$ was taken.

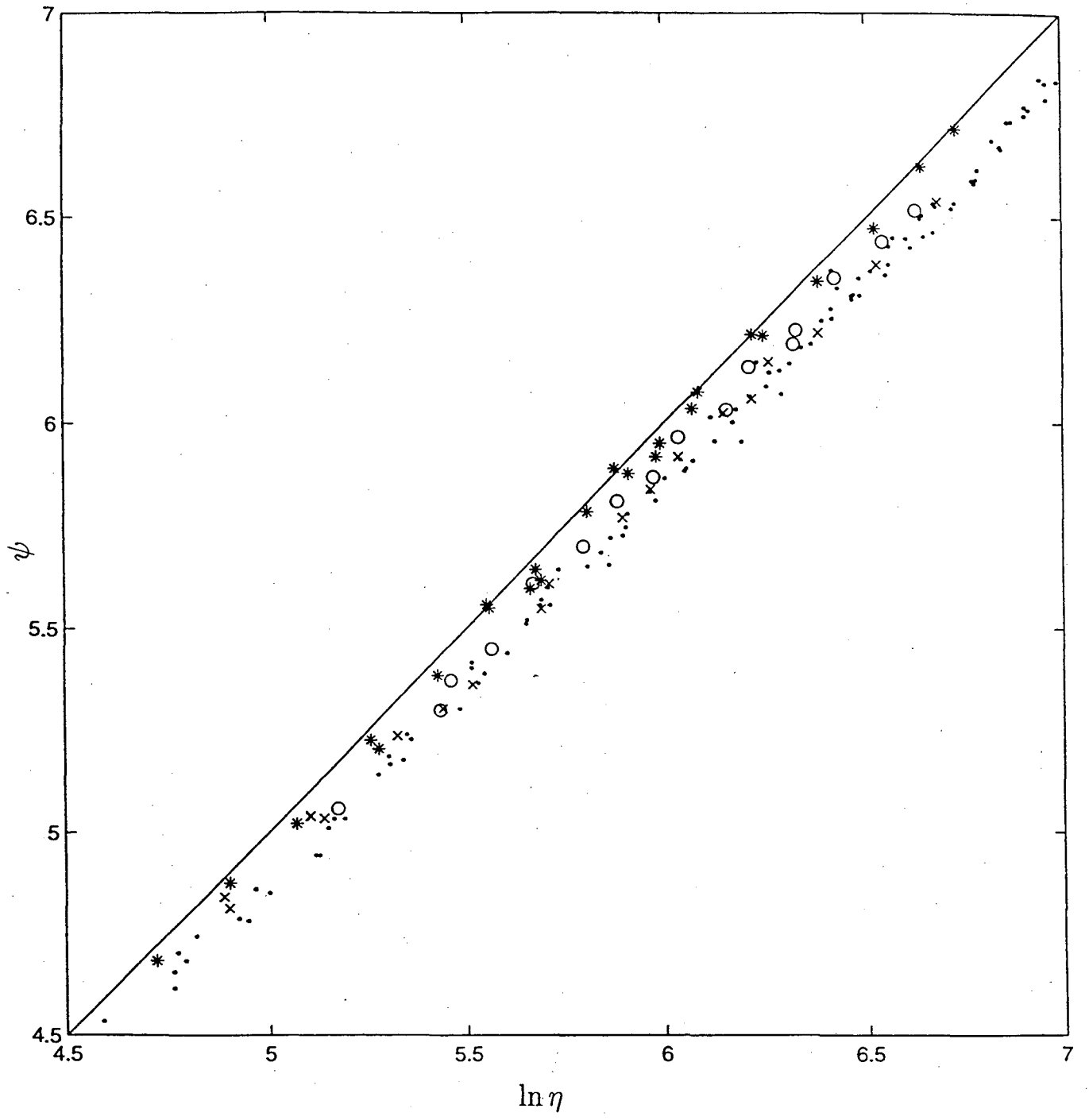

Figure 16. (f) The data of Hancock and Bradshaw, (1989), show the parallel shift from the bisectrix of the same order as in the experiments by Nagib et al. (·) Nagib et al., (⋆) Hancock and Bradshaw, $u'/U = 0.0003$; 0.024; 0.026; (×) Hancock and Bradshaw, $u'/U = 0.040, 0.041$, (○) Hancock and Bradshaw, $u'/U = 0.058$.

6 Conclusion

The Reynolds-number-dependent scaling law

$$\phi = \frac{u}{u_*} = (\frac{1}{\sqrt{3}}\ln\ \mathrm{Re} + \tfrac{5}{2})\eta^{3/2\ln\ \mathrm{Re}}\ , \qquad \eta = \frac{u_* y}{\nu} \tag{15}$$

was established earlier for the intermediate region of pipe flows between the viscous sublayer and the close vicinity of the pipe axis. The Reynolds number Re was determined as Re $= \bar{u}\ d/\nu$, where $\bar{u}$ is the average velocity, and d the pipe diameter. Attempts (Zagarola and Smits (1998)) to adjust the constants of the universal logarithmic law so that this law is valid in a small region of distances from the wall (y less than 0.07 of the pipe radius) are immaterial because these data correspond to the envelope of the family of scaling laws.

In the present work we show that the scaling law (5) gives an accurate description of the mean velocity distribution over the self-similar intermediate region adjacent to the viscous sublayer for a wide variety of zero-pressure-gradient boundary layer flows. The Reynolds number is defined as $\mathrm{Re} = U\Lambda/\nu$, where U is the free stream velocity and Λ is a length scale which is well defined for all the flows under investigation.

We also show that under conditions of weak free stream turbulence there exists a second intermediate self-similar region between the first one, where the scaling law is valid, and the free stream. This second region deteriorates under the influence of free stream turbulence.

The validity of the scaling law for boundary layer flows constitutes strong argument in favor of its validity for a wide class of wall-bounded turbulent shear flows at large Reynolds numbers. The plotting of the experimental data in universal coordinates yields a sensitive gauge of the presence of wall roughness.

Finally, we feel that the affirmation of the effectiveness of incomplete similarity and of vanishing-viscosity asymptotics for turbulent shear flows at large Reynolds numbers has broad implications for other manifestations of turbulence, e.g. in jets, wakes, mixing layers, and local structure, and should lead to a reconsideration of the basic tools used in the study of turbulent flows.

Acknowledgements. The authors would like to thank Professors P. Bradshaw and P.-A. Krogstad for providing them with their recent data.

This work was supported in part by the Applied Mathematics subprogram of the U.S. Department of Energy under contract DE-AC03-76-SF00098, and in part by the National Science Foundation under grants DMS94-14631 and DMS97-32710.

References

Barenblatt, G. I., 1996. *Scaling, Self-Similarity and Intermediate Asymptotics*, Cambridge University Press.

Barenblatt, G. I. 1991. On the scaling laws (incomplete self-similarity with respect to Reynolds number) in the developed turbulent flow in pipes, *C.R. Acad. Sci. Paris*, series II, **313**, 309–312.

Barenblatt, G. I., 1993. Scaling laws for fully developed shear flows. Part 1: Basic hypotheses and analysis, *J. Fluid Mech.* **248**, 513–520.

Barenblatt, G. I. and Chorin, A. J., 1996. Small viscosity asymptotics for the inertial range of local structure and for the wall region of wall-bounded turbulence, *Proc. Nat. Acad. Sciences USA* **93**, 6749–6752.

Barenblatt, G. I. and Chorin, A. J., 1997. Scaling laws and vanishing viscosity limits for wall-bounded shear flows and for local structure in developed turbulence, *Comm. Pure Appl. Math.* **50**, 381–398.

Barenblatt, G. I., Chorin, A. J., Hald, O. H., and Prostokishin, V. M., 1997. Structure of the zero-pressure-gradient turbulent boundary layer, 1997. *Proc. Nat. Acad. Sciences USA* **94**, 7817–7819.

Barenblatt, G. I., Chorin, A. J., Prostokishin, V. M., 1997,a. Scaling laws in fully developed turbulent pipe flow: discussion of experimental data, *Proc. Nat. Acad. Sci. USA* **94a**, 773–776.

Barenblatt, G. I., Chorin, A. J. and Prostokishin, V. M., 1997,b. Scaling laws in fully developed turbulent pipe flow, *Applied Mechanics Reviews* **50**, no. 7, 413–429.

Barenblatt, G. I. and Prostokishin, V. M., 1993. Scaling laws for fully developed shear flows. Part 2. Processing of experimental data, *J. Fluid Mech.* **248**, 521–529.

Chorin, A. J., 1988, Scaling laws in the vortex lattice model of turbulence, *Commun. Math. Phys.* **114**, 167-176.

Chorin, A. J., 1994. *Vorticity and Turbulence*, Springer, New York.

Chorin, A. J., 1998. New perspectives in turbulence. *Quart. Appl. Math.* **56**, 767–785.

Erm, L.P. and Joubert, P. N., 1991. Low Reynolds-number turbulent boundary layers, *J. Fluid Mech.* **230**, 1–44.

Fernholz, H. H. and Finley, P. J., 1996. The incompressible zero-pressure-gradient turbulent boundary layer: an assessment of the data. *Progr. Aerospace Sci.* **32**, 245–311.

Hancock, P. E. and Bradshaw, P., 1989. Turbulence structure of a boundary layer beneath a turbulent free stream, *J. Fluid Mech.* **205**, 45–76.

Krogstad, P.-Å. and Antonia, R. A., 1998. Surface roughness effects in turbulent boundary layers, *Experiments in Fluids*, in press.

Landau, L. D. and Lifshits, E. M., 1987. *Fluid Mechanics*, Pergamon Press, New York.

Monin, A. S. and Yaglom, A. M., 1971. *Statistical Fluid Mechanics*, vol. 1, MIT Press, Boston.

Nagib, H. and Hites, M., 1995. High Reynolds number boundary layer measurements in the NDF. AIAA paper 95–0786, Reno, Nevada.

Naguib, A. N., 1992. Inner- and Outer-layer effects on the dynamics of a turbulent boundary layer, Ph.D. Thesis. Illinois Institute of Technology.

Nikuradze, J., 1932. Gesetzmaessigkeiten der turbulenten Stroemung in glatten Rohren, *VDI Forschungheft*, No. 356.

Prandtl, L., 1932. Zur turbulenten Stroemung in Rohren und laengs Platten, *Ergeb. Aerodyn. Versuch.*, Series 4, Goettingen, 18–29.

Schlichting, H., 1968. *Boundary Layer Theory*, McGraw-Hill, New York.

Spurk, J., 1997. *Fluid Mechanics*, Springer, New York.

von Kármán, Th., 1930. Mechanische Ähnlichkeit und Turbulenz, *Proc. 3rd International Congress for Applied Mechanics*, C.W.Oseen, W.Weibull, eds. AB Sveriges Litografiska Tryckenier, Stockholm, vol. 1, pp.85–93.

Zagarola, M. V., Smits, A. J., Orszag, S. A., and Yakhot, V., 1996. Experiments in high Reynolds number turbulent pipe flow, AIAA paper 96-0654, Reno, NV.

Zagarola, M. V. and Smith, A. J., 1998. Mean-flow scaling of turbulent pipe flow, *J. Fluid Mech.* **373**, 33–79.

Ernest Orlando Lawrence Berkeley National Laboratory
One Cyclotron Road | Berkeley, California 94720

Prepared for the U.S. Department of Energy under Contract No. DE-AC03-76SF00098